NOTICE

The quality of this microform is heavily dependent upon the quality of the original thesis submitted for microfilming. Every effort has been made to ensure the highest quality of reproduction possible.

If pages are missing, contact the university which granted the degree.

Some pages may have indistinct print especially if the original pages were typed with a poor typewriter ribbon or if the university sent us an inferior photocopy.

Previously copyrighted materials (journal articles, published tests, etc.) are not filmed.

Reproduction in full or in part of this microform is governed by the Canadian Copyright Act, R.S.C. 1970, c. C-30.

AVIS

La qualité de cette microforme dépend grandement de la qualité de la thèse soumise au microfilmage. Nous avons tout fait pour assurer une qualité supérieure de reproduction.

S'il manque des pages, veuillez communiquer avec l'université qui a conféré le grade.

La qualité d'impression de certaines pages peut laisser à désirer, surtout si les pages originales ont été dactylographiées à l'aide d'un ruban usé ou si l'université nous a fait parvenir une photocopie de qualité inférieure.

Les documents qui font déjà l'objet d'un droit d'auteur (articles de revue, tests publiés, etc.) ne sont pas microfilmés.

La reproduction, même partielle, de cette microforme est soumise à la Loi canadienne sur le droit d'auteur, SRC 1970, c. C-30.

Canada

THE APPLICATION OF SPECTRAL DOMAIN ANALYSIS TO THE SIMULATION OF FINLINE HYBRID COUPLERS

by

Sylvain Labonté

A THESIS SUBMITTED TO THE
SCHOOL OF GRADUATE STUDIES AND RESEARCH
IN PARTIAL FULFILLMENT OF THE REQUIREMENTS
FOR THE DEGREE OF
MASTER OF APPLIED SCIENCE

Ottawa-Carleton Institute for Electrical Engineering
Department of Electrical Engineering
Faculty of Engineering
University of Ottawa

February 1988

ISBN 0-315-46794-0

UNIVERSITÉ D'OTTAWA
UNIVERSITY OF OTTAWA

STATEMENT ON THE CONTRIBUTION OF THIS THESIS

The work reported here deals with the computer simulation of E-plane directional couplers. It is part of an effort to develop a complete CAD package for millimeter-wave circuits undertaken by Dr. Hoefer at University of Ottawa.

The contribution achieved by this work includes the development of a computer program based on the spectral domain approach for the analysis of coupled finline slots. Also, a simulation procedure for E-plane coupled slot circuits in general, and directional couplers in particular, has been developed and proved adequate. The procedure is simple enough to be easily incorporated in a CAD package with computer optimization based on user-defined models.

ABSTRACT

A procedure for the numerical simulation of finline coupled slot hybrids is proposed. The circuit is analyzed as a cascade of uniformly coupled subsections whose characteristics are calculated individually with the spectral domain method. The validity of the approach is confirmed by the measurements of several couplers. A review of coupled transmission line theory and the description of the spectral domain program developed for this purpose are also given.

ACKNOWLEDGEMENTS

I want to express my gratitude to my supervisor Dr. W.J.R. Hoefer for his guidance during the course of this work. Thanks are also due to the people at the Communications Research Center who helped me realize some of the circuits for this research, and in particular Greg Gajda for some very helpful discussions.

I also want to express my sincere appreciation to Eswarappa for his thorough revision of a part of the manuscript.

Finally, I want to thank Sylvie, my life companion, for her constant encouragement.

Contents

List of Tables

List of Figures

Chapter 1

Introduction

Directional couplers, and in particular hybrid couplers, are a basic component of various electronic systems: balanced mixers, image-rejection mixers, QPSK modulators, etc... In E-plane technology a few different configurations have been investigated for the realization of hybrid couplers. Among them is the coupled slot structure. The principle behind this approach is that when two transmission lines are brought close to each other, some of the energy flowing in the first one is coupled into the second one and becomes available at its ports. By properly designing the coupled line arrangement, a hybrid coupler can be realized. Coupled slot finline hybrids constitute the focus point of this thesis.

Coupled slot finline hybrids are usually composed of two parallel slots in unilateral finline. Often, they are preferred to the other alternatives in E- plane technology for their simplicity of fabrication, or because they produce a so-called codirectional coupling which simplifies the connections with the other components of an integrated system. Unfortunately, the design of these circuits has so far necessitated an empirical approach based on trial and error. The major reason for this is the difficulty of evaluating the excess (and non-uniform) coupling produced by the curved slots necessary to establish a connection to the coupled slots. In an attempt to alleviate this problem, a simulation procedure taking into consideration these non-uniform sections is reported here. Prior to this though, some background information on directional couplers and

coupled transmission line theory is presented.

After defining in general terms what directional couplers are, chapter 2 contains a review of the various coupler configurations used up to now in E-plane technology. Their respective performances are outlined and compared on the basis of the results reported in the literature. The comparison reveals the advantages that coupled slot finline hybrids have over the other alternatives, and explains the interest in these circuits.

In Chapter 3, an in-depth investigation of the coupling mechanism between transmission lines is presented. Such a study is essential for the comprehension of the simulation procedure described later. This analysis also sheds some light on the relationship between codirectional and contradirectional couplers, which are two classes of coupled transmission line circuits. The key point of this section is the conclusion that the behavior of coupled line systems can be entirely determined from the characteristics of their normal modes of propagation.

In the case of finlines, the evaluation of the normal-mode characteristics (propagation constant and impedance) is not a simple task at all. The spectral domain analysis is a numerical method that can be applied to the problem of uniformly (parallel) coupled slots yielding both accuracy and computation efficiency. A program based on this approach has been developed in Turbo-Pascal. Chapter 4 presents a detailed description of it, along with all the necessary theory and developments. Together with Appendix A, it constitutes the only reference document for this program.

In Chapter 5 a simulation procedure for non-uniform (curved) slot arrangements is proposed. The theory and the numerical method developed in Chapters 3 and 4 form the basis of it. The determination of this procedure constitutes the main objective of the present work. It consists in analyzing the non-uniform structure as a cascade of short uniform subsections which are characterized independently. The approach is verified by the simulation of many circuits and proves to yield very good results.

It is believed that the simulation procedure put forward in this work can be of great help for the design of E-plane directional couplers because it is accurate and simple.

Chapter 2

E-Plane Directional Couplers

2.1 Introduction

Ideal directional couplers are lossless junctions with four perfectly matched ports divided into 2 conjugate pairs. The terminals of a conjugate pair are isolated from each other. When the ports are properly terminated in their characteristic impedance, directional couplers have the property that the RF power incident at any port couples power to each port of the other conjugate pair only. In general, directional couplers are symmetrical devices so that the pairs of terminals are indistinguishable from one another.

Figure 2.1 shows a schematic drawing of a directional coupler illustrating its directional behavior. When a signal is propagating from port 1 to 3, a fraction of its energy is coupled to port 4. Accordingly in this case, 4 is called the coupled port, and 3 and 2 the direct and isolated ports, respectively. The same fraction of the energy traveling in the opposite direction is diverted to port 2. The ratio of the coupled power to the incident power is called the coupling coefficient and is expressed in dB. It is determined by the particular design and can take any value from 0 dB down. The earliest application of directional couplers was to provide a simultaneous indication of the powers flowing in both directions on a main transmission line. Consequently the circuits were designed to yield fairly low coupling coefficients of -10 or -20 dB.

Because of their construction some directional couplers present an inherent phase

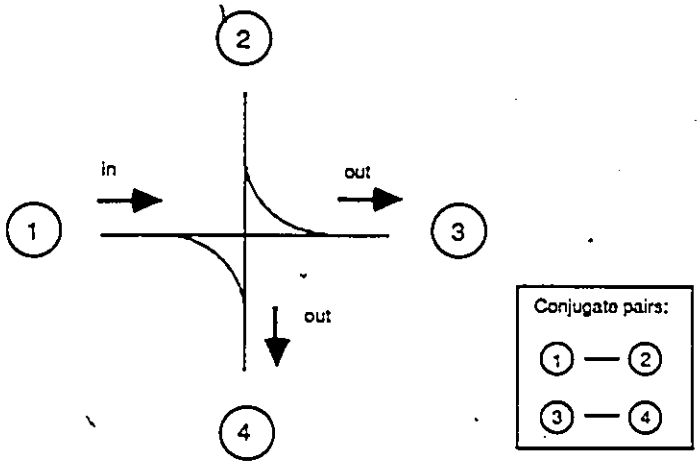

Figure 2.1: Schematic representation of a directional coupler.

shift of 0, 90 or 180 degrees between their two output signals. When designed for −3 dB coupling, this particular class of directional couplers is referred to as hybrid couplers. These are used in many circuit components and systems. Figure 2.2 shows a schematic diagram of a 90- and a 180-degree hybrid. In the first case, the two output voltages differ in phase by 90 degrees regardless of the input port. In the 180-degree case they differ by 0 or 180 degrees depending upon which port is chosen as the input. Some applications of 90- and 180-degree 3 dB hybrids are shown in Figure 2.3.

Directional couplers can be realized in a number of different ways: Branch-line hybrid, multi-hole coupler, hybrid ring, magic-tee, coupled transmission line coupler, etc. Depending on the transmission medium (waveguide, stripline, E-Plane, etc.) all configurations may not be possible or practical. To the author's knowledge, directional couplers of four different types have been reported in E-Plane technology: The 180-degree hybrid junction between a finline and a coplanar line, the printed-probe, the deRonde and the coupled slot 90-degree hybrids.

In this chapter, these hybrids are described and compared on the basis of the results published in the literature. This comparison will justify the interest for the coupled slot

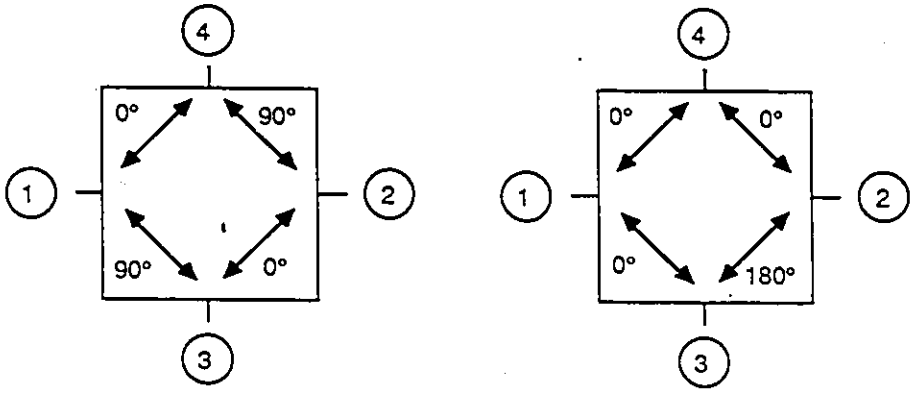

Figure 2.2: Schematic drawings of a 90- and a 180-degree hybrid.

finline hybrid investigated in this thesis.

2.2 180-degree E-Plane Hybrid Junction

This type of arrangement was first introduced by Gysel [1] for millimeter-wave balanced mixers. It has since been extensively utilized in many mixer applications for it yields an excellent LO-to-RF isolation and has broadband characteristics as demonstrated by Meier [2].

This 180-degree hybrid is formed by juxtaposing an unbalanced line such as finline and a balanced line such as coplanar waveguide or microstrip in a configuration shown in Figure 2.4. If a good symmetry is maintained, the balanced signal coming from the left (its E field is represented by thick arrows), only excites a balanced mode in the coplanar line on the right. On the other hand, the unbalanced signal coming from the right (E field represented by thin arrows) does not couple energy into the slot due to this one's inability to propagate an unbalanced signal. Therefore, if a reflective load is provided for the balanced mode on the coplanar line, the isolation between the two ports is inherently very good.

This structure is used in balanced mixers with the diodes located at the junction

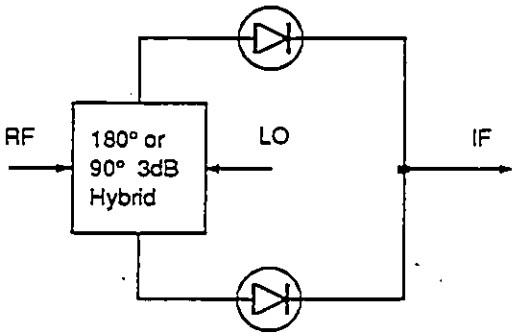

BALANCED MIXER

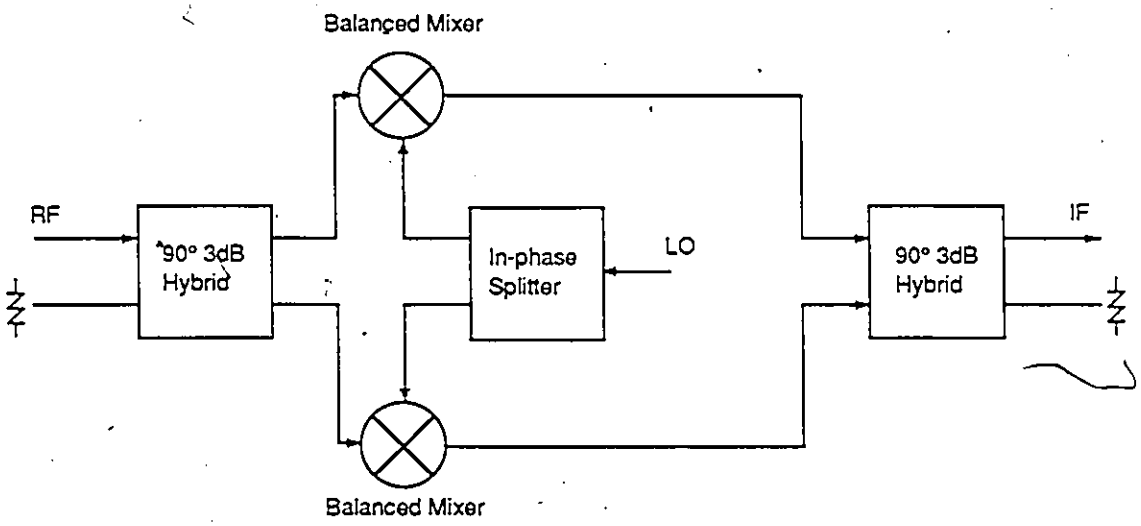

IMAGE REJECTION MIXER

Figure 2.3: Some applications of 90- and 180-degree 3-dB hybrids.

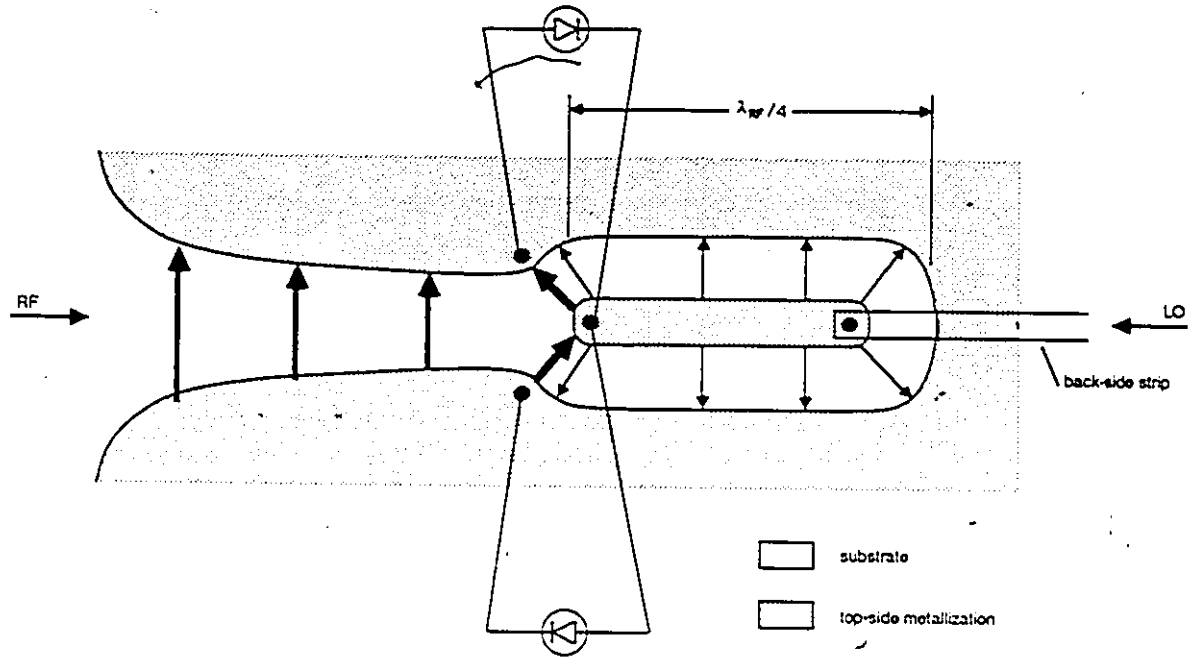

Figure 2.4: 180-degree E-Plane hybrid junction.

and the signals fed in as indicated in Figure 2.4. The LO signal provides in-phase excitation while the RF provides out-of-phase excitation of the diodes. In that respect, this junction acts as a low-loss 180-degree 3-dB hybrid. It is the only type of 180-degree hybrid reported so far in E-Plane technology.

2.3 The Printed-Probe Hybrid Coupler

In this configuration, two parallel waveguides share a common broadwall which is slotted along the E-Plane to accept a pair of dielectric boards as shown in Figure 2.5. An array of printed probes on one of the boards achieves directional coupling between the two waveguides. The other board simply insulates the probes from the metallic housing. This type of coupler was first reported by Meier [3].

The design uses the techniques of multi-hole coupling arrays on the basis of experimental data obtained for the (bi-directional) coupling of individual probes of various dimensions. A 94-GHz 3-dB codirectional[1] hybrid based on this technique has been

[1]Both coupled output signals travel in the direction of the incident signal. In contradirectional couplers, one of the outputs travels in a direction opposite that of the incident signal.

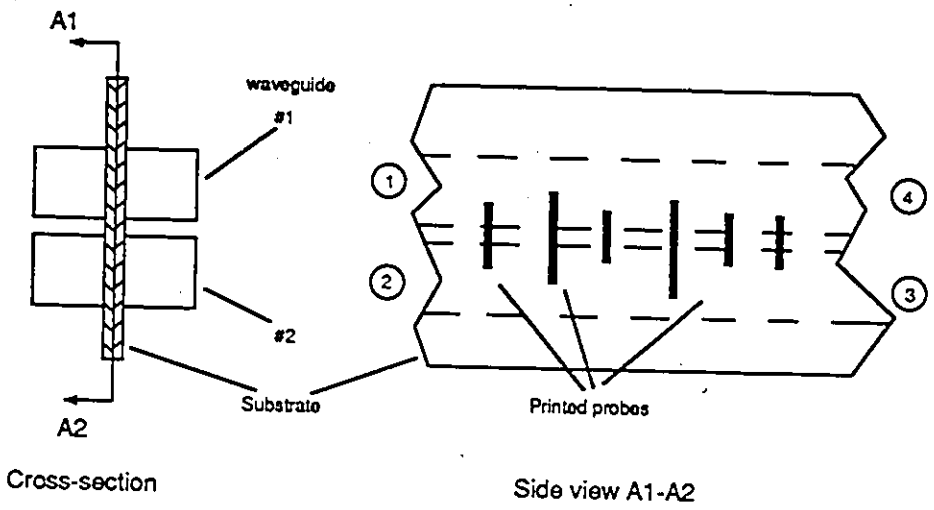

Figure 2.5: Printed-probe hybrid coupler.

demonstrated [4;5]. Figure 2.6 shows the results. A good isolation of more than 22 dB is obtained from 92 to 96 GHz with 0.3 dB insertion loss. However the behavior is very narrowband, with less than 3% bandwidth for a 1-dB imbalance of the output signals.

2.4 deRonde Type 90-degree Hybrid Couplers

A deRonde hybrid coupler [6] consists in two microstrip lines connected by two quarter wavelength long branches: a shunt branch, and a series one in the form of a slot etched in the ground-plane as in Figure 2.7. Ideally, the coupling takes place at the junction of the shunt and the series branches only, the two being otherwise decoupled. An even-odd mode analysis by Callsen and Schmidt [7] reveals that under even excitation only the shunt branch is excited while in the odd mode only the series branch is. By properly choosing the impedances of the branches, perfect isolation and contradirectional 3-dB coupling can in principle be achieved. The propagation constant in both branches is assumed equal, and dielectric overlays are used to ensure this.

Two slightly different implementations of this coupler in E-Plane technology have

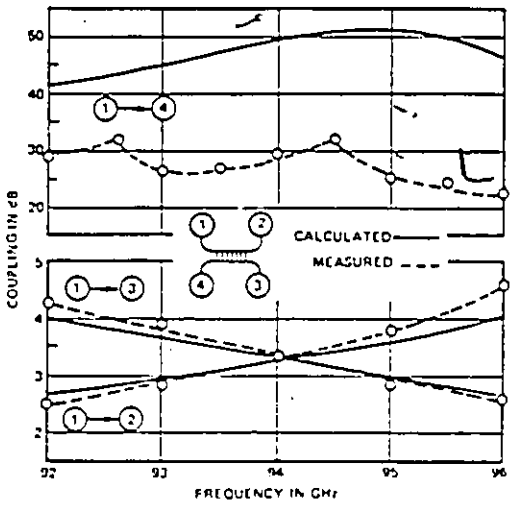

Figure 2.6: Printed-probe hybrid performances obtained by Meier [4]

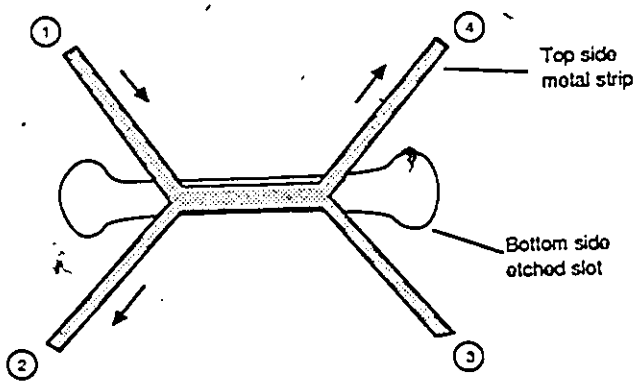

Figure 2.7: deRonde's microstrip coupler.

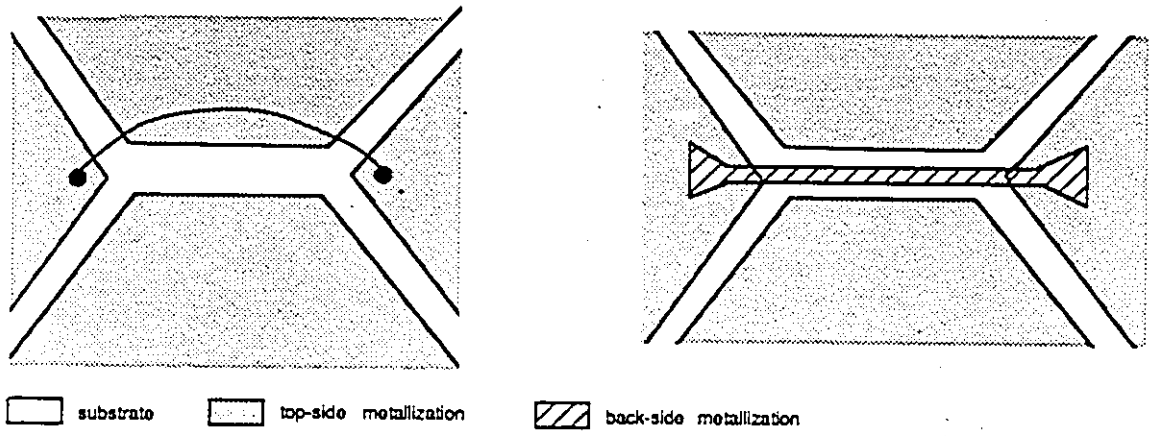

Figure 2.8: Slot-line versions of deRonde's coupler.

been reported [7,8]. In [8] the dual of the deRonde hybrid is presented with the strips replaced by slots and the slot by a wire as in Figure 2.8. Alternatively, the wire can be replaced by a strip printed on the backside and capacitively loaded at both ends [9]. In [7], antipodal finlines are used to essentially reproduce the microstrip configuration inside a waveguide housing.

After some empirical optimization, the two implementations resulted in 3-dB hybrids characterized by 0.5 dB insertion loss (including the losses of the transitions to the empty waveguide), less than 0.5 dB imbalance and 20-25 dB isolation over the entire Ka-band. The circuits proved to be broadband and very compact.

On the other hand, the implementation with a wire as the parallel branch suffers from a bad reproducibility and requires additional mounting steps. The other circuit requires metallization on both sides of the substrate, and both approaches require dielectric overlays to equalize the phase velocities in the branches. Also, even though compactness represents an advantage for circuit integration, fabrication problems appear as frequency increases. For this reason the use of these circuits is limited to frequencies below 40 GHz [2].

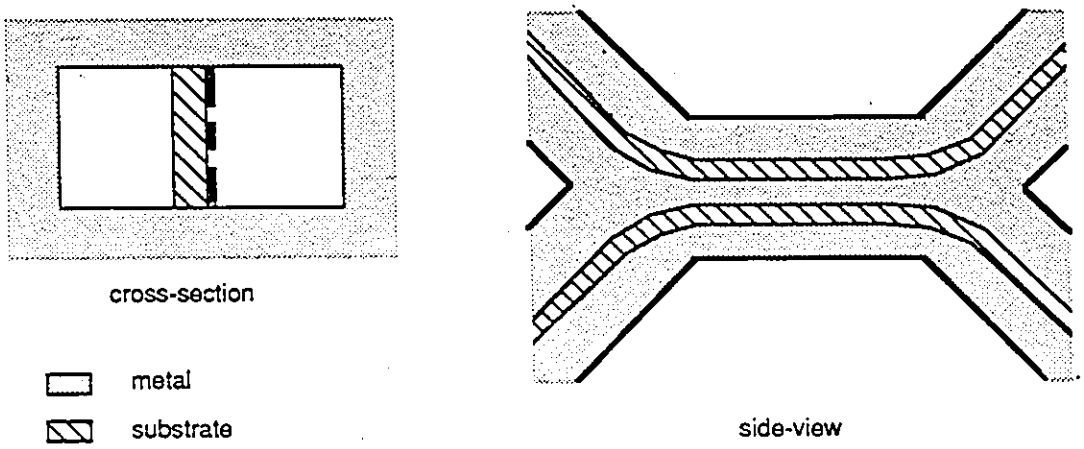

Figure 2.9: Unilateral coupled slot hybrid.

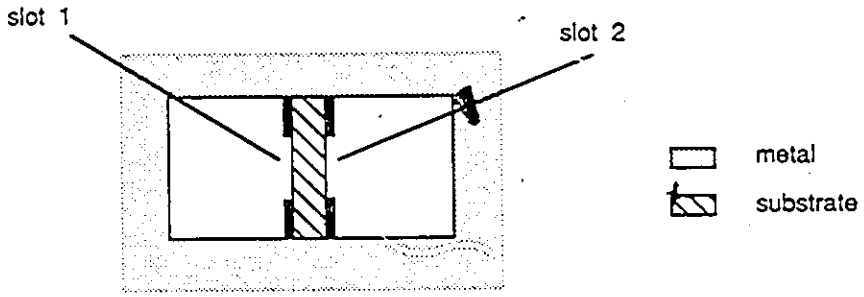

Figure 2.10: Bilateral coupled slot hybrid proposed by Mirshekar-Syahkal [10].

2.5 Coupled Slot 90-degree Hybrid Couplers

This type of coupler is realized with a double slot structure in a waveguide housing. It can take the form of two slots in unilateral finlines as in Figure 2.9 or, as recently proposed in [10], bilateral coupled slots (see Figure 2.10). No realization of the latter type has been reported yet, but the operation is similar to the former except for the connections to the terminals.

In unilateral coupled slots, the even mode of propagation (TEM-like mode) interferes

with the odd mode by virtue of their different phase velocities, creating a beating effect. Hence, a periodical codirectional coupling[2] is obtained with insertion loss corresponding to the attenuation of the coupled lines (taking into account the losses of the transitions to empty waveguide). The degree of coupling is a function of the width, the spacing and the length of the coupled slots. The concept of a slot-line directional coupler was first demonstrated in [11], where an empirical design resulted in a 3-dB hybrid usable between 2.6 and 3 GHz.

Since then, the technique has been adapted to E-Plane circuits [2] (balanced mixers [12] and QPSK modulators [13,14]) with broadband results. In [13] an equal power split was obtained with 0.3 dB insertion loss between 13-17 GHz with an isolation better than 20 dB and a reflection coefficient varying between -30 and -17 dB. In [2], a Ka-band 3-dB hybrid is reported featuring 0.3 dB insertion loss, a return loss and an isolation better than -17 dB, and less than 1 dB imbalance across the entire band. Furthermore the approach has been demonstrated to be feasible at frequencies as high as 90 GHz [2] where coupling varying between 3-5 dB and better than 21 dB isolation were achieved over the full waveguide band of 60 to 90 GHz.

The major disadvantage of this type of coupler is that one has to rely upon a fair amount of empirical optimization of the coupling parameters to achieve satisfactory results [13,14]. A theoretical design approach has been attempted in [15] but the results were not satisfying. The main reason is that the curved sections connecting the finline to the coupled slots were not taken into account. Previous work on dielectric waveguides has demonstrated that they have a non-negligible effect on the coupling. A contribution originally published in German [16] and just recently made available in English, presents a design approach that does consider, to some extent, the non-uniform coupling of the curved sections. The concept of *effective coupling length* is used there to predict the

[2]See section 3:5.2.

actual level of coupling between the two slots. This method relies on the approximation that the impedance of the curved slots is constant over their length. Nonetheless, the approach leads, after empirical optimization, to very good coupler performance.

2.6 Conclusion

The performance of the E-Plane hybrids discussed above are summarized in Table 2.1 to facilitate a comparison.

Regarding the 180 degree hybrid, it is the only one of its type and features excellent performance. It is a close relative of the waveguide magic-tee and offers large bandwidth, low insertion loss, and simplicity. The reasons are clear for its wide utilization.

Concerning the performance of the 90-degree hybrids, the coupled slot and the deRonde types are superior to the printed-probe coupler regarding the usable bandwidth. On the other hand, the deRonde coupler requires the most complex fabrication process of the three types, which could be a major drawback in mass production applications.

The coupled slot coupler appears to be a superior approach. Its codirectional rather than contradirectional (see Chapter 3) behavior also proves to be an advantage for microwave integrated circuits, allowing easier connections between adjacent subsystems. A major inconvenience, however, is that no systematic and accurate design technique has been reported yet for this type of coupler. So far, researchers have mostly relied on empirical optimization based on trial and error. In order to better understand the phenomenon of coupling between two adjacent parallel transmission lines an analysis is given in the next chapter.

coupler type	direction	phase shift	bandwidth	conjugate port isolation	com-pact-ness	simplicity of design	fabrication	comments
180 deg hybrid junction	n/a	180	depends on the termination used for the balanced mode	very good	yes	yes	easy	- extensively used for balanced mixers
printed-probe hybrid	forward	90	narrow	good	no	no	complicated housing	- not suitable for circuit integration
deRonde type	backward	90	wide	good	very	yes	double-sided or bond wire necessary	- limited to frequencies below 40 GHz - backward can be a disadvantage for system integration
coupled slots	forward	90	wide	good	yes	empirical approach	easy	- better overall results than printed probe - demonstrated up to 90 GHz - forward is convenient for integration - design is inconvenient

Table 2.1: Comparison of the performances of the various hybrids

Bibliography

[1] U.H. Gysel, "A 26.5 to 40-GHz Planar Balanced Mixer," in *Proc. 5th Eur. Microwave Conf.*, 1975, pp. 491-495.

[2] P.J. Meier, "Integrated Finline: The Second Decade. Part 1," *Microwave Journal*, Nov. 1985, pp. 31-36.

[3] P.J. Meier, "Millimeter Integrated Circuits Suspended in the E- Plane of Rectangular Waveguide," *IEEE Trans. Microwave Theory Tech.*, vol. MTT-26, pp. 726-733, Oct. 1978.

[4] P.J.Meier, "Printed-probe Hybrid Coupler for the 3 mm Band," in *9th Eur. Microwave Conf Dig.*, (Brighton, England), 1979, pp. 443-447.

[5] K. Solbach, "The Status of Printed Millimeter-Wave E-Plane Circuits," *IEEE Trans. Microwave Theory Tech.*, vol. MTT-31, pp. 107-121, Feb. 1983.

[6] F.C. deRonde, "A New Class of Microstrip Directional Couplers," *Proc. 1970 European Microwave Conf.*, pp. 184-189.

[7] H. Callsen, L.-P. Schmidt, "Quasiplanar 3 dB Hybrid for Millimeter-Wave Integrated Circuits," *Electron. Letters*, vol. 18, no 14, 18 Feb. 1982.

[8] H.E. Hennawy, R. Knöchel, K. Schünemann, "Octave-Band Fin-Line Hybrid," in *Proc. 11th Eur. Microwave Conf.*, Amsterdam, 1981, pp. 301-304.

[9] E. Kpodzo, L. Szabo, E. Jensen, K. Schünemann, "Integrated Fin-Line Millimeter-Wave Transceiver," in *12th Eur. Microwave Conf. Dig.*, 1982, pp. 702-706.

[10] D. Mirshekar-Syahkal, B. Jia, "Analysis of Bilateral Finline Couplers," *Electron. Letters*, vol. 23, no. 11, pp. 577-578, 21st May 1987.

[11] E.A. Mariani and J.P. Agrios, "Slot-Line Filters and Couplers," *IEEE Trans. Microwave Theory Tech.*, vol. MTT-18, pp. 1089-1095, Dec. 1970.

[12] G. Begemann, "An X-Band Balanced Fin-Line Mixer," *IEEE Trans. Microwave Theory Tech.*, vol. MTT-26, pp. 1007-1011, Dec. 1978.

[13] E. Kpodzo, K. Schünemann, G. Begemann, "A Quadriphase Fin-Line Modulator," *IEEE Trans. Microwave Theory Tech.*, vol. MTT-28, pp. 747-752, July 1980.

[14] G.B. Cajda and C.J. Verver, "Millimeter-Wave QPSK Modulator in Fin Line," in *1986 IEEE MTT-S Int. Microwave Symp. Digest*, pp. 233-236.

[15] A. Beyer, D. Köther, I. Wolff, "Development of a Coupler in Finline Technique," in *1985 IEEE MTT-S Int. Microwave Symp. Digest*, pp. 139-142.

[16] H. Callsen, L.-P. Schmidt, K. Solbach, "Broadband Finline Directional Couplers", translated from German in "E-Plane Integrated Circuits", by Bhartia and Pramanick, Artech House, 1987.

Chapter 3

Coupled Transmission Lines: Analysis and Application to Directional Couplers

3.1 Introduction

Coupled transmission lines are obtained by placing two or more lines side by side in such a way as to allow their respective electromagnetic fields to interact with each other. In terms of circuit theory models, this interaction is represented by mutual inductance and capacitance. In terms of field quantities, the different phase velocities and impedances of the system's so-called normal propagating modes express the same inter-relationship.

In general, many transmission lines of different types, dielectric media and characteristic impedances can be coupled together. In these cases the coupling is often an undesirable effect deteriorating the performances of the system. The first efforts spent on coupled transmission lines were driven by telephone companies having to cope with crosstalk problems between telephone lines in the 1920's. Eventually however, researchers found useful applications for coupled lines, and these are now widely used to realize filters, directional couplers and impedance transformers.

Coupled transmission lines can be asymmetric or symmetric, uniformly or non-uniformly coupled, with homogeneous or inhomogeneous dielectric medium. The symmetry refers to the characteristics of the isolated lines: if they have the same charac-

teristic impedance and propagation constant then they are symmetric, if not, they are asymmetric. Uniform coupling means that along the longitudinal axis the structure is uniform. Finally, the lines can be embedded in a homogeneous dielectric medium, as in the case of striplines, or not, as in the case of finlines. This chapter deals with the analysis of uniformly coupled transmission lines and investigates their applications to directional couplers. Our analysis will be restricted to the cases involving only two lines.

Firstly, a general procedure to analyze coupled asymmetric lines in an inhomogeneous medium will be outlined. This is introduced here in order to show that such a system is entirely characterized by its *normal modes* of propagation and that the signals on the lines are superpositions of these modes. Following this, a short section is devoted to a comparison of these normal modes and the well-known even and odd modes.

In the case of interest to us, namely E-Plane couplers made of a pair of identical slots, a different formulation of the problem is possible, assuming *a priori* the *normal mode* decomposition. This analysis is detailed in Section 3.4. It results in expressions that can be readily used for the design of directional couplers.

Finally, Section 3.5 applies these formulae to obtain directional couplers with codirectional and contradirectional behavior, whose frequency responses are then compared.

3.2 Case of Two Asymmetric Lines in an Inhomogeneous Medium

Coupled transmission line circuits have in general four terminals corresponding to ports of the two lines. It is often desirable to characterize such circuits by their 4×4 [Y], [Z] or ABCD matrices. Tripathi [1] has presented a particularly clear analysis resulting in the general expressions for the four-port's parameters. He shows that these parameters can be determined from the propagation constants and the impedances of the independent *normal modes* of the system. To gain some insight into the mechanism of coupling and

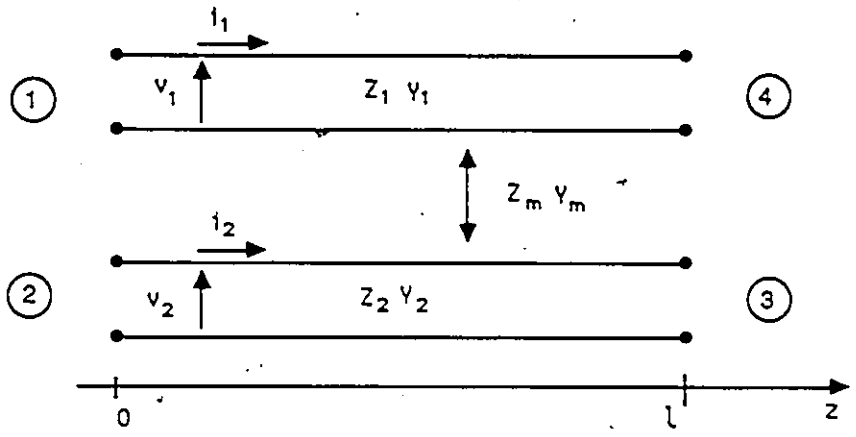

Figure 3.1: System of two coupled lines.

to provide a justification for the normal mode decomposition used in Section 3.4, this analysis is outlined step by step.

Step 1/ The generalized Telegraphist's Equations for the system of coupled lines of Figure 3.1 are written down by applying Kirchoff's law to an element dz of each line, and then reduced to second order differential equations for the voltage on each line.

The generalized Telegraphist's Equations are:

$$-\frac{dv_{1,2}}{dz} = Z_{1,2}i_{1,2} + Z_m i_{2,1} \tag{3.1}$$

$$-\frac{di_{1,2}}{dz} = Y_{1,2}v_{1,2} + Y_m v_{2,1}$$

where $Z_{1,2}$ and $Y_{1,2}$ are, respectively, the self impedance and admittance per unit length of each line and Z_m, Y_m are the mutual impedance and admittance per unit length. Subscripts 1 and 2 refer to the line numbers and the notation $_{1,2}$ in the expressions is a short-hand notation for expressing the relation for both lines.

Equations (3.1) can then be reduced to two second-order differential equations for the voltages:

$$\frac{d^2v_1}{dz^2} - a_1v_1 - b_1v_2 = 0 \tag{3.2}$$

$$\frac{d^2v_2}{dz^2} - a_2v_2 - b_2v_1 = 0$$

where a_i's and b_i's are functions of Z_1, Z_2, Y_1, Y_2, Z_m, Y_m.

Step 2/ A particular solution of (3.2) is sought in the form of a wave propagating in the z direction simultaneously in the two lines. Such a solution will be called a *mode* of the system.

Let us therefore assume:

$$v_{1,2}(z) = U_{1,2}\, e^{\gamma z} \tag{3.3}$$

where γ is the propagation constant of the mode. The mode's structure may assume different voltage amplitudes U_1 and U_2 on the two lines.

Step 3/ Combining (3.3) and (3.2) yields a 2×2 system of simultaneous equations $[A][v] = 0$. The eigenvalues of the system are obtained by setting $\det A = 0$. This results in four possible values for γ or, in other words, four *normal modes* of two different types: the c modes and the π modes. We have:

$$\gamma = \pm\gamma_c \quad \text{and} \quad \gamma = \pm\gamma_\pi \tag{3.4}$$

where $\gamma_{c,\pi}$ are expressed in terms of a_i's and b_i's in (3.2). The $\pm$ sign simply indicates the directions of propagation of the modes.

Clearly, two types of waves or modes are particular solutions to the Telegraphist's Equations. For these waves the two coupled lines are a *single directional system.* Each mode represents a certain distribution of voltages (and currents) among the conductors. In other words, each mode is characterized by its own field structure.

Step 4/ For each type of mode, the ratios R_c and R_π of the voltage amplitudes in the lines can be determined by replacing the expressions obtained for the γ's back into (3.2). These ratios are defined as

$$R_c = \frac{v_2}{v_1} \quad \text{for} \quad \gamma = \pm\gamma_c \tag{3.5}$$

$$R_\pi = \frac{v_2}{v_1} \quad \text{for} \quad \gamma = \pm\gamma_\pi$$

and are functions of the line parameters through the a_i's and b_i's. Next, the impedance of each line for each mode is found using (3.5), (3.3) and (3.1). These are:

$$Z_{1c},\ \ Z_{2c},\ \ Z_{1\pi},\ \ Z_{2\pi}, \tag{3.6}$$

and are functions of the line parameters Y and Z and the mode parameters γ and R.

Step 5/ A linear combination of the four possible modes yields a general solution to (3.2). We get:

$$v_1(z) = (A_1 e^{-\gamma_c z} + A_2 e^{+\gamma_c z}) + (A_3 e^{-\gamma_\pi z} + A_4 e^{+\gamma_\pi z}) \tag{3.7}$$

$$v_2(z) = (A_1 R_c e^{-\gamma_c z} + A_2 R_c e^{+\gamma_c z}) + (A_3 R_\pi e^{-\gamma_\pi z} + A_4 R_\pi e^{+\gamma_\pi z})$$

and the associated currents can be deduced from the mode impedances.

Step 6/ Finally, the port voltages and currents are expressed in terms of the A_i's in Step 5, resulting in two 4×4 systems. From these the A_i's can be eliminated leading to the 4×4 impedance matrix [Z] of the structure. The [Z] matrix representation allows the characterization of the two-port's behavior with any terminations connected to it.

The general expression for [Z] reveals that a knowledge of the mode parameters γ, R and Z is sufficient to characterize entirely the coupled line system. Therefore, the behavior of a circuit can be predicted by an analysis of the properties of the field distribution corresponding to each mode. The fact that the modes are normal justifies that they be analyzed independently. The very existence of these modes has been experimentally observed by Speciale [2]. They have the properties of *equal voltage amplitude on the two lines for the c mode ($R_c = 1$) and equal but opposite currents for the π mode.*

The *coupled mode approach* of Adair and Haddad [3] is another formulation that can also be adopted to investigate the coupling process between transmission lines. The voltages and currents need not be resolved into the *normal modes* of the system but may be considered as the voltages and currents of waves each of which is propagating

in only one partial line. By virtue of the coupling of these lines, an exchange of energy occurs between the waves propagating in them.

The two viewpoints are, of course, equivalent. For various reasons (physical insight, convenience for design) one approach might be preferred to the other. For the cases where more than two lines are involved, the coupled mode approach is more attractive due to the complexity in defining the normal modes.

3.3 Notes on the Normal Modes

The EM field propagating on a system of two transmission lines is distributed as prescribed by the normal modes of the system. The existence of these modes was demonstrated in the previous section, and their main characteristics were outlined.

The analysis of the propagation of these modes (a total of four of two different types traveling in both directions along the line) is sufficient to characterize entirely the four-port network. It is interesting to note that the well-known even and odd mode analysis often used in similar problems [4,5,6] is applicable in particular cases only. These modes are defined as having *equal voltage magnitude on the two lines, with equal and opposite polarity, respectively.* In the cases of symmetric coupled lines (both in the homogeneous or inhomogeneous case) they are equivalent to the c and π modes because each line has the same impedance.

For asymmetric lines however, the even and odd modes do not correspond to the normal modes of the system. Speciale [2] interprets them as being linear combinations of the fundamental c and π modes. The even-odd mode analysis remains valid though for asymmetric coupled lines in a homogeneous medium because in this case, both the normal modes have the same phase velocity. Consequently, the linear combinations forming the even and odd modes propagate in an independent fashion as simple waves (without breaking down into a fast c and a slow π waves) and can be analyzed separately.

On the other hand, when an inhomogeneous dielectric medium is considered, the normal modes have different phase velocities and the even and odd modes do not propagate independently. In these cases, the analysis of an excitation in terms of its even and odd components would not reflect the physical reality and would lead to incorrect results.

The configuration of interest in this thesis involves identical lines in an inhomogeneous dielectric medium. On the basis of what has just been presented, the even and odd mode formulation is justified and will be used in the next section.

3.4 Case of Two Symmetric Lines in an Inhomogeneous Medium

The analysis presented in Section 3.2 is very general and the parameter matrix proves to be a very flexible means of describing the four-port circuit. This type of approach is advantageous when various port terminations must be considered as in the investigation of filters conducted in [6]. However, for the simple case of symmetric directional couplers where one port is excited and the three other ports are terminated in their characteristic impedance, a very straightforward formulation of the problem exists. It parallels that of Reed and Wheeler [7]. Its results, in terms of the ports' emerging waves, are not directly applicable to the analysis of filters but are adequate for the present work. This elegant approach will be presented in detail here, and the results will be used to design directional couplers in the following section.

The directional coupler of interest is shown in Figure 3.2. It is composed of two symmetric uniform coupled transmission lines of length l in an inhomogeneous medium. Each port is terminated in an impedance Z_L. We are interested in studying the behavior of this four-port circuit under a single input at port 1. It has been shown in the previous sections how similar structures support two types of *independent normal modes* traveling in both directions. In this particular case these two types correspond to the even and

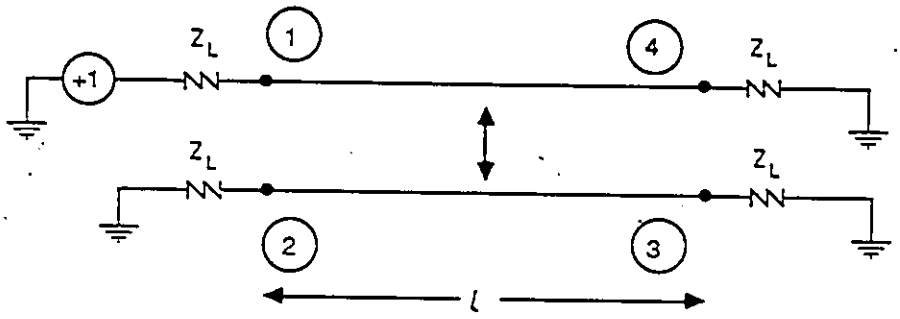

Figure 3.2: Coupled line directional coupler with a unit input at port 1

odd modes as explained in Section 3.2. Accordingly, the circuit response to a unit voltage input at port 1 can be obtained by the superposition of the responses to an even and an odd mode excitation of amplitude 1/2 at ports 1 and 2.

By virtue of the independence of the chosen modes, the two excitations can be considered separately. In each case, the analysis reduces to that of a two port network. The equivalent circuits for each mode are shown in Figure 3.3 along with their line parameters: $\beta_{e,o}$, the propagation constants of the two modes and $Z_{e,o}$, the impedances of each line in the presence of the other for each mode.

The amplitude and phase of the total signals emerging from each port are expressed by:

$$V_1 = \frac{1}{2}(\Gamma_e + \Gamma_o) \tag{3.8}$$

$$V_2 = \frac{1}{2}(\Gamma_e - \Gamma_o)$$

$$V_3 = \frac{1}{2}(T_e - T_o)$$

$$V_4 = \frac{1}{2}(T_e + T_o)$$

where $\Gamma_{e,o}$ and $T_{e,o}$ are, respectively, the reflection and transmission coefficients of the two-port networks in the even and odd modes.

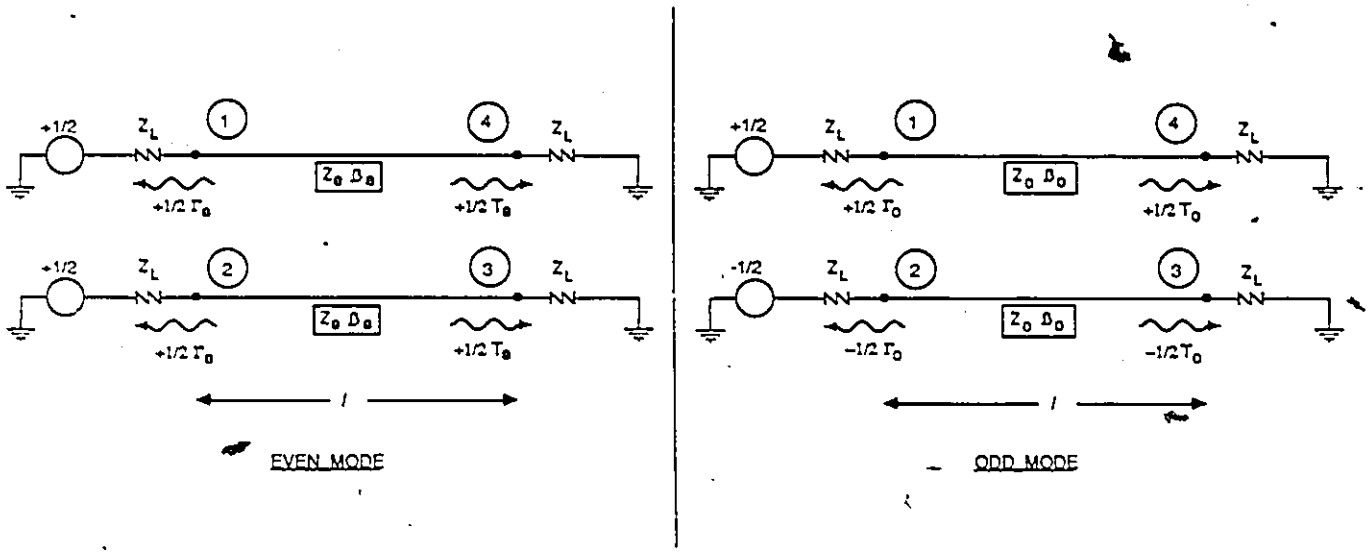

Figure 3.3: Even and odd mode excitations at ports 1 and 2

The general expressions for Γ and T of a two-port network in terms of its ABCD parameters are:

$$\Gamma = \frac{AZ_L + B - CZ_L{}^2 - DZ_L}{AZ_L + B + CZ_L{}^2 + DZ_L} \qquad (3.9)$$

$$T = \frac{2}{AZ_L + B + CZ_L{}^2 + DZ_L}$$

where Z_L is the embedding characteristic impedance of the two-port.

The ABCD matrix of a section of transmission line of length l with a characteristic impedance Z and a propagation constant β is:

$$\begin{pmatrix} \cos\theta & jZ\sin\theta \\ \frac{j}{Z}\sin\theta & \cos\theta \end{pmatrix} \qquad (3.10)$$

where $\theta = \beta l$.

Using (3.10) in (3.9) for each mode we obtain the following expressions for the reflection and transmission coefficients:

$$\begin{aligned} \Gamma_e &= \frac{j\sin\theta_e\,(\frac{Z_e}{Z_L} - \frac{Z_L}{Z_e})}{DE} \\ \Gamma_o &= \frac{j\sin\theta_o\,(\frac{Z_o}{Z_L} - \frac{Z_L}{Z_o})}{DO} \end{aligned} \qquad (3.11)$$

$$T_e = \frac{2}{DE}$$
$$T_o = \frac{2}{DO}$$

where

$$DE = 2\cos\theta_e + j\sin\theta_e\,(\frac{Z_e}{Z_L} + \frac{Z_L}{Z_e})$$
$$DO = 2\cos\theta_o + j\sin\theta_o\,(\frac{Z_o}{Z_L} + \frac{Z_L}{Z_o})$$

Relations (3.11) and (3.8) can now be used to compute the emerging signals for a given set of even and odd parameters. They are all we need to undertake the design of directional couplers.

The even and odd parameters can be obtained theoretically for a specific physical implementation assuming the known field structure of each mode. The particular case of coupled finline slots will be studied in Chapter 4 using the spectral domain method. Prior to this though, directional couplers themselves will be investigated more deeply in the following section.

3.5 Application of Coupled Transmission Lines to Directional Couplers

3.5.1 Introduction

In order to gain a clear understanding of directional couplers, relations (3.11) and (3.8) will now be looked at under two realistic sets of assumptions for the various parameters. The first one results in contradirectional coupling, the second one in codirectional coupling. The respective frequency responses will then be compared emphasizing the relation between these two apparently very different behaviors. In an application environment, the task of the designer is to realize transmission lines satisfying the particular set of assumptions associated with the desired results.

3.5.2 Backward or Contradirectional Coupling

Using the solutions for the coupled lines obtained in Section 3.4 let us make the assumption that the phase velocities of the two modes are the same, that is:

$$\beta_e = \beta_o = \beta$$

Clearly, this can be obtained only for lines in a homogeneous dielectric medium. Furthermore let us assume that the impedance of the even and odd modes are related in the following way:

$$Z_e Z_o = {Z_L}^2$$

where Z_L is the load impedance.

Under these special conditions the reflection and transmission coefficients of the two-port (3.11) become

$$\Gamma_e = \frac{j \sin\theta \,(A - \frac{1}{A})}{D} \qquad (3.12)$$

$$\Gamma_o = \frac{j \sin\theta \,(\frac{1}{A} - A)}{D}$$

$$T_e = T_o = \frac{2}{D}$$

with

$$D = 2\cos\theta + j \sin\theta \,(A + \frac{1}{A})$$

$$A = \frac{Z_e}{Z_L} = \frac{Z_L}{Z_o}$$

$$\theta = \beta l.$$

Using these expressions to compute the wave emerging at each terminal of the four-port yields:

$$\begin{aligned} V_1 &= 0 \quad \text{for all frequencies} \\ V_2 &= j \frac{2\sin\theta}{D} (A - \frac{1}{A}) \end{aligned} \qquad (3.13)$$

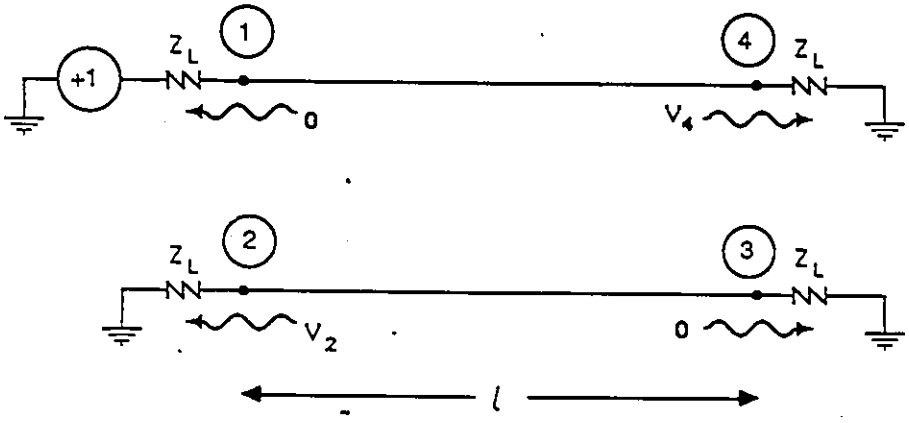

Figure 3.4: Backward coupling obtained with $\beta_e = \beta_o$ and $Z_L^2 = Z_e Z_o$

$$V_3 = 0 \quad \text{for all frequencies}$$
$$V_4 = \frac{4}{D}.$$

This reveals that, at all frequencies, the circuit presents a perfect match, that port 3 is perfectly isolated and that the power is divided between ports 2 and 4. As shown in Figure 3.4 contradirectional coupling is obtained. Equations (3.13) further reveal that

- The maximum coupling is obtained when $\theta = (2n+1)\frac{\pi}{2}$ or $l = (2n+1)\frac{\lambda}{4}$, where λ is the wavelength in the medium;
- V_2 is always in phase quadrature with V_4. The structure is consequently a 90-degree hybrid as defined in Chapter 2;
- Once $\theta = (2n+1)\frac{\pi}{2}$ has been fixed, the ratio $\frac{|V_2|}{|V_4|}$ depends only on the expression $\frac{1}{2}(A - \frac{1}{A})$ which is a function of Z_e and Z_o. To increase the coupling one has to increase A which makes it difficult to achieve tight coupling coefficients (> -3 dB) in practice.
- For -3 dB coupling, $\frac{|V_2|}{|V_4|} = 1$ implying that $A = 2.414$
- For -20 dB coupling, $\frac{|V_2|}{|V_4|} = \frac{0.1}{0.995}$ implying that $A = 1.105$

The assumptions leading to these results, the "design goals", can be well approximated with striplines and microstrips, and the hybrids obtained in this manner are very good. Numerous papers treat the design of this type of 90-degree hybrid, and sophisticated means of improving the bandwidth have been devised. Figure (3.7) in Section 3.5.4 shows the theoretical frequency response of these hybrids.

3.5.3 Forward or Codirectional Coupling

A second set of conditions imposed on the line characteristics can be the following:

$$\beta_e \neq \beta_o \quad \text{and} \quad Z_e \approx Z_o \approx Z_L$$

In this case, equations (3.11) reduce to:

$$\Gamma_e \approx 0 \qquad \Gamma_o \approx 0 \tag{3.14}$$

$$T_e \approx e^{-j\theta_e} \qquad T_o \approx e^{-j\theta_o}$$

and we get:

$$V_1 = V_2 = 0 \quad \text{for all frequencies} \tag{3.15}$$

$$V_3 = -2j\ e^{-j(\frac{\theta_e+\theta_o}{2})} \sin(\frac{\theta_e-\theta_o}{2})$$

$$V_4 = 2\ e^{-j(\frac{\theta_e+\theta_o}{2})} \cos(\frac{\theta_e-\theta_o}{2})$$

We now see in Figure 3.5 that while still displaying a perfect match and perfect isolation at all frequencies, the circuit now splits the power between ports 3 and 4 resulting in forward coupling. The following observations can be made:

- $\frac{V_3}{V_4} = -j\tan(\frac{\theta_e-\theta_o}{2})$. As long as $\beta_e \neq \beta_o$, any level of coupling can be achieved, including 0 dB, by varying l. The power simply transfers back and forth between the two lines as the length is increased;

- V_3 and V_4 are in quadrature, so that the coupler is a 90-degree hybrid;

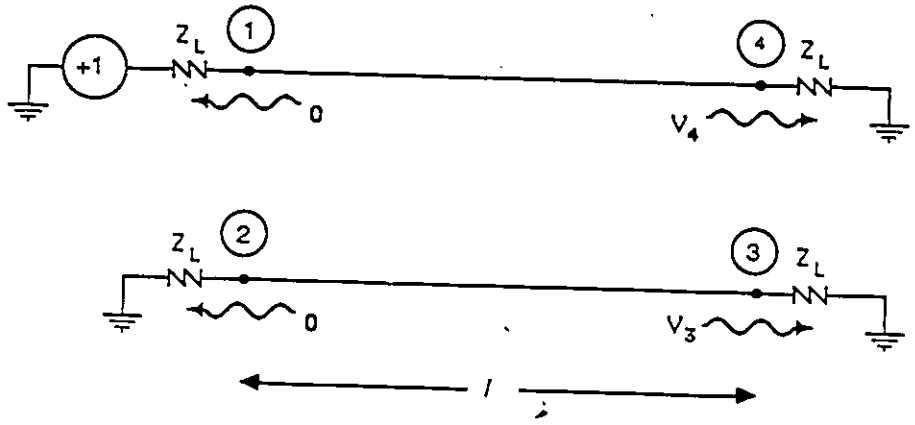

Figure 3.5: Forward coupling obtained with $\beta_e \neq \beta_o$ and $Z_e \approx Z_o \approx Z_L$

- 0 dB coupling is obtained when $(\frac{\theta_e - \theta_o}{2}) = \frac{\pi}{2}$ or when $l_0 = \frac{\lambda_0}{2(\sqrt{\epsilon_e} - \sqrt{\epsilon_o})}$, where λ_0 is the free space wavelength;

- -3 dB coupling is obtained when $(\frac{\theta_e - \theta_o}{2}) = \frac{\pi}{4}$ or when $l_3 = \frac{\lambda_0}{4(\sqrt{\epsilon_e} - \sqrt{\epsilon_o})}$.

This second set of assumptions can be well approximated with coupled finline slots. The hybrids discussed in Section 2.4 are all such realizations.

The frequency responses of the forward and the backward coupled line hybrids are compared in the following section and are seen to have very different behaviors.

3.5.4 Frequency Responses of Codirectional and Contradirectional Couplers

It has been shown in the previous section that under special sets of assumptions, coupled transmission lines were capable of producing codirectional or contradirectional coupling. The frequency responses of these circuits are very different. A number of theoretical responses have been calculated and are shown here to emphasize the relations between them. It will be shown how a backward coupler is transformed into a forward coupler when its line parameters depart from the ideal values.

The following plots show the amplitude of the voltage outputs for a unit excitation

at port 1, with respect to a normalized frequency (see Figure 3.6). These responses have been calculated with equations (3.8) and (3.11) for different values of even and odd parameters. The normalized frequency is defined as

$$\text{normalized frequency} = \frac{4l}{c} f \tag{3.16}$$

where c is the speed of light in vacuum and l is the length of the lines. From the definition of $\theta_{e,o}$ we obtain:

$$\theta_{e,o} = \beta_{e,o} l = \frac{2\pi l}{c} \sqrt{\epsilon_{e,o}}\, f = \frac{\pi}{2} \sqrt{\epsilon_{e,o}}\, \text{normalized frequency} \tag{3.17}$$

where the effective dielectric constant $\epsilon_{e,o}$ has been introduced to describe the propagation constant.

Figure 3.7 shows the response of an ideal -3 dB backward coupler as described in Section 3.5.2. It has been computed with $\epsilon_e = \epsilon_o = 1$ and $A = 2.414$. As expected, $V_1 = V_3 = 0$ for all frequencies, and the maximum coupling of 0.707 (-3 dB) occurs at $\theta = (2n+1)\frac{\pi}{2}$ (normalized frequency $= 2n+1$).

Figure 3.8 shows the same circuit when ϵ_e departs from its ideal value and becomes $\epsilon_e = 1.1$ instead. The response is fairly similar but as frequency (or length) increases, the levels of outputs 1 and 3 increases significantly, producing input mismatch and forward coupling.

If the non-ideality is further increased by choosing $\epsilon_e = 1.5$, a response similar to that of Figure 3.9 will be obtained. Clearly, the overall behavior is strongly affected and does not much resemble the original one. It is interesting to note that at a normalized frequency of 9, an equal power split between ports 3 and 2 is obtained, described as *side-coupling*.

Now let us redo the same progression starting this time with a -20 dB ideal backward coupler (Figure 3.10). In this case, $\epsilon_e = \epsilon_o = 1$ and $A = 1.105$, meaning that Z_e and Z_o

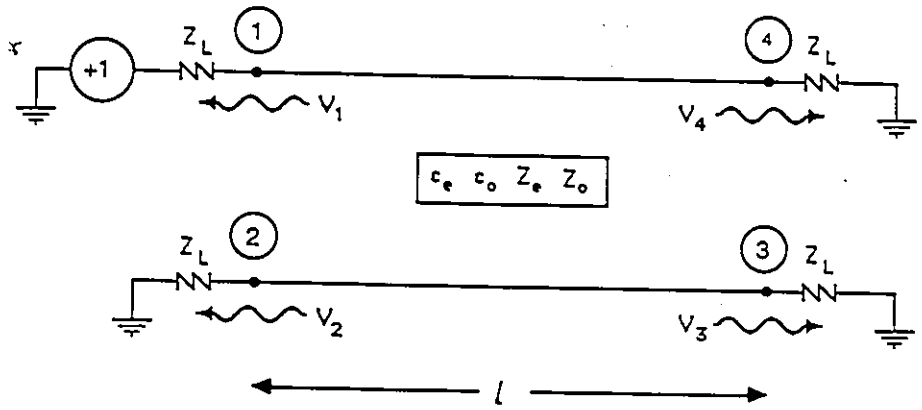

Figure 3.6: Coupler diagram showing the port numbering

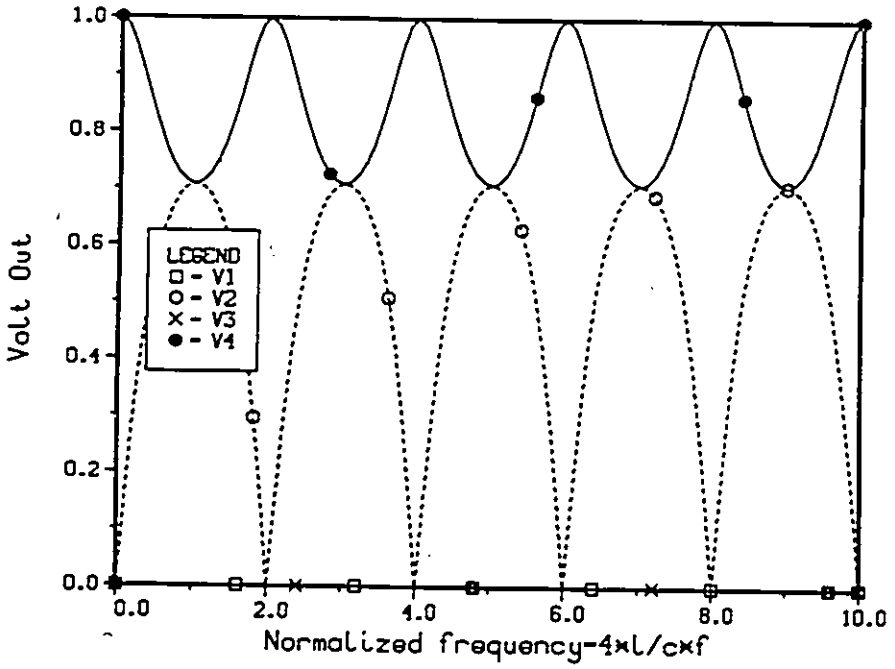

Figure 3.7: Frequency response of a coupler with $\epsilon_e = \epsilon_o = 1$, $Z_e = 2.414$, $Z_o = 1/2.414$ (-3 dB ideal backward coupler).

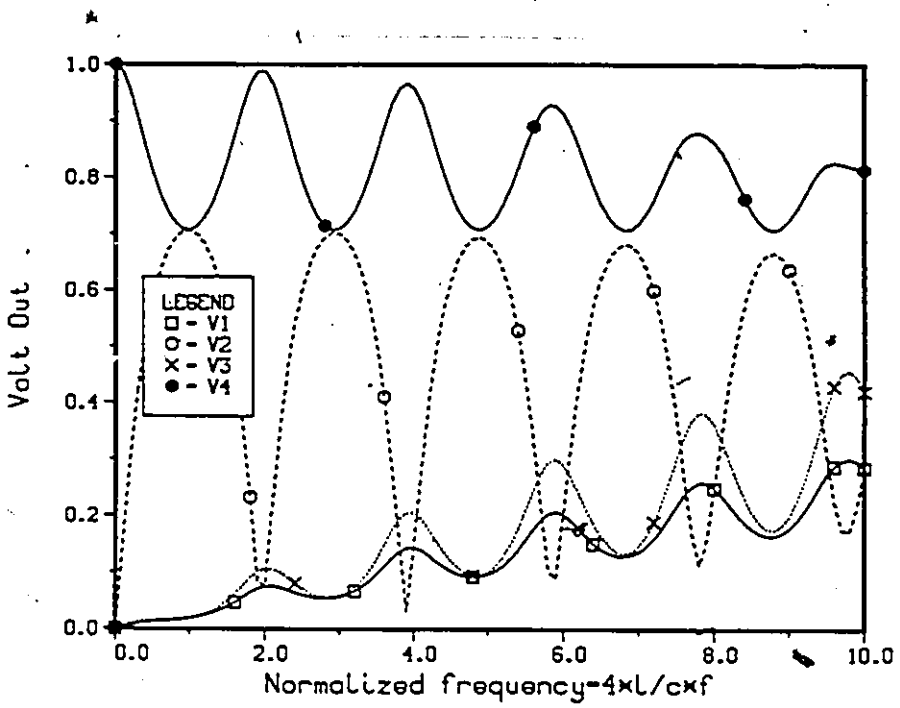

Figure 3.8: Frequency response of a coupler with $\epsilon_e = 1.1$, $\epsilon_o = 1$, $Z_e = 2.414$, $Z_o = 1/2.414$

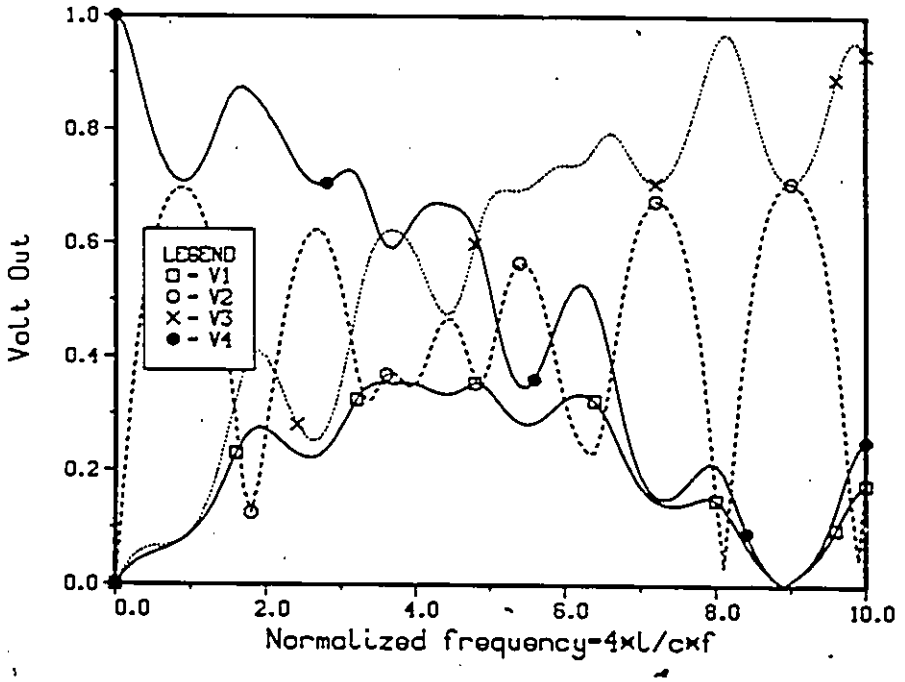

Figure 3.9: Frequency response of a coupler with $\epsilon_e = 1.5$, $\epsilon_o = 1$, $Z_e = 2.414$, $Z_o = 1/2.414$

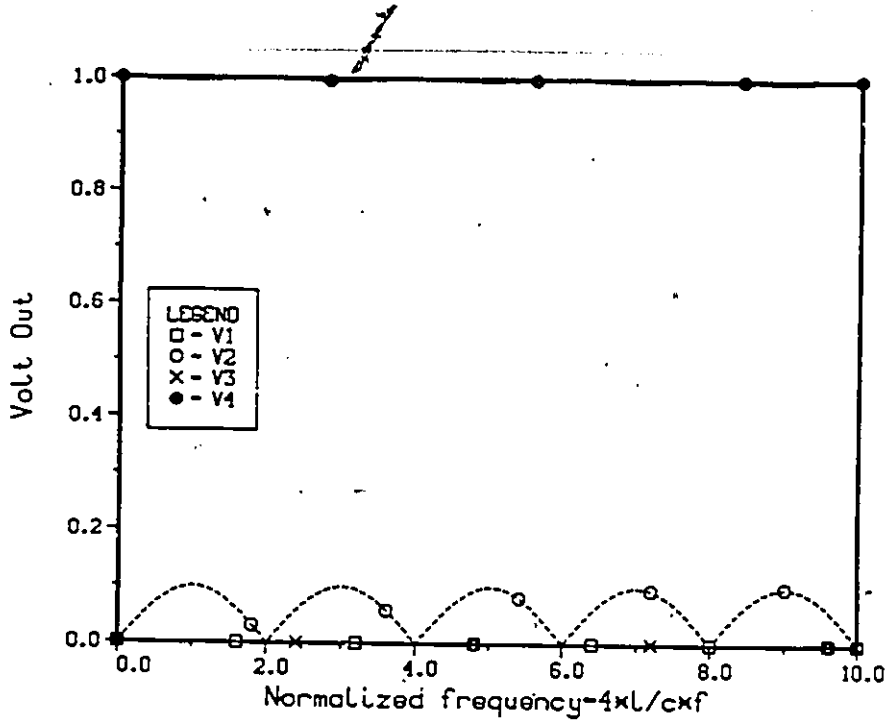

Figure 3.10: Frequency response of a coupler with $\epsilon_e = \epsilon_o = 1$, $Z_e = 1.105$, $Z_o = 1/1.105$ (-20 dB ideal backward coupler).

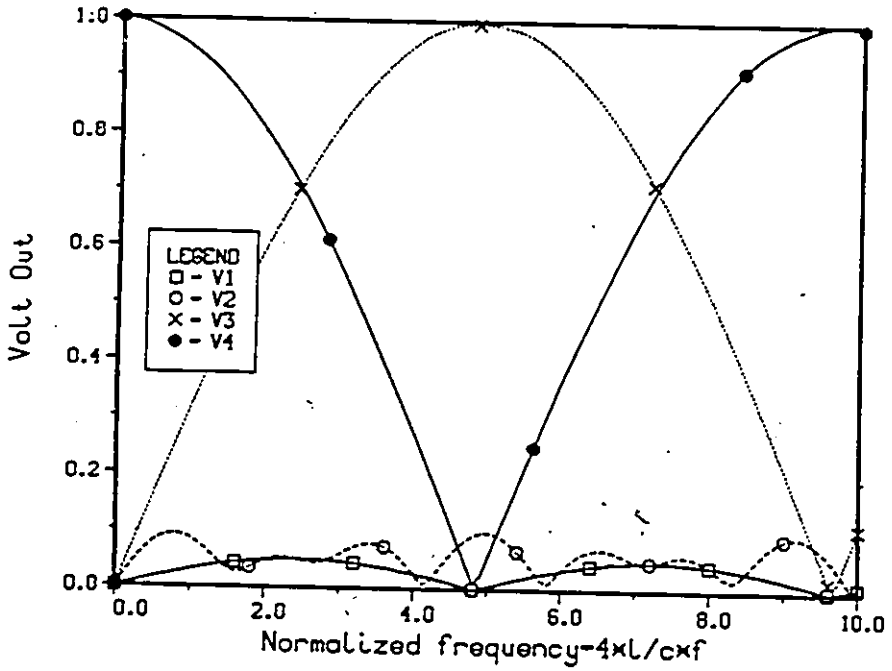

Figure 3.11: Frequency response of a coupler with $\epsilon_e = 2$, $\epsilon_o = 1$, $Z_e = 1.105$, $Z_o = 1/1.105$ (almost ideal forward coupler)

are getting closer to each other. Again, the maximum of coupling occurs at $\theta = (2n+1)\frac{\pi}{2}$, and $V_1 = V_3 = 0$ as expected.

If the value of ϵ_e is chosen so as to depart strongly from the ideal case, say $\epsilon_e = 2$, the response of Figure 3.11 results. The power oscillates back and forth periodically between outputs 4 and 3. An almost ideal forward coupler (as described in Section 3.5.3) is obtained, with equal power split (-3 dB coupling) at $\frac{\theta_e - \theta_o}{2} = \frac{\pi}{4}$ (normalized frequency ≈ 2.42) as expected.

The relationships existing between the behaviors of the forward and backward couplers are now clear from these figures. The forward coupler can be loosely defined as a non-ideal backward coupler with a weak coupling coefficient. The non-ideality refers to the even and odd modes having different values of propagation constants.

As mentioned earlier, forward couplers can be easily implemented in finline. They will be discussed in more detail later on where experimental frequency responses similar to these will be presented.

3.6 Conclusion

This chapter has presented the analysis of uniform coupled transmission line circuits. A very general approach was first introduced to explain the physical origin and the significance of the normal mode decomposition of the signal on coupled lines. It has been shown how a coupled line circuit is entirely described by the characteristics of its normal modes. These boil down to the even and odd modes when applied to symmetric lines. Symmetric lines have then been studied in detail, and hybrid couplers of two different types have been obtained under special assumptions for the line parameters: forward and backward couplers. Finally, the theoretical frequency responses for these circuits have been presented in a fashion that emphasizes their relationship.

This chapter has been included in this thesis to provide a clear explanation for the

operation of finline couplers. In Chapter 5, we will present a simulation procedure for these circuits but, prior to this, the determination of the even and odd mode parameters for coupled finline slots will be undertaken in the next chapter.

Bibliography

[1] V.K. Tripathi, "Asymmetric Coupled Transmission Lines in an Inhomogeneous Medium," *IEEE Trans. Microwave Theory Tech.*, vol. MTT-23, pp. 731-739, Sept. 1975.

[2] R.A. Speciale, "Fundamental Even- and Odd-Mode Waves For Non- Symmetrical Coupled Lines in Non-Homogeneous Media," in *1974 IEEE MTT-S Int. Microwave Symp. Digest*, pp. 156-158.

[3] J.E. Adair, G.I. Haddad, "Coupled-Mode Analysis of Non-Uniform Coupled Transmission Lines," *IEEE Trans. Microwave Theory Tech.*, vol. MTT-17, pp. 746-752, Oct. 1969.

[4] E. Cristal, "Coupled-Transmission-Line Directional Couplers with Coupled Lines of Unequal Characteristic Impedances," *IEEE Trans. Microwave Theory Tech.*, vol. MTT-14, pp. 337-346, July 1966.

[5] G.I. Zysman and A.K. Johnson, "Coupled Transmission Line Networks in an Inhomogeneous Dielectric Medium," *IEEE Trans. Microwave Theory Tech.*, vol. MTT-17, pp.753-759, Oct. 1969.

[6] E.M.T. Jones and J.T. Bolljahn, "Coupled-Strip-Transmission- Line Filters and Directional Couplers," *IRE Trans. Microwave Theory Tech.*, vol MTT-4, pp. 75-81, April 1956.

[7] J. Reed and G.J. Wheeler, "A Method of Analysis of Symmetrical Four-Port Networks," *IRE Trans. Microwave Theory Tech.*, vol. MTT-4, pp. 246-252, Oct. 1956. Corrections in IRE T-MTT, p. 162, April 1957.

Chapter 4

Spectral Domain Analysis of Coupled Finline Slots

4.1 Introduction

At this point, we are interested in the calculation of the even and odd mode parameters (propagation constants and characteristic impedances) for coupled slots in finline. As mentioned in Chapter 3, these parameters are sufficient to characterize coupled transmission line circuits. This calculation is fairly complex in the case of finlines due to the non-homogeneous nature of the dielectric medium, and it requires a numerical treatment. Accordingly, a computer program has been developed to deal with our specific structure.

The numerical method chosen here is called the Spectral Domain Approach, and it allows the analysis of a structure at a given frequency. One of the advantages of this approach is that it is numerically more efficient than the methods that work directly in the space domain. This is due primarily to the fact that the coupled integral equations obtained in the space domain (see Denlinger [1]) are transformed in the spectral domain into algebraic equations that are relatively easier to handle. The method also offers higher efficiency than other numerical methods at the price of an increased analytical work for the formulation of the problem.

The Spectral Domain Approach (SDA) was first explicitly described in these terms

by Itoh and Mittra [2] in 1973. However, its development has been an ongoing process since at least the 1960's. Many authors have reported applications of the SDA dealing with microstrip, slot line, finline and various other problems with or without losses. For finline problems, some important contributions are due to Mirshekar-Syakhal, Schmidt, Davies, Itoh and Hofmann [3,4,5]. The SDA is the object of a review paper by Jansen [6] which includes an extensive bibliography. It seems pointless here to repeat this general survey, and the interested readers should refer to that important contribution. Instead, our attention will focus on the description of the method itself and the problem of coupled finline slots.

Section 4.2 presents the application of the SDA to the unilateral finline problem. The expressions derived there remain general enough to be easily extended to other structures, but it is believed that the consideration of a specific example somewhat clarifies the presentation. The concepts common to all unilateral finline structures (single or multi-slots) will be presented.

Following this, Section 4.3 presents the application of the SDA to symmetric coupled finline slots. In the first subsection, the theoretical development and the computer implementation are discussed on the basis of the notions introduced in Section 4.2. The general expressions used in the computer program are given there. Because these expressions are not always directly applicable for programming (particularly those involving complex quantities) their final forms are given in Appendix A. The computer code itself (in Turbo-Pascal) and its algorithm are also included in Appendix A. Together, this whole chapter and that appendix constitute the reference document for the utilization of the program for coupled finline slots. Finally, in Subsection 4.3.2, the results of the computer calculations are compared to similar ones obtained from the literature, and the good agreement confirms the accuracy of our program.

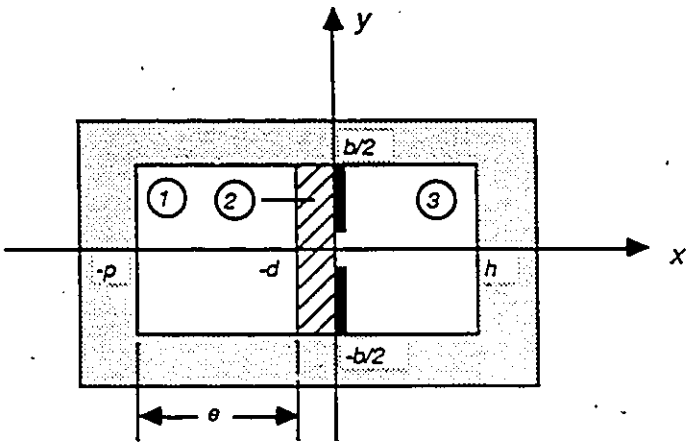

Figure 4.1: Cross-section of a unilateral finline structure

4.2 General SDA Formulation for Unilateral Finline Structures

Let us now present the SDA in a step by step fashion as applied to a general unilateral finline problem. As alluded to earlier, the technique is very flexible and the specialization described here is only one of the possible applications of the general approach. However it is felt that the consideration of a practical case helps clarify the presentation. For other types of application see, for instance, [3,7,8,9]. The global development has been divided into five logical steps, each describing a specific aspect of the method. Four of these, namely the transformation into the spectral domain, the application of the boundary conditions, Galerkin's procedure and the choice of the basis functions are fundamental to the SDA and lead to the evaluation of the propagation constant. The final step, the evaluation of the characteristic impedance, is in principle a straightforward process but it involves tedious derivations.

The cross-section of the structure considered here is shown in Figure 4.1. It consists of a dielectric board mounted across an empty perfectly conducting metallic enclosure. The structure is considered infinite and uniform in the z direction. One side of the substrate bears a metallic pattern that is here considered symmetric with respect to

the x axis[1]. The metallization is assumed lossless and of negligible thickness. The dimensions and the various regions of the cross-section are identified on the drawing.

Transformation into the Spectral Domain

The normal modes of propagation in a dielectric slab loaded waveguide (without metallization) are TE to x, or Longitudinal Section Electric (LSE) modes, and TM to x or LSM modes (see Collin [10, Chap. 6]). The basic modes may be derived respectively from a magnetic and an electric Hertz potential having a single component in the x direction. Each type of mode is a solution to the field problem when no metallic fins are present and, together, they form a complete set in terms of which an arbitrary field configuration can be decomposed. In our case, the fields inside the structure must be a superposition of the basic modes in order to fulfill the additional boundary conditions at $x = 0$.

In the SDA, the Hertz potentials and the field components derived therefrom are Fourier transformed with-respect to the y axis and all the computations are performed in the Fourier or spectral domain. If necessary the spatial field components can be recovered using the inverse Fourier transform. The Hertz potentials are therefore expressed as:

$$\Pi^e(x,y) = \Pi^e(x,y)\, e^{-j\beta z}\, \hat{\mathrm{a}}_x \qquad (4.1)$$
$$\Pi^h(x,y) = \Pi^h(x,y)\, e^{-j\beta z}\, \hat{\mathrm{a}}_x$$

with their Fourier transforms defined by:

$$\tilde{\Pi}^e(x,\alpha) = \int_{-\infty}^{+\infty} \Pi^e(x,y) e^{j\alpha y}\, dy \qquad (4.2)$$
$$\tilde{\Pi}^h(x,\alpha) = \int_{-\infty}^{+\infty} \Pi^h(x,y) e^{j\alpha y}\, dy.$$

[1] If one were to solve for unsymmetric slots, the x axis would be made to coincide with one of the broad guide walls.

Throughout this chapter, the quantities with a $\tilde{}$ will represent the spectral counterparts of the quantities without $\tilde{}$. Boldface symbols will indicate vectorial quantities and a $\hat{}$ will identify the unit vectors. A temporal dependence $e^{j\omega t}$ and a propagation in z according to $e^{-j\beta z}$ where β is the unknown propagation constant are assumed. Due to the limited extent of the structure in the y direction and considering the mirror effect of the electric walls at $y = -b/2$ and $+b/2$ that creates multiple images of the fields, the Fourier transforms become Fourier series whose coefficients are expressed by:

$$\tilde{\Pi}^e(x,n) = \frac{1}{2b}\int_{2b} \Pi^e(x,y)e^{j\alpha_n y}\,dy \qquad (4.3)$$
$$\tilde{\Pi}^h(x,n) = \frac{1}{2b}\int_{2b} \Pi^h(x,y)e^{j\alpha_n y}\,dy$$

with

$$\alpha_n = \frac{n2\pi}{2b} = \frac{n\pi}{b} \qquad n = 0, \pm 1, \pm 2, \ldots$$

and where n becomes the Fourier variable. A basic spatial period of $2b$ has been chosen here to maintain a formulation that can be directly applied to the coupled slot problem treated in the next section. Even though $2b$ is also valid, in principle, the basic period in this case should be b. The spectral field components can be derived from the potentials as follows:

LSE modes

$$\tilde{\mathbf{E}} = -j\omega\mu_0 \nabla \times \tilde{\mathbf{\Pi}}^h \qquad (4.4)$$
$$\tilde{\mathbf{H}} = \nabla \times \nabla \times \tilde{\mathbf{\Pi}}^h$$

LSM modes

$$\tilde{\mathbf{H}} = j\omega\epsilon_i \nabla \times \tilde{\mathbf{\Pi}}^e \qquad (4.5)$$
$$\tilde{\mathbf{E}} = \nabla \times \nabla \times \tilde{\mathbf{\Pi}}^e.$$

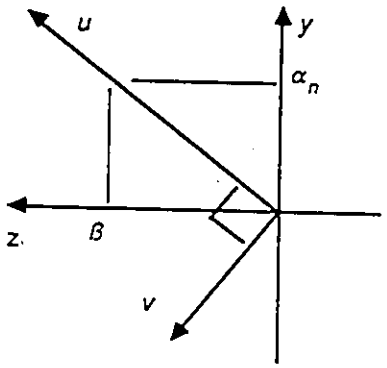

Figure 4.2: Alternative coordinate system x, u, v

At this point, solutions satisfying the boundary conditions could be assumed for the potentials, and one could apply the continuity conditions at $x = 0$ to eliminate the unknown coefficients. However Itoh [8] has proposed a method based on the transverse equivalent transmission line concept that achieves the same result with considerably less effort. It will be used here.

Application of the Continuity Condition at the Interface x = 0

Remembering that the fields propagate in the $+z$ direction we can express the spatial Hertz potentials as

$$\Pi^e(x,y)\,e^{-j\beta z} = \sum_{n=-\infty}^{\infty} \tilde{\Pi}^e(x,n)\,e^{-j(\alpha_n y+\beta z)} \qquad (4.6)$$

$$\Pi^h(x,y)\,e^{-j\beta z} = \sum_{n=-\infty}^{\infty} \tilde{\Pi}^h(x,n)\,e^{-j(\alpha_n y+\beta z)}.$$

These expressions can be interpreted as the summations of non-uniform plane waves propagating in the $(\alpha_n y + \beta z)$ direction. Taking this fact into account, a new system of coordinates is defined for each n whereby the u axis is the direction of propagation and axes v and x are normal to it as shown in Figure 4.2. We obtain:

$$\hat{\mathbf{a}}_u = N_y \hat{\mathbf{a}}_y + N_z \hat{\mathbf{a}}_z \qquad (4.7)$$

$$\hat{\mathbf{a}}_v = -N_z\hat{\mathbf{a}}_y + N_y\hat{\mathbf{a}}_z$$

with

$$N_y = \frac{\alpha_n}{\sqrt{\alpha_n^2+\beta^2}} \qquad (4.8)$$
$$N_z = \frac{\beta}{\sqrt{\alpha_n^2+\beta^2}}.$$

Rewriting the sum of the plane waves of (4.6) in the new coordinate system (x,u,v) we get:

$$\Pi^e(x,y)\,e^{-j\beta z} = \sum_{n=-\infty}^{\infty} \tilde{\Pi}^e(x,n)\,e^{-j\sqrt{\alpha_n^2+\beta^2}u} \qquad (4.9)$$
$$\Pi^h(x,y)\,e^{-j\beta z} = \sum_{n=-\infty}^{\infty} \tilde{\Pi}^h(x,n)\,e^{-j\sqrt{\alpha_n^2+\beta^2}u}.$$

The spectral potentials in the right-hand side depend only on u and x with $d/dv = 0$ and, furthermore, they have only an x component. Accordingly, for each value of n, the spectral electromagnetic fields (from (4.4) and (4.5)) propagating in the u direction are LSE waves with only three components $(\tilde{E}_v, \tilde{H}_x, \tilde{H}_u)$ and LSM waves with only three components $(\tilde{H}_v, \tilde{E}_x, \tilde{E}_u)$: in other words two *decoupled* normal modes[2]. Remembering the topology with its metallization in the $x = 0$ or u–v plane, we recognize that the boundary conditions at this point can be taken into account by introducing current densities $\tilde{J}_u$ and $\tilde{J}_v$, generating the LSM and LSE modes respectively. Using the transmission line analogy in the x direction we can draw an equivalent circuit for each mode as in Figure 4.3 where the subscripts $i = 1,2,3$ indicate the different regions of the structure. All the boundary conditions for the LSE and LSM waves are incorporated in these circuits. For instance, the electric walls at $x = h$ and $x = -p$ are represented by short circuits at these points. The continuity of the electric field and the discontinuity

[2]Let us recall here that the spatial LSE and LSM modes introduced earlier in this section both have 5 field components. They are coupled via the boundary conditions at $x = 0$. For instance, the z component of the current density on the metallization excites both types of modes by generating a y component of the magnetic field.

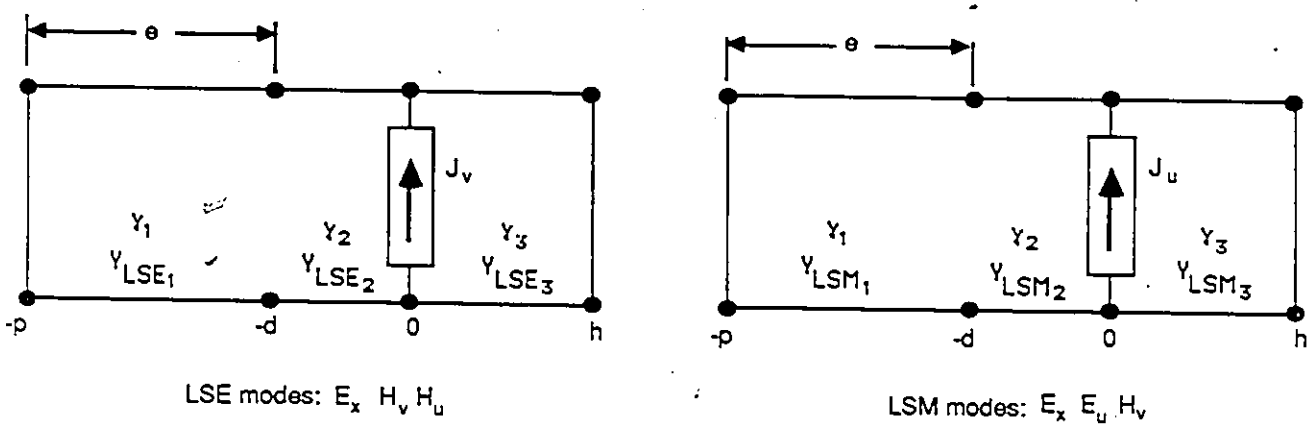

Figure 4.3: Equivalent transverse transmission line circuits for the LSE and LSM modes.

of the tangential magnetic field at $x = 0$ are expressed in terms of the transmission line analogy by

$$Y^e \tilde{E}_u(x=0,n) = \tilde{J}_u(0,n) \qquad (4.10)$$
$$Y^h \tilde{E}_v(0,n) = \tilde{J}_v(0,n)$$

where Y^e and Y^h are the driving point admittances at $x = 0$ in the LSM and LSE equivalent circuits. For unilateral finline Y^e is given by

$$Y^e = Y_{LSM_1} \coth(\gamma_1 h) + Y_{LSM_2} \left[\frac{Y_{LSM_1} \coth(\gamma_1 e) + Y_{LSM_2} \tanh(\gamma_2 d)}{Y_{LSM_2} + Y_{LSM_1} \coth(\gamma_1 e) \tanh(\gamma_2 d)} \right] \qquad (4.11)$$

and Y^h is obtained with the same formula by simply replacing the $_{LSM}$ by $_{LSE}$ subscripts. These formulae are functions of the geometry and of the transverse wave admittances of each region which are given by:

$$Y_{LSE_i} = -\frac{\widetilde{H}_{u_i}}{\widetilde{E}_{v_i}} = \frac{\gamma_i}{j\omega\mu} \qquad (4.12)$$
$$Y_{LSM_i} = \frac{\widetilde{H}_{v_i}}{\widetilde{E}_{u_i}} = \frac{j\omega\epsilon_i}{\gamma_i}$$

where a dependence of the type $e^{-\gamma_i z}$ has been assumed. The values of γ_i are obtained with Helmholtz equation and are expressed by

$$\gamma_i = (\alpha_n^2 + \beta^2 - \epsilon_{ri} k_0^2)^{1/2} \qquad (4.13)$$

or equivalently by

$$\gamma_i = (\alpha_n^2 + (\epsilon_{\text{eff}} - \epsilon_{ri})k_0^2)^{1/2} \tag{4.14}$$

where ϵ_{eff} is defined as

$$\epsilon_{\text{eff}} = \frac{\beta^2}{k_0^2}. \tag{4.15}$$

Equations (4.10) establish the relation between the unknown electric field and current density components at the interface $x = 0$. Returning to x, y, z coordinates with (4.7) and (4.8), (4.10) becomes[3]

$$\begin{pmatrix} Y_{11} & Y_{12} \\ Y_{21} & Y_{22} \end{pmatrix} \begin{pmatrix} \tilde{E}_y(0,n) \\ \tilde{E}_z(0,n) \end{pmatrix} = \begin{pmatrix} \tilde{J}_y(0,n) \\ \tilde{J}_z(0,n) \end{pmatrix} \tag{4.16}$$

where

$$\begin{aligned} Y_{11}(n) &= N_y^2 Y^e + N_z^2 Y^h \\ Y_{12}(n) = Y_{21}(n) &= N_y N_z (Y^e - Y^h) \\ Y_{21}(n) &= N_y^2 Y^h + N_z^2 Y^e. \end{aligned} \tag{4.17}$$

The method described here is applicable to problems with many dielectric layers and metallic surfaces, and the final system of equation (4.16) can practically be written down only by inspection of the physical structure.

Galerkin's procedure

To solve system (4.16) two of the four unknowns must be eliminated. To this end, let us first realize that at $x = 0$ (in the space domain) either the tangential electric field or the current density is 0 at every point on y. In other words, they are orthogonal functions and they satisfy

$$\frac{1}{b} \int_{-b/2}^{b/2} J(0,y) \cdot E(0,y)\, dy = 0. \tag{4.18}$$

[3]It is worth mentioning here that the coupling between the LSE and LSM modes is re-established by this axis rotation.

We will use this property to eliminate the J's in system (4.16).

Let us first expand the electric field components at $x = 0$ in terms of known orthogonal basis functions $\xi(y)$ and $\zeta(y)$ that vanish on the fin surfaces. We get

$$E_y(0,y) = \sum_{r=1}^{R} a_r \xi_r(y) \qquad (4.19)$$
$$E_z(0,y) = \sum_{s=1}^{S} b_s \zeta_s(y)$$

and in the spectral domain

$$\tilde{E}_y(0,n) = \sum_{r=1}^{R} a_r \tilde{\xi}_r(n) \qquad (4.20)$$
$$\tilde{E}_z(0,n) = \sum_{s=1}^{S} b_s \tilde{\zeta}_s(n)$$

where the a's and b's are the unknown amplitudes of the basis functions ξ and ζ respectively. R and S represent the total number of basis functions used to approximate the field components. Substituting (4.20) in (4.16) we obtain

$$\sum_{r=1}^{R} a_r Y_{11}(n)\tilde{\xi}_r(n) + \sum_{s=1}^{S} b_s Y_{12}(n)\tilde{\zeta}_s(n) = \tilde{J}_y(0,n) \qquad (4.21)$$
$$\sum_{r=1}^{R} a_r Y_{21}(n)\tilde{\xi}_r(n) + \sum_{s=1}^{S} b_s Y_{22}(n)\tilde{\zeta}_s(n) = \tilde{J}_z(0,n). \qquad (4.22)$$

Because the basis functions for the E fields have been chosen to vanish on the metallization, we can transform equation (4.18) and with Parseval's theorem obtain the following relationship:

$$\frac{1}{b}\int_{-b/2}^{b/2} J(0,y)\xi_r(y)\,dy = \sum_{n=-\infty}^{\infty} \tilde{J}(0,n)\tilde{\xi}_r^*(n) = 0. \qquad (4.23)$$

If we now multiply (4.21) by $\tilde{\xi}_{r'}^*(n)$, $r' = 1,\ldots,R$ and (4.22) by $\tilde{\zeta}_{s'}^*(n)$, $s' = 1,\ldots,S$ and sum up all the spectral terms from $n = -\infty$ to $n = +\infty$, we can eliminate the right hand side by virtue of (4.23). What remains is the following homogeneous system of

$(R+S)$ equations for the a's and b's,

$$\begin{pmatrix} \sum_{r=1}^{R} P_{r',r} & \sum_{s=1}^{S} Q_{r',s} \\ \sum_{r=1}^{R} R_{s',r} & \sum_{s=1}^{S} T_{s',s} \end{pmatrix} \begin{pmatrix} \vdots \\ a_r \\ \vdots \\ b_s \\ \vdots \end{pmatrix} = 0 \qquad \begin{matrix} r' = 1, \ldots, R \\ s' = 1, \ldots, S \end{matrix} \tag{4.24}$$

where

$$\begin{aligned} P_{r',r} &= \sum_{n=-\infty}^{\infty} Y_{11}(n) \tilde{\xi}_r(n) \, \tilde{\xi}^*_{r'}(n) \\ Q_{r',s} &= \sum_{n=-\infty}^{\infty} Y_{12}(n) \tilde{\zeta}_s(n) \, \tilde{\xi}^*_{r'}(n) \\ R_{s',r} &= \sum_{n=-\infty}^{\infty} Y_{21}(n) \tilde{\xi}_r(n) \, \tilde{\zeta}^*_{s'}(n) \\ T_{s',s} &= \sum_{n=-\infty}^{\infty} Y_{22}(n) \tilde{\zeta}_s(n) \, \tilde{\zeta}^*_{s'}(n). \end{aligned} \tag{4.25}$$

A non-trivial solution to (4.24) can be obtained by using an iteration scheme to find the value of the propagation constant β that sets the determinant of the matrix equal to zero. Calling this matrix the *eigenmatrix* we have:

$$\det[\text{eigenmatrix}] = 0 \tag{4.26}$$

Equation (4.26) will be referred to as the *characteristic equation* and the propagation constant of the dominant mode will be the highest value of β ($\epsilon_{\text{eff}} < \epsilon_r$) to satisfy this equation. The accuracy of the solution can be systematically improved by increasing the number of basis functions and solving a system of a larger order. Note here that the infinite summations in (4.25) can be truncated to a finite number depending upon the rate of decay of the integrand which in turn varies with the basis functions used.

Choice of the basis functions

For an efficient use of the SDA the choice of the basis functions for the electric field components is crucial. In order to keep the size of the final system as small as possible,

the first few terms of the field expansion should be chosen such as to approximate the unknown fields reasonably well. It is interesting to note that in some cases, quite accurate solutions for the propagation constant result even if only 2 or even 1 carefully chosen basis functions are used ($R = S = 1$ or $R = 1,\ S = 0$). This is so because certain attributes of the aperture field components, such as symmetry and edge conditions can be incorporated in the choice of the expansion functions. If one were interested in solving for many different modes in the structure, therefore for different field configurations, a more general set of basis functions would be necessary and R and S would have to be increased.

For finline problems, trains of rectangular pulses, constant functions, sinusoidal functions with an edge correction term, and Legendre polynomials are commonly used as basis functions. An efficient alternative also reported is the one-term expansion satisfying the edge conditions and the symmetry of the fields used in [4] by Schmidt and Itoh. This is the type of basis function that has been used in our case, and it is discussed in details in Subsection 4.3.1.

Characteristic impedance

The final step of the analysis is the evaluation of the impedance. Once the propagation constant in the structure has been found, the homogeneous system can be solved for the expansion coefficients a_r and b_s. Hence, by assuming suitable solutions for the potential vectors, and knowing the value of the electric field components at $x = 0$, one can deduce the expressions for all the fields in the structure. From these, one can calculate the impedance. For a finline slot the generally accepted definition of impedance is

$$\frac{V^2}{2P_{\text{slot}}} \tag{4.27}$$

where V is the slot voltage and P_{slot} is the total power transmitted by this slot. The former is directly calculated by the integration of E_y across the aperture (along the

shortest path),

$$V = -\int_{\text{slot}} E_y(x = 0, y)\, dy. \tag{4.28}$$

To get the transmitted power, the integral of the Poynting vector is performed over the cross-section of the structure:

$$P_{\text{tot}} = \frac{1}{2}\,\text{Re}\iint_{\text{c-sect}} S_z\, dx\, dy \tag{4.29}$$

where the z component of the Poynting vector is given by:

$$S_z = (E_x H_y^* - E_y H_x^*) \tag{4.30}$$

For a single finline, $P_{\text{tot}} = P_{\text{slot}}$. It is not a simple task to derive the expressions for the field components and in particular for the total transmitted power. These will be introduced in the next section which presents the details of the application of the spectral domain method.

4.3 Application to Symmetric Coupled Slots

Now that the general formulation of the SDA has been presented, we will proceed with a description of its application in the case of symmetric coupled slots.A Turbo-Pascal program called CPLFIN has been written for that purpose. For a given frequency and geometry it first calculates the propagation constant and the impedance for the even mode, then for the odd mode of propagation. To obtain the dispersion characteristic, the program must be run many times with different frequency values. Two basis functions ($R = S = 1$) are used to approximate the slot field components, and the accuracy of the results (compared with results in the literature obtained with four basis functions) seems sufficient for most applications.

This section describes our implementation of the SDA by presenting the important steps of the program and their main features. The progression follows that of the

previous section, and the same variable names have been used here. Besides, reference will often be made to the general formulation of Section 4.2. In an effort to facilitate comprehension of the code itself, we will also refer specifically to the procedure names used in the program, although it is not necessary to be familiar with it or even have a listing of it to follow the developments.

Many of the mathematical expressions originating in the SDA are fairly cumbersome and some of them require tedious derivations. In addition, because Turbo-Pascal does not support complex number arithmetic, most of the expressions obtained gracefully on paper could not be programmed directly. Accordingly, for the sake of completeness but to avoid overloading this chapter, some important derivations and the exact expressions used in the program have been included in Appendix A. The algorithm and the listing of the Turbo-Pascal code are also included. We avoided as much as possible the use of fancy tricks in the program in order to keep it as easy to read as possible. It is written simply with meaningful variable names, and the reader should not have too much difficulty finding his way through it. The program has not been optimized for speed but rather for simplicity with the idea in mind that accelerating features can always be included later.

4.3.1 Computer Program

The topology studied here is shown together with the dimensions in Figure 4.4. It is assumed that $\epsilon_3 = \epsilon_1$, and that $\mu_1 = \mu_2 = \mu_3 = \mu_0$. The field structures of the different modes are also shown. Eight major portions of the program are identified here with reference to the related procedures (Pascal subroutines). To have an idea of how each portion fits into the problem as a whole, it is essential to refer to Section 4.2.

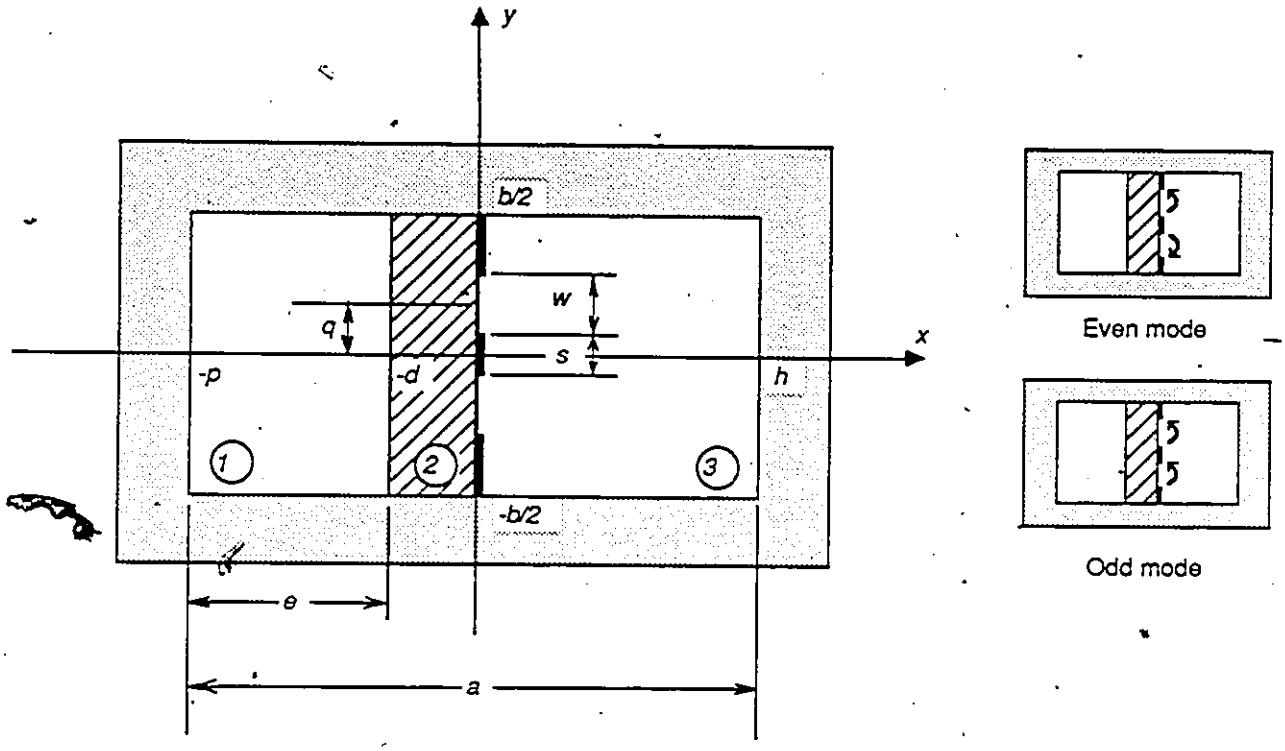

Figure 4.4: Cross-section of symmetric unilateral coupled slots and dimensions

The admittances (Procedure get_transv_adm(n, ϵ_{eff})**)**

The transverse admittances Y^e and Y^h are given by equation (4.11) in the previous section. They are valid for all unilateral finlines and therefore apply to both our even and odd mode analyses. The quantities γ_i that they contain can be either imaginary or real, leading to the various expressions for the admittance matrix (4.16) used in the program. The exact expressions are given in the appendix. They are identical for the even and odd modes of excitation. It can be easily shown that the elements of the matrix (4.17) satisfy the following relationship,

$$\begin{aligned} Y_{ij}(n) &= -Y_{ij}(-n) \quad \text{if} \quad i \neq j \\ &= Y_{ij}(-n) \quad \text{if} \quad i = j \\ & \qquad i, j = 1, 2 \end{aligned} \tag{4.31}$$

that will be used for the formulation of the characteristic equation.

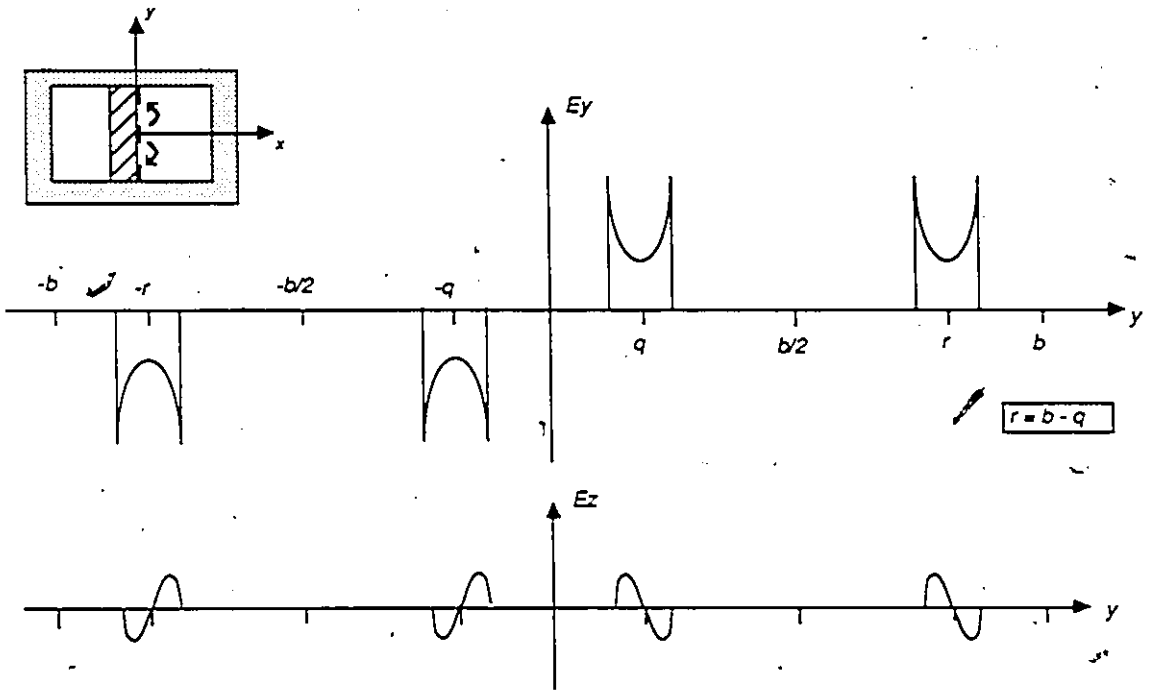

Figure 4.5: Expansion functions for the even mode excitation.

Basis-functions (Procedure get_basis_func(n))

The even and odd mode excitations represent two different cases calling for two different sets of basis functions. In each case, a one term expansion has been chosen to approximate both the y and z components of the E field.

Even mode Figure 4.5 shows the approximate field structures in the plane of the slots. At $x = 0$, E_y is odd symmetric along the y axis with respect to the $y = 0$ plane. A function $g(y)$, known to represent fairly well the distribution of E_y across *one* slot (of width w centered at $y = 0$), is given in [4,11] and has been used here. Its spatial and spectral expressions are:

$$g(y) = \frac{1}{\sqrt{1 - \left(\frac{2y}{w}\right)^2}} \qquad \overset{\mathcal{F}}{\Rightarrow} \qquad \tilde{g}(n) = \frac{\pi w}{4b} J_0\left(\frac{\alpha_n w}{2}\right) \qquad \alpha_n = \frac{n\pi}{b}. \tag{4.32}$$

Using these expressions for each aperture in our structure (centered at $y = -r, -q, q, r$) we finally obtain the following form for the spectral basis function of E_y:

$$\tilde{\xi}(n) = j[\sin(\alpha_n q) + \sin(\alpha_n r)]\, J_0\left(\frac{\alpha_n w}{2}\right) \qquad \alpha_n = \frac{n\pi}{b} \tag{4.33}$$

$$\tilde{\xi}(0) = 0$$

$$\tilde{\xi}(n) = -\tilde{\xi}(-n)$$

$$\tilde{\xi}(n) \neq 0 \qquad \text{for } n \text{ odd only}^4$$

where the constant factors have been left out because the basis functions are weighted by the SDA anyway. At $x = 0$, E_z is even symmetric along the y axis with respect to the $y = 0$ plane (Figure 4.5). A function $h(y)$ approximating E_z across one aperture of width w can also be found in [4,11]. Its spatial and spectral forms are:

$$h(y) = \frac{2y}{w}\sqrt{1 - \left(\frac{2y}{w}\right)^2} \quad \overset{\mathcal{F}}{\Rightarrow} \quad \tilde{h}(n) = -j\frac{\pi}{2\alpha_n b} J_2\left(\frac{\alpha_n w}{2}\right) \qquad \alpha_n = \frac{n\pi}{b} \tag{4.34}$$

From these, the expression of the spectral basis function for E_z in our problem is easily obtained as:

$$\tilde{\zeta}(n) = \frac{1}{\alpha_n}[\sin(\alpha_n q) + \sin(\alpha_n r)]\, J_2\left(\frac{\alpha_n w}{2}\right) \qquad \alpha_n = \frac{n\pi}{b} \tag{4.35}$$

$$\tilde{\zeta}(0) = 0$$

$$\tilde{\zeta}(n) = \tilde{\zeta}(-n)$$

$$\tilde{\zeta}(n) \neq 0 \qquad \text{for } n \text{ odd only}$$

Odd mode Please refer to Figure 4.6. The basis functions for the y and z components are similar to those used for the even mode above. We obtain:

$$\tilde{\xi}(n) = [\cos(\alpha_n q) + \cos(\alpha_n r)]\, J_0\left(\frac{\alpha_n w}{2}\right) \qquad \alpha_n = \frac{n\pi}{b} \tag{4.36}$$

$$\tilde{\xi}(0) = 2$$

[4] In the program the calculations are made for all values of n. The execution time could be reduced by almost 50% if this property were to be taken into account.

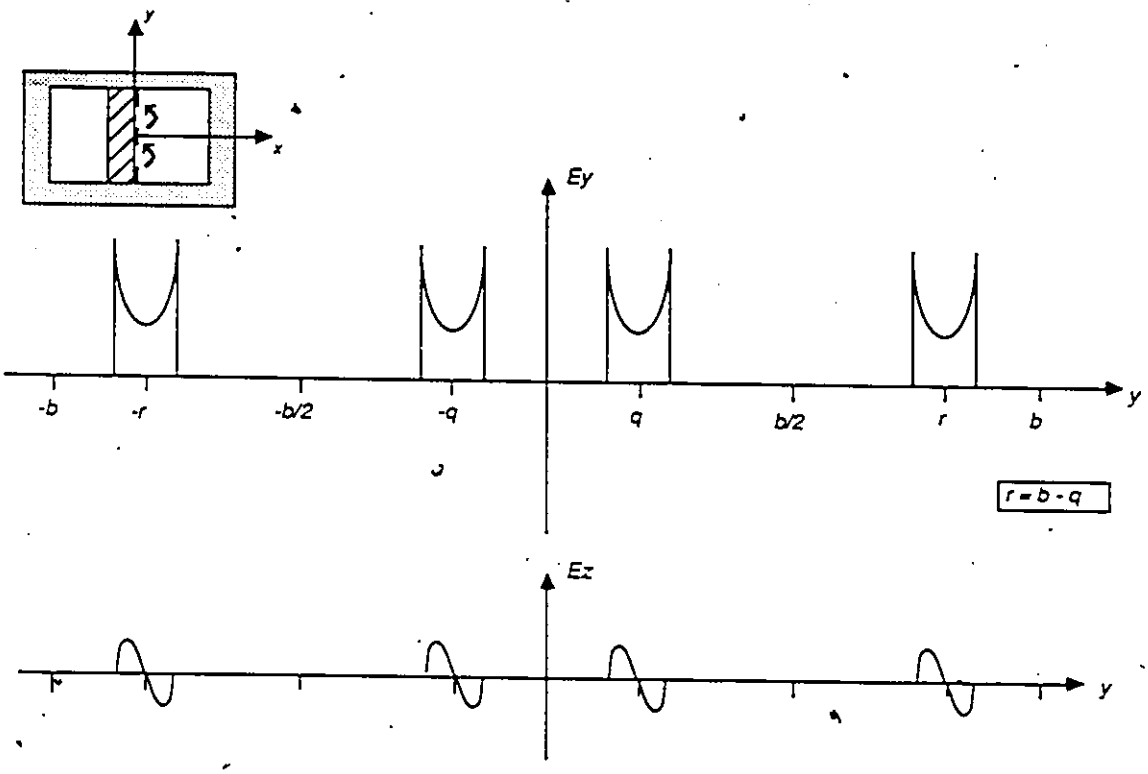

Figure 4.6: Expansion functions for the odd mode excitation.

$$\tilde{\xi}(n) = \tilde{\xi}(-n)$$

$$\tilde{\xi}(n) \neq 0 \qquad \text{for } n \text{ even only}^4$$

and

$$\tilde{\zeta}(n) = \frac{j}{\alpha_n}[\cos(\alpha_n q) + \cos(\alpha_n r)]\, J_2\left(\frac{\alpha_n w}{2}\right) \qquad \alpha_n = \frac{n\pi}{b} \tag{4.37}$$

$$\tilde{\zeta}(0) = 0$$

$$\tilde{\zeta}(n) = -\tilde{\zeta}(-n)$$

$$\tilde{\zeta}(n) \neq 0 \qquad \text{for } n \text{ even only}$$

Note here that for programming simplicity, the definition for α_n in the even mode has been maintained for the odd mode as well, even though the basic spatial period in the second case is b and not $2b$. In the program, when the basis functions are modified the procedure **get_voltage** (which calculates the integral of the basis function across one

slot) must be modified accordingly.

Characteristic equation (Procedure char_eq(ϵ_{eff}))

The characteristic equation (4.26) must be solved to obtain the propagation constant[5]. In our case, the eigenmatrix (4.24) is simplified for two basis functions and manipulated to a form adequate for programming. First, the infinite summations of equation (4.25) are modified to semi-infinite ones from $n = 0$ to ∞ by consideration of the symmetry of the integrands (equations (4.31), (4.33), (4.35), (4.36),(4.37)).

Next, one must realize that when $\tilde{\xi}(n)$ is real, $\tilde{\zeta}(n)$ is imaginary and vice versa. This entails that the $(1,2)$ and the $(2,1)$ terms in the eigenmatrix can be considered as real without affecting the value of its determinant.

Finally, since only the roots of the determinant are of interest, the constant multipliers can be dropped. A simplified matrix is obtained which, as far as the characteristic equation (4.26) is concerned, is *equivalent* to the one in equation (4.24). It is expressed by

$$\text{eigen matrix} = \begin{pmatrix} \sum_{n=1}^{\infty} Y_{11}(n)\ |\tilde{\xi}(n)|^2 & \sum_{n=1}^{\infty} Y_{12}(n)\{\tilde{\xi}(n)\}\{\tilde{\zeta}(n)\} \\ \sum_{n=1}^{\infty} Y_{21}(n)\{\tilde{\xi}(n)\}\{\tilde{\zeta}(n)\} & \sum_{n=1}^{\infty} Y_{22}(n)\ |\tilde{\zeta}(n)|^2 \end{pmatrix} \tag{4.38}$$

for the even mode and by

$$\text{eigen matrix} = \begin{pmatrix} \frac{1}{2}Y_{11}(0)\ |\tilde{\xi}(0)|^2 + \sum_{n=1}^{\infty} Y_{11}(n)\ |\tilde{\xi}(n)|^2 & \sum_{n=1}^{\infty} Y_{12}(n)\{\tilde{\xi}(n)\}\{\tilde{\zeta}(n)\} \\ \sum_{n=1}^{\infty} Y_{21}(n)\{\tilde{\xi}(n)\}\{\tilde{\zeta}(n)\} & \sum_{n=1}^{\infty} Y_{22}(n)\ |\tilde{\zeta}(n)|^2 \end{pmatrix} \tag{4.39}$$

for the odd mode. The $\{\}$ indicate that the quantity enclosed is to be considered real (that is, if it is imaginary the j must be dropped). Consequently the characteristic

[5]Actually, in CPLFIN the procedure char_eq computes det[eigenmatrix] and the procedure get_eps_eff finds the root of char_eq.

equation is a purely real equation and can directly be programmed in Turbo-Pascal. Practically the infinite summations of the eigen matrix are truncated after **nterms_eps** terms as chosen by the user. More will be said later about the summation boundaries.

Root finding algorithm (Procedure get_eps_eff)

First of all, let us mention that CPLFIN solves the system for ϵ_{eff} (see Equation (4.15)) instead of the propagation constant β because as a numerical value it is more informative. The root-finding procedure starts with an initial guess for the value of ϵ_{eff}. From this guess, a low and a high value for ϵ are derived (simple multiplication factors) until a root of **char_eq** is enclosed between them (seek a change of sign of the characteristic equation). Then the **regula falsi** algorithm is used to rapidly converge towards the root. The convergence criterion is set by the procedure **conv_criterion**. As it is now, the calculated root (ϵ_{eff}) will differ from the real root by at most an absolute quantity of 0.0005. The initial estimates for ϵ_{eff} are the parameters **eps_even_guess** and **eps_odd_guess** and they are specified by the user. Generally one has a fairly good idea of the value of ϵ_{eff}, enough so to be able to give an initial estimate. If this is not the case, in this type of algorithm, a relatively high value should be specified to make sure to get the highest root. See the computer code for more details.

The previous sections constitute the algorithm for the calculation of the propagation constant. The next ones are necessary to compute the impedance.

Solution for the expansion coefficients (Procedure get_basis_func_ratio)

In order to calculate the impedance, in addition to the propagation constant, it is necessary to know the expansion coefficients a and b, the unknowns of the system (4.24). Actually the ratio a/b is all we can calculate, and it is obtained as the ratio of two elements on a same row of the eigenmatrix. Usually the eigenmatrix itself requires

a larger number of spectral terms to converge than it is necessary for the root of its determinant to converge. In other words, the eigenmatrix calculated with **nterms_eps** spectral terms for the evaluation of ϵ_{eff} is not a converging value, so to speak. In principle, in order to get a realistic value, one has to add more terms to the summations of the eigenmatrix prior to the solution of a/b. The procedure **get_basis_func_ratio** does just that and it adds terms up to **nterms_ratio** as specified by the user. The quantity a/b is called the **basis_func_ratio**.

Calculation of voltage (Procedure get_voltage)

With the type of basis function used, the voltage integral (4.28) can be calculated analytically. It is important here to include a multiplicative term to take into account the relative amplitude of the basis functions, **basis_func_ratio** obtained as a solution for system (4.24).

Calculation of Power (Procedure get_total_power)

Because of the symmetry of the problem considered here, the power associated with each slot is half the total power,

$$P_{\text{slot}} = \frac{P_{\text{tot}}}{2} \tag{4.40}$$

In order to evaluate equation (4.29) for the total power transmitted in the structure, we must first find the expressions for the field components. To this end, appropriate solutions for the potentials in equation (4.6) are assumed. For LSE modes we have:

$$\tilde{\Pi}_i^h(x,n) = \Phi_i Ch_i(x) + \Theta_i Sh_i(x) \tag{4.41}$$

and for LSM modes

$$\tilde{\Pi}_i^e(x,n) = \Upsilon_i Ch_i(x) + \Gamma_i Sh_i(x) \tag{4.42}$$

where $i = 1,2,3$ refers to the various regions of the cross-section. For compactness we use:

$$\begin{aligned} Ch_1(x) &= \cosh\gamma_1(x+p); \quad Sh_1(x) = \sinh\gamma_1(x+p) \\ Ch_2(x) &= \cosh\gamma_2(x+d); \quad Sh_2(x) = \sinh\gamma_2(x+d) \\ Ch_3(x) &= \cosh\gamma_3(x-h); \quad Sh_3(x) = \sinh\gamma_3(x-h). \end{aligned} \tag{4.43}$$

where the γ_i's come from (4.14). By assuming that each spectral component fulfills the boundary conditions at $x = -p, -d$ and $-h$, and by applying the continuity conditions at $x = 0$ (in terms of the basis functions) to the superposition of the two modes[6] we eventually get:

LSE modes

$$\begin{aligned} \tilde{\Pi}_1^h &= \Theta_1 Sh_1(x); \\ \tilde{\Pi}_2^h &= \Theta_1[Sh_{1d}\, Ch_2(x) + \gamma_{12} Ch_{1d}\, Sh_2(x)]; \\ \tilde{\Pi}_3^h &= \Theta_3 Sh_3(x). \end{aligned} \tag{4.44}$$

with

$$\begin{aligned} \Theta_1 &= \frac{1}{\Delta\rho G_1}\left[\frac{\alpha_n}{\beta}\tilde{\zeta}(n) - r\tilde{\xi}(n)\right] \\ \Theta_3 &= \frac{1}{\Delta\rho Sh_{30}}\left[\frac{\alpha_n}{\beta}\tilde{\zeta}(n) - r\tilde{\xi}(n)\right] \\ r &= \text{ratio of expansion coefficients } a/b \end{aligned} \tag{4.45}$$

LSM modes

$$\begin{aligned} \tilde{\Pi}_1^e &= j\Upsilon_1 Ch_1(x); \\ \tilde{\Pi}_2^e &= j\Upsilon_1[\epsilon_{12} Ch_{1d}\, Ch_2(x) + \gamma_{12} Sh_{1d}\, Sh_2(x)]; \\ \tilde{\Pi}_3^e &= j\Upsilon_3 Ch_3(x). \end{aligned} \tag{4.46}$$

with

$$\begin{aligned} \Upsilon_1 &= -\left(\frac{\rho\alpha_n G_{12}}{\gamma_2}\Theta_1 - \frac{1}{\beta\gamma_2 G_2}\tilde{\zeta}(n)\right) \\ \Upsilon_3 &= -\left(\frac{\rho\alpha_n}{\gamma_3}\Theta_3 - \frac{1}{\beta\gamma_3 Sh_{30}}\tilde{\zeta}(n)\right). \end{aligned} \tag{4.47}$$

[6]For a discussion on the coupling of the LSE and LSM modes see [12].

The auxiliary quantities used in these expressions are defined as

$$\begin{array}{ll} Sh_{1d} = Sh_1(-d) & \gamma_{12} = \gamma_1/\gamma_2 \\ Ch_{1d} = Ch_1(-d) & \epsilon_{12} = \epsilon_1/\epsilon_2 \\ Sh_{30} = Sh_3(0) & G_{12} = G_1/G_2 \\ \Delta = \alpha_n^2 + \beta^2 & G_1 = Sh_{1d}\, Ch_2(0) + \gamma_{12} Ch_{1d}\, Sh_2(0) \\ \rho = \omega\mu_0/\beta = \eta_0/\sqrt{\epsilon_{eff}} & G_2 = \epsilon_{12} Ch_{1d}\, Sh_2(0) + \gamma_{12} Sh_{1d}\, Ch_2(0) \end{array} \tag{4.48}$$

Next, using equation (4.6) and the spatial counterparts of (4.4) and (4.5), the spatial field components in the guide ($E_{x,y,z}$ and $H_{x,y,z}$) can be obtained as a sum of the contributions from each mode.

Following this, the z component of the Poynting vectors (4.30) are calculated. These terms involve the product of two infinite summations as in, for instance,

$$\begin{aligned} E_{xi}H_{yi}^* &= \sum_{n=-\infty}^{\infty} \tilde{E}_{xi}(x,n) e^{-j(\alpha_n y + \beta z)} \sum_{m=-\infty}^{\infty} \widetilde{H}_{yi}^*(x,m) e^{j\alpha_m y + \beta z} \\ &= \sum_{n=-\infty}^{\infty} \sum_{m=-\infty}^{\infty} \tilde{E}_{xi}(x,n) \widetilde{H}_{yi}^*(x,m) e^{j(\alpha_m - \alpha_n)y}. \end{aligned} \tag{4.49}$$

In order to calculate the power, these expressions must be integrated over y from $y = -b/2$ to $y = b/2$. From the orthogonality of the exponential factors *and* considering that the spectral terms always vanish either for n odd or for n even (see equations for basis functions), the field products can be replaced by

$$E_{xi}H_{yi}^* \Rightarrow \sum_{n=-\infty}^{\infty} \tilde{E}_{xi}(x,n) \widetilde{H}_{yi}^*(x,n). \tag{4.50}$$

This expression is not an equality but, as far as the evaluation of the total power is concerned, it is an *equivalence*. For the total power in the guide we finally get:

$$P_{tot} = \frac{1}{2} \mathrm{Re} \int_{-b/2}^{b/2} \left[\int_{-p}^{-d} S_{z1} dx + \int_{-d}^{0} S_{z2} dx + \int_{0}^{h} S_{z3} dx \right] dy \tag{4.51}$$

which is transformed via (4.50) and (4.30) to

$$P_{tot} = \frac{b}{2} \mathrm{Re} \sum_{n=-\infty}^{\infty} \int_{-p}^{-d} \left(\tilde{E}_{x1}(n) \widetilde{H}_{y1}^*(n) - \tilde{E}_{y1}(n) \widetilde{H}_{x1}^*(n) \right) dx + \tag{4.52}$$

$$\int_{-d}^{0} \left(\tilde{E}_{x2}(n)\widetilde{H}^{*}_{y2}(n) - \tilde{E}_{y2}(n)\widetilde{H}^{*}_{x2}(n) \right) dx +$$
$$\int_{0}^{h} \left(\tilde{E}_{x3}(n)\widetilde{H}^{*}_{y3}(n) - \tilde{E}_{y3}(n)\widetilde{H}^{*}_{x3}(n) \right) dx$$

As for the eigenmatrix, the infinite summations in (4.52) can be simplified to a semi-infinite one for reasons of symmetry. Practically, the program truncates it at **nterms_z** terms, chosen by the user.

Needless to say that the final expression for the total power is quite cumbersome. Furthermore, because the programming language did not support complex numbers, modifications to the expressions had to be incorporated for each possibility of γ_i real or imaginary. The exact expressions for the program are given in the appendix.

Limits of the summations, number of spectral terms

There are three different parameters for the limits of summations that must be supplied by the user: **nterms_eps**,**nterms_ratio**, and **nterms_z**. The first one is used to truncate the summations in eigenmatrix for the calculation of ϵ_{eff} (equation (4.38) and (4.39)). **nterms_ratio** $\geq$ **nterms_eps**, is used to find a converging value for eigenmatrix in the calculation of **basis_func_ratio**. Finally, **nterms_z** is used to truncate the power summation in (4.52). Generally, **nterms_z** must be larger than **nterms_eps** for converging values of impedance. For most applications we tried, stable results were obtained with values in the following ranges:

$$50 \leq \text{nterms\_eps} \leq 500$$
$$\text{nterms\_ratio} \approx 1.5\ \text{nterms\_eps}$$
$$\text{nterms\_z} \approx \text{nterms\_ratio}.$$

This completes the description of the program. The input-output operations will not be discussed here for they are fairly self-explanatory. It is hard to give a number to describe the numerical efficiency of the program. With a reasonable initial guess for ϵ_{eff} (let us say within 20% of its real value), a 200 spectral term computation of ϵ_{eff} and

Z for one mode of propagation takes less than 2 minutes time for each frequency point on an XT-compatible computer with an 8087 coprocessor and an 8 MHz clock. This compares very well with the finite-element method algorithm used at this time in this department that would require at least half an hour to obtain a similar result. There is no doubt that the program can be improved by, for instance, including accelerating features or by using more basis functions. However, as will be seen in the next section, the accuracy achieved by this program is satisfactory for most applications.

4.3.2 Numerical Results

The results of our program have been checked against those obtained with the same method in [5] and [13]. In the first case, 2 edge-corrected sinusoidal functions have been used to approximate each of the field components in the slots. In [13], four of these basis functions were used. Results for a wide range of slotwidths and waveguide sizes were calculated and, in all cases, the values for epsilon effective in both modes of propagation agree very well with the published data. Regarding the impedances, the agreement is also very good with, in the worst case, our results being larger than the published ones by less than 10%. This proves that for most practical cases, the basis functions used here seem to give a sufficient accuracy.

Figure 4.7 compares the present results with some of the values published in [5]. The dimensions of the structure considered are given in the caption of the figure. The curves show the even and odd mode characteristics of the slots for values of s varying between 0 and 3.2 mm at a frequency of 33 GHz. The agreement obtained is typical of all the comparisons performed.

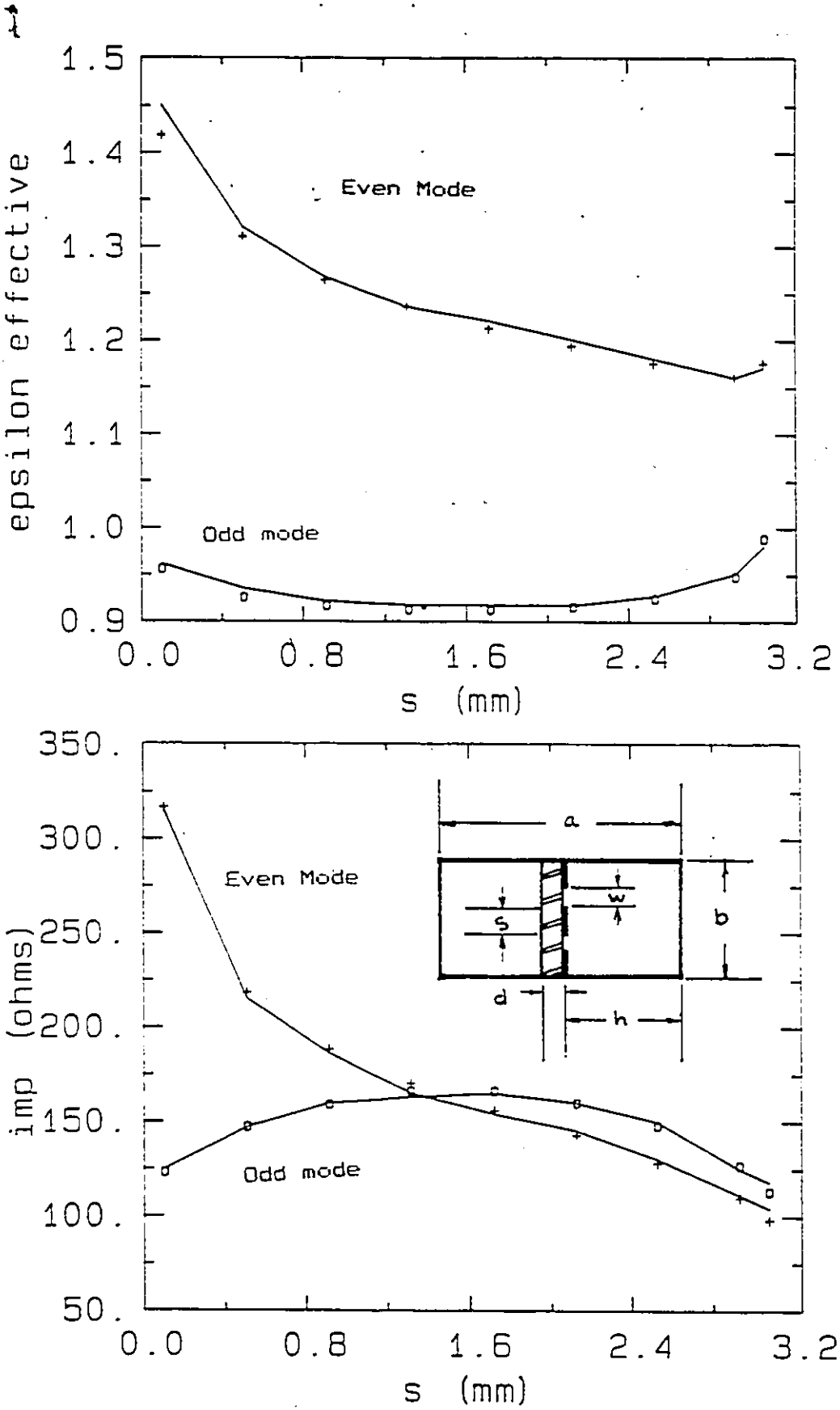

Figure 4.7: This program's results (discrete points) and values from [5] (continuous lines). In mm, $a = 7.112$, $b = 3.556$, $h = 3.494$, $w = 0.25$, $d = 0.125$, $\epsilon_r = 2.2$, $f = 33$ GHz.

4.4 Conclusion

A Turbo-Pascal program, CPLFIN, has been developed to compute the even and odd mode characteristics of coupled finline slots. It uses the Spectral Domain Approach with two basis functions to approximate the slot field's components. The analytical formulation of the analysis has been presented in this section. In addition, much emphasis has been put on a detailed description of the program's main features. It is hoped that this will help future workers trying to improve this program. Besides, a complete listing has also been included in appendix for reference. The results of the program have been checked against similar ones published in the literature, and their accuracy is very good.

In the following section, the computer program developed here will be used in the simulation of finline hybrid couplers.

Bibliography

[1] E.J. Denlinger, "A Frequency Dependent Solution for Microstrip Transmission Lines", *IEEE Trans. Microwave Theory Tech.*, vol. MTT-19, pp. 30-39, Jan. 1971.

[2] T. Itoh, R. Mittra, "Spectral-Domain Approach for Calculating the Dispersion Characteristics of Microstrip Lines," *IEEE Trans. Microwave Theory Tech.*, vol. MTT-21, pp. 496-499, July 1973.

[3] D. Mirshekar-Syakhal, J.B. Davies, "An Accurate Unified Solution to Various Fin-Line Structures, of Phase Constant, Characteristic Impedance, and Attenuation," *IEEE Trans. Microwave Theory Tech.*, vol. Mtt-30, pp. 1854-1861, 1982.

[4] L.P. Schmidt, T. Itoh, "Spectral Domain Analysis of Dominant and Higher Order Modes in Fin-Lines," *IEEE Trans. Microwave Theory Tech.*, vol. MTT-28, pp. 981-985, Sept. 1980.

[5] L.P. Schmidt, T. Itoh, H. Hofmann, "Characteristics of Unilateral Fin-Line Structures with Arbitrarily Located Slots," *IEEE Trans. Microwave Theory Tech.*, vol. MTT-29, pp. 352-357, April 1981.

[6] R.H. Jansen, "The Spectral-Domain Approach for Microwave Integrated Circuits," *IEEE Trans. Microwave Theory Tech.*, vol. MTT-33, pp. 1043-1056, Oct. 1985.

[7] T. Itoh, "Analysis of Microstrip Resonators," *IEEE Trans. Microwave Theory Tech.*, vol. MTT-22, pp. 946-951, 1974.

[8] T. Itoh, "Spectral Domain Immitance Approach for Dispersion Characteristics of Generalized Printed Transmission Lines," *IEEE Trans. Microwave Theory Tech.*, vol. MTT-28, pp. 733-736, July 1980.

[9] J.B. Knorr, K.D. Kuchler, "Analysis of Coupled Slots and Coplanar Strips on Dielectric Substrate," *IEEE Trans. Microwave Theory Tech.*, vol. MTT-23, pp. 541-548, July 1975.

[10] R.E. Collin, Field Theory of Guided Waves, New York: McGraw- Hill, 1960.

[11] A.K. Sharma, W.J.R. Hoefer, "Propagation in Coupled Unilateral and Bilateral Finlines," *IEEE Trans, Microwave Theory and Tech.*, vol. MTT-31, pp.498-502, June 1983.

[12] A.S. Omar, K. Schünemann, "Space Domain Decoupling of LSE and LSM Fields in Generalized Planar Guiding Structures, " in *1984 IEEE MTT-S Int. Microwave Symp. Dig.*, pp. 59-61.

[13] *AEG Telefunken*, private communication.

Chapter 5

Computer Simulation of E-Plane Hybrid Couplers

5.1 Introduction

In the overview of finline couplers presented in Chapter 2, we recognized that coupled slot hybrids offered superior performances compared to the other E-plane structures. The fundamental concept behind this type of coupler is that the transfer of energy from one slot to the other is a consequence of their proximity only. They constitute a coupled transmission line arrangement comparable to those studied in Chapter 3. Ignoring parasitic effects such as resonances and evanescent modes, it appears feasible to model a coupler by uniformly coupled lines of an appropriate length, and use the relations worked out in chapter 3 to describe them. Previous attempts to design hybrid couplers in this manner [1,2] did not yield satisfying results. The main reason for that appears to be the excess coupling produced by the sections where the single slots converge towards the main coupling section. The excess coupling is non-uniform in nature because the geometry itself is non-uniform. The resulting coupling length is therefore somewhat larger than that of the main coupling section and, *a priori* it is difficult to evaluate by what amount.

Callsen *et al* [3] reported a design approach that takes into account, to some extent, this non-uniform coupling. They used the *effective coupling length* concept introduced

in [4]. For uniform lines with similar even and odd mode impedance values (see Section 3.5.3), we obtained earlier (equation (3.15)):

$$\left|\frac{V_3}{V_4}\right| = \tan\left(\frac{\theta_e - \theta_o}{2}\right).$$

In the case of non-uniform lines, assuming that the impedances are constant over their length, it can be shown that the *effective coupling length* is equal to the summation of the coupling lengths of an infinite number i of subsections, each considered uniform:

$$\left|\frac{V_3}{V_4}\right| = \tan\sum_i\left(\frac{\theta_{ei} - \theta_{oi}}{2}\right). \tag{5.1}$$

This represents an approximation because the effect of the reflections caused by the variation of the impedances is neglected. Unfortunately, in [3] no mention is made of the accuracy achieved with this design-approach.

The simulation procedure put forward here extends this principle to include the effect of the varying impedances in the analysis. The non-uniform coupled slots are modeled by a cascade of uniformly coupled lines and analyzed with simple circuit theory. This model has been used to simulate a number of couplers and, in most cases, a good agreement with the experimental results has been found. The simulation procedure is simple enough to be considered for implementation in a CAD package with computer optimization based on user-defined models.

The first step in the development of the general simulation procedure has been the study of a uniformly coupled slot finline hybrid. No report is made in the literature of the accuracy achieved by the uniformly coupled transmission-line analog applied to this problem. In order to get a feeling for it, we investigated that simple structure before attempting to simulate the more complex non-uniform configurations. For this purpose, some finline couplers approximating as closely as possible a uniformly coupled line arrangement have been designed. The comparison of their performances with those predicted by the theory confirmed the realism of the coupled transmission line analog

and the correctness of the spectral domain analysis for coupled slots. This work is summarized in Section 5.2.

Section 5.3 contains the description of the proposed simulation approach for non-uniformly coupled slots with the application to five different hybrids. In all cases but one, a good agreement between the simulated and the experimental scattering parameters has been obtained. The data for the circuits studied here have been provided by the Communications Research Center of the Government of Canada, in Ottawa.

5.2 Simulation of Uniformly Coupled Finline Slots

Before trying to develop any general simulation procedure we wanted to verify the validity of the SDA program (Chapter 4) and the coupled transmission line analogy (Chapter 3) when applied to finlines. To the author's knowledge, no experimental verification of the spectral domain analysis results has been published. Therefore, we had no idea at the time of how good the correlation would be between the theoretical and the experimental results. To this end, a few hybrids have been designed with a configuration that is as close to the ideal model of two uniform transmission lines as possible. Their topology is shown in Figure 5.1.

5.2.1 Description of the circuits

Two uniform parallel slots form the coupling section. Four single finlines, at 90 degrees with the coupled slots, are connected to them by rounded elbows. Waveguide-to-finline tapers are used at each port for compatibility with waveguide test equipment.

These couplers were also built in view of another application which dictated the design specifications. Consequently, the housing dimensions for the input ports are $a = 10.668$ mm and $b = 4.318$ mm (WR–42), and for the coupling section, $a = 10.668$ mm and $b = 5.207$ mm. The distance from the metallic pattern to the side wall of

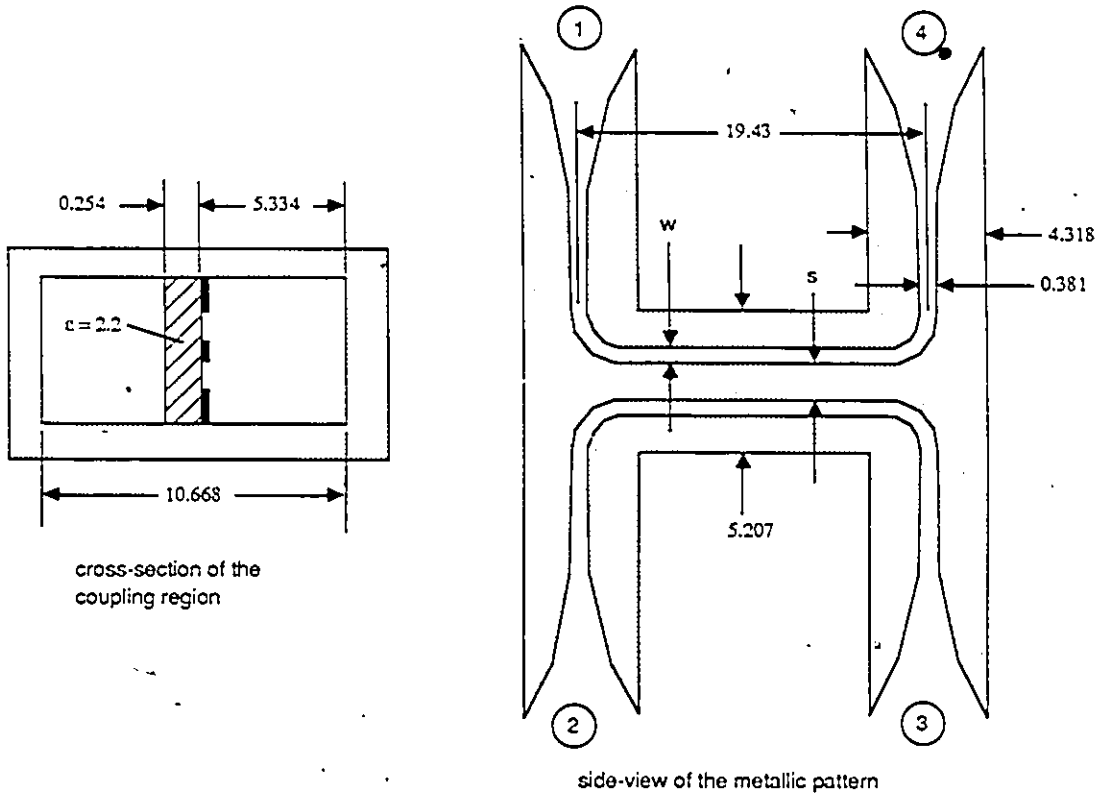

Figure 5.1: Topology of uniform finline hybrids S94W15 and S94W85 with the dimensions in mm

the enclosure is $h = 5.334$ mm. The dielectric used is RT/Duroid, $\epsilon_r = 2.2$ with a thickness of 0.254 mm. The slotwidth of the single finlines is 0.381 mm corresponding to an impedance of 172 ohms. The nominal coupling length was chosen to be 19.43 mm. Since no reliable procedure was available to carry out the design, a trial and error approach was followed to obtain the equal power split at 19 GHz required in the specifications. The optimization was done by varying the slot width and spacing (w and s) in the coupling section from one circuit to the other.

The 90 degree junctions in these hybrids are not optimum to minimize the reflections. They have been used to make the coupling section as uniform as possible over its entire length. Two of the prototypes that were built, circuits S94W15 and S94WS5, have been simulated here using the uniformly coupled transmission line analogy.

5.2.2 The Model and the Simulation

The simulations proceeded as follows. First, given the geometry of the coupling section, the even/odd mode parameters of the equivalent coupled lines were computed with the program CPLFIN (Chapter 4). Next, the coupling length was obtained from the dimensions of the circuit as shown in Figure 5.2. Even with this simple topology, the coupled slots are not exactly uniform due to the rounded elbows at each end. Therefore the determination of the coupling length is not totally objective and depends on one's opinion as to where the coupling effect stops taking place. On the other hand, these end portions are small as compared to the overall length and their effect is minimal. It was decided here to include half the length of arc of the elbows (l_r) in the total coupling length, which ends up being approximately 18.9 mm for both circuits. The data for each circuit are given in Figures 5.3 and 5.4.

Following this, the circuit analysis was performed with TOUCHSTONE using its CLINP element. This is the name used by TOUCHSTONE to describe a section of coupled transmission lines with a given length and a set of even/odd effective dielectric

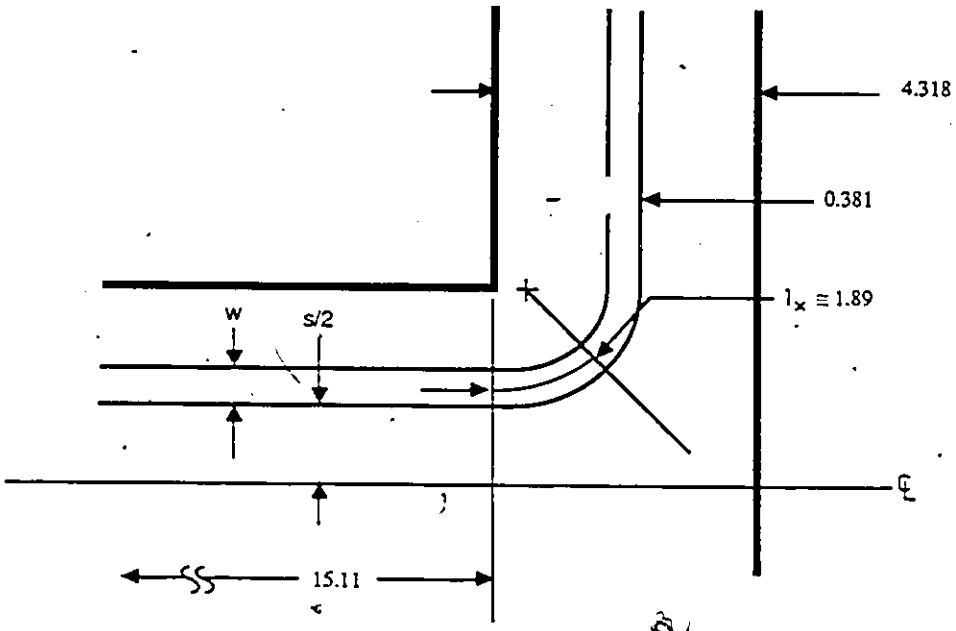

Figure 5.2: Determination of the coupling length for S94W15 and S94W85 (in mm). One quarter of the structure is shown.

constants and impedances. The load impedance used at each of the four ports in the coupled line circuit was 172 ohms, the characteristic impedance of the 0.381 mm slots of the coupler's arms. The waveguide-to-finline tapers (−20 to −25 dB return loss) were not included in the analysis, nor were the effects of the elbows and the line losses. Because of the dispersive nature of finlines, a frequency sweep analysis was not possible and, therefore, only a few points were calculated. The results are compared with experiment in Figures 5.3 and 5.4 over the 18–26 GHz band.

5.2.3 Results and Discussion

The frequency responses reveal that the transmission coefficients (s_{31} and s_{41}) are relatively well approximated by the simulations. Their magnitude is predicted within 1 dB but, more importantly, the general trend of their frequency dependence is in good agreement for both circuits. The simulations predict an equal power split around 18.5 GHz for S94W15 and, for S94W85, a clear undercoupling over the entire band. These

circuit S94W15

Subsection data

i \ mm	w_i	s_i	b_i	l_i
1	0.381	2.39	5.207	18.9

Experimental (continuous curves) and calculated (discrete points) responses

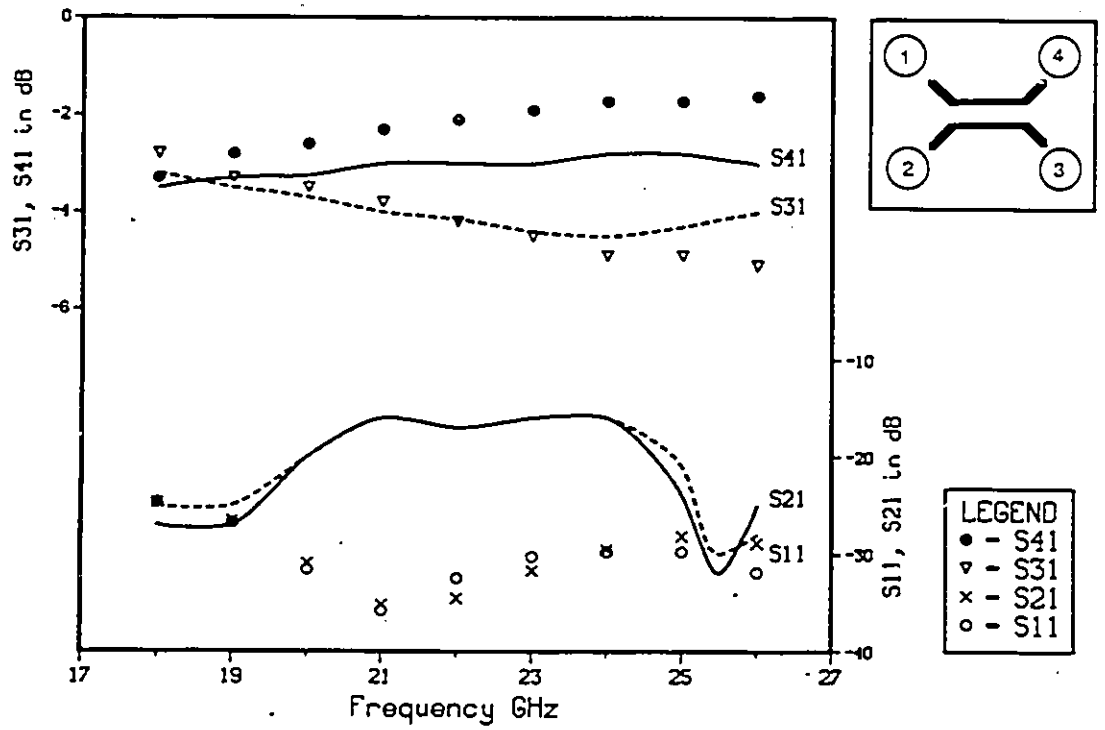

Figure 5.3: Data and experimental and calculated frequency responses of circuit S94W15.

circuit S94W85

Subsection data

i \ mm	w_i	s_i	b_i	l_i
1	0.216	2.39	5.207	18.9

Experimental (continuous curves) and calculated (discrete points) responses

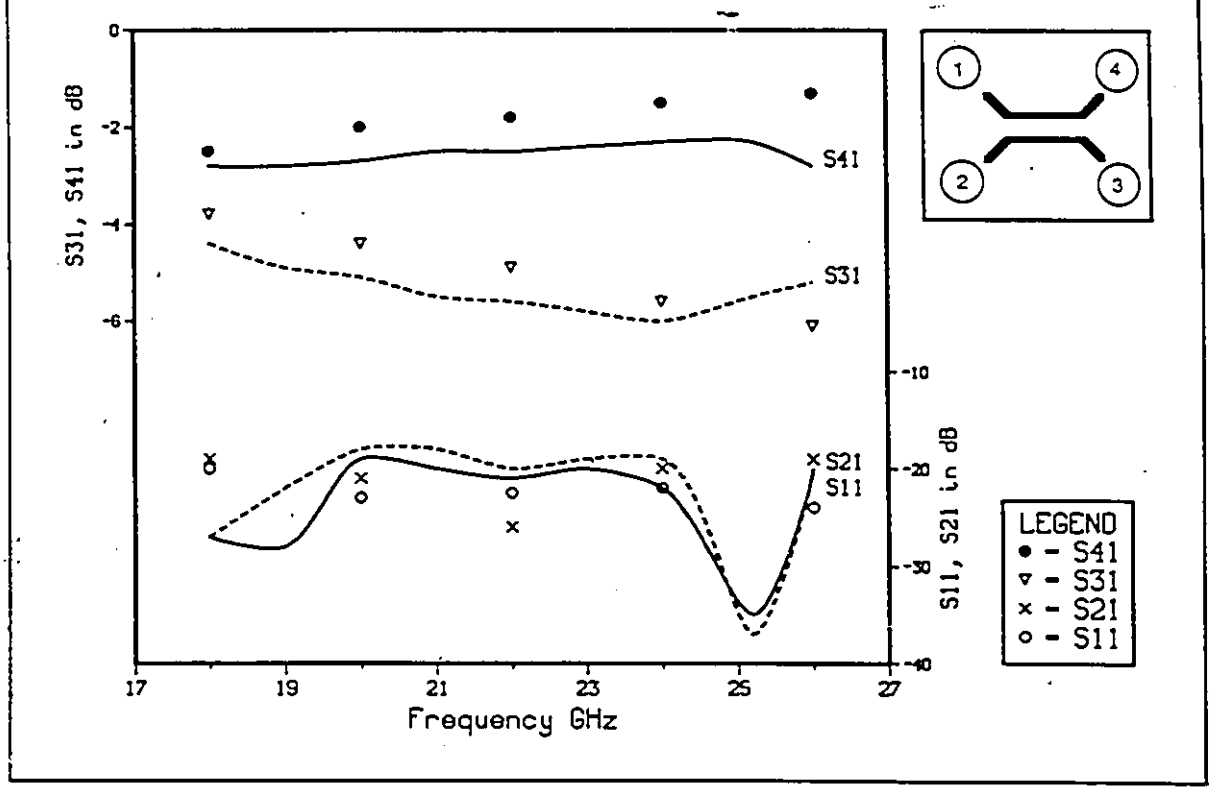

Figure 5.4: Data and experimental and calculated frequency responses of circuit S94W85.

behaviors are confirmed by the measurements.

Concerning the reflection coefficients[1] there is not much correlation (although their overall levels seem to agree for S94W85) between the theoretical and the measured responses. However, this was expected because the mismatch introduced by the elbows was not considered in the simulations and is certainly not negligible in practice. The validity of the agreement for the transmission coefficients is not really undermined by the lack of correlation observed for the reflection coefficients. The level of these is too low to affect the former significantly.

The similarity of the calculated and the measured transmission coefficients obtained for both circuits appeared very encouraging, considering that the parasitic effects produced by the elbows had been neglected in the simulations. On this basis, it was concluded that the transmission line model is reasonably accurate for the description of parallel finline slots. Besides, these simulations have also contributed to establish a good level of confidence in the results of the spectral domain program.

The difficulty in determining the coupling length in this case had been minimized by the use of 90 degree elbows. Nevertheless, there remained a certain uncertainty as to which portion of the elbow was to be considered in the analysis. One can thus appreciate the corresponding problem arising for most practical cases where smoother junctions are used. The approach followed here becomes, in those cases, inapplicable. However, in the next section, we show how the spectral domain method and the coupled transmission line analogy can still be used successfully for non-uniform coupled slots.

[1]This terminology will be used throughout this chapter to refer to the s_{11} and s_{21} coefficients

5.3 Simulation of Non-Uniformly Coupled Finline Slots

In practice, in order to achieve better return loss, the input slots of a finline coupler are connected smoothly to the coupled lines at an angle smaller than 90 degrees. The region of convergence of these slots has a coupling effect that influences the overall response of the circuit. In addition, to optimize the performance, the coupled slots themselves can be chosen not to be parallel. Therefore, in general, the geometry of the coupled slots in an E-Plane hybrid is simply not uniform longitudinally. This fact makes a rigorous field theory analysis very difficult and a uniform coupled line analogy impractical. Consequently, it has not been possible up to now to simulate accurately this type of circuit and a mostly empirical approach has been used for their design.

On the other hand, it has been confirmed in the previous section that parallel slots in finline were fairly well modeled by two uniformly coupled transmission lines with the parameters computed by the program CPT.FIN. The idea then arose to model non-uniform finline coupled slots by a *cascade* of short uniform coupled transmission lines. This suggestion will be investigated here by the simulation of 5 different circuits. First, the circuits and the modeling procedure will be described. Next, a comparison of the simulated and experimental responses is presented confirming the validity of the approach.

5.3.1 Description of the Circuits

The experimental data and the geometries of the couplers investigated here have been obtained from the Communications Research Center [5]. The circuits had been realized by empirically optimizing a finline hybrid for -3dB coupling at around 32 GHz. They all have the topology shown in Figure 5.5.

The four input slots are connected to the uniform coupled slots at an angle of 45

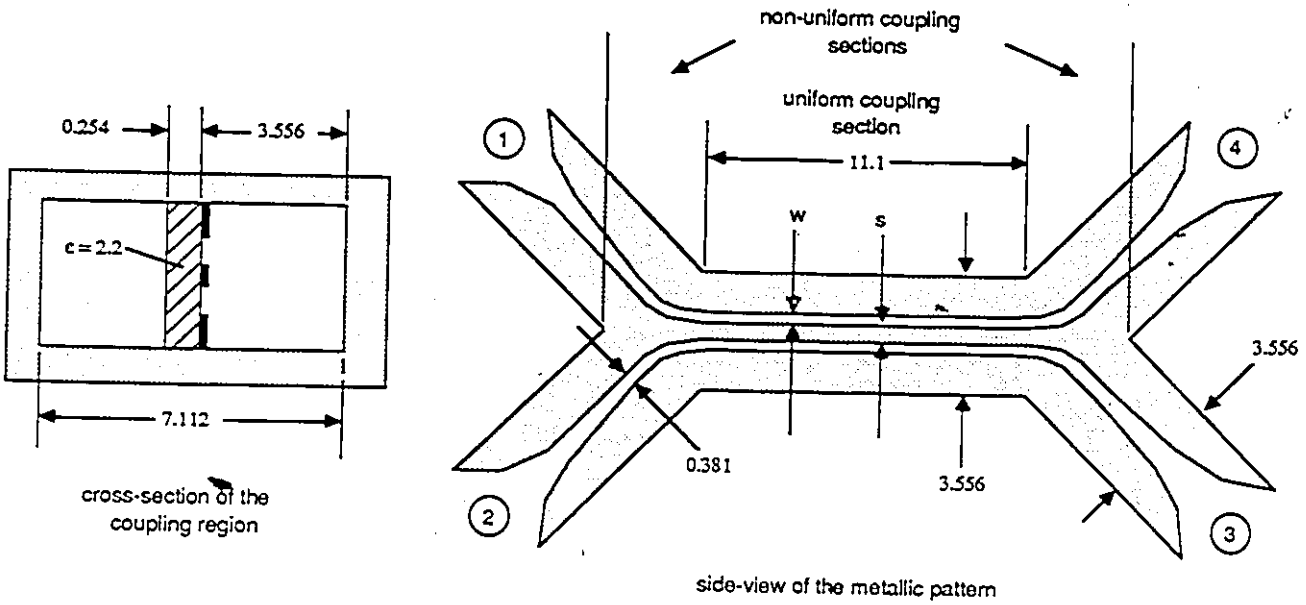

Figure 5.5: Topology of non-uniform finline hybrids obtained from [5] and dimensions in mm.

degrees to minimize parasitic reflections. The housing dimensions for the input lines and the coupling section are those of a WR–28 waveguide: $a = 7.112$ mm, $b = 3.556$ mm. The substrate used is RT/Duroid with $\epsilon_r = 2.2$ and a thickness of 0.254 mm. The distance between the metallic pattern and the housing is 3.556 mm and the input slotwidth is 0.381 mm. At each port, smooth tapers are used for compatibility with waveguide test equipment.

The circuits are all mounted in the same housing therefore they all have the same physical length. The optimization was done by empirically varying the slot width w and spacing s of the main coupling section from one circuit to another. In each case, a smooth profile was used to connect the main coupling section to the output slots resulting, as explained earlier, in non-uniform coupling. 5 different circuits have been studied here. They will be called by the names used in [5], namely: GREXXX with XXX=049,054,063,064 and 101.

The physical dimensions of the circuits were obtained from [5] and the data points

of the rubylith masks. The overetch effect has been considered. In none of the cases was the exact expression for the profile of the rounded elbows between the input slots and the main coupling section available. However, knowing the position of the parallel slots and that of the single slots, it was easy to interpolate a smooth curve between the two, such as to resemble the actual circuit. The error introduced by this somewhat subjective interpolation is considered minimal, especially so because of the discretization errors introduced afterwards.

5.3.2 The Model and the Simulation Procedure

The model for non-uniform coupled lines follows a suggestion by Saad [6]. The basic idea is to approximate a non-uniform geometry by a cascade of short uniform subsections. Saad used this principle to analyze finline couplers and tapers using a mode matching technique. His method requires extensive calculations and to this author's knowledge, no experimental evidence have been reported to support his approach concerning the couplers.

The simulation procedure proposed here for non-uniform slots uses a similar discretization in conjunction with simple circuit theory. The total coupling region of the circuit is first decomposed longitudinally into a number of subsections. Each subsection is then considered uniform, with dimensions corresponding to their average values over the length of the subsection. They are subsequently analyzed individually with the spectral domain program of Chapter 4, resulting in equivalent coupled transmission lines with even and odd mode parameters. The equivalent line circuits are finally connected in cascade and analyzed at various frequencies with TOUCHSTONE (CLINP elements) to obtain the overall response. This modeling approach has the advantage of including the information related to the reflections produced along the coupled slots by consideration of the equivalent lines' impedances. Consequently, the reflection coefficients as well as the transmission ones should be reasonably well predicted by this method (as

opposed to the effective coupling length concept used in [3] which gives no information about the reflections).

The details of the decomposition for the circuits studied here are shown in Figure 5.6. The first step is to determine the desired number of subsections in the effective coupling region which extends up to the point where the two slots are separated by the enclosure. A number of 9 has been chosen in all cases. This number is arbitrary but, as will be shown later, the larger it is the better the approximation is.

The uniform section constitutes the longest subsection. The non-uniform sections at each end are segmented into three subsections of equal length and one slightly longer where the coupling is known to be less important. The slotwidth and spacing, w_i and s_i, and the waveguide height b_i for each subsection i are then simply taken as their average values over the length of the subsection. Once these are determined, the spectral domain approach is used to obtain the equivalent coupled transmission line parameters.

In the TOUCHSTONE simulation the cascade of coupled lines (see Figure 5.6) is terminated at each port by a resistive termination of 194 ohms, corresponding to the characteristic impedance of the 0.381 mm slots. The waveguide-to-finline tapers (return loss of -20 to -25 dB) have not been included in the simulations. The discontinuities arising from the discretization process have not been considered either because no data is available to describe them.

5.3.3 Results of the Simulations

The simulations of the five different circuits have been performed. Summaries for each one are presented in Figures 5.7 to 5.13, showing the dimensions of the subsections and their calculated and measured performances at Ka-band. It was not felt necessary to include the equivalent transmission line parameters obtained with CPLFIN. These can always be recovered knowing the subsections' geometry. As mentioned earlier a 9 subsection model has been used to simulate each circuit. In addition, the results of a 3

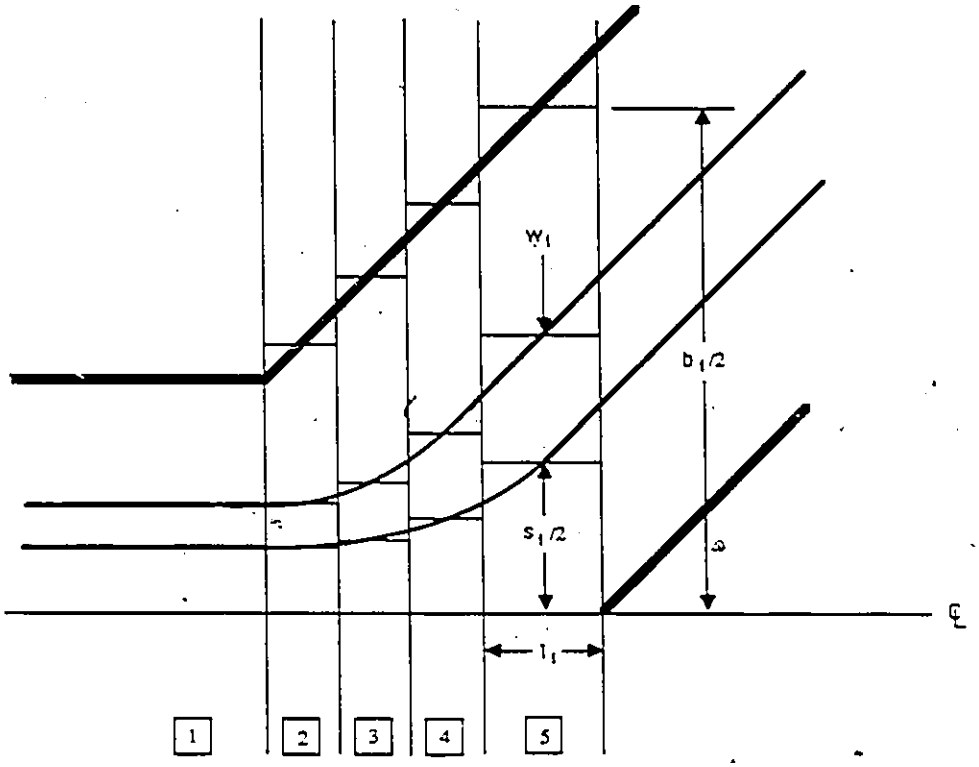

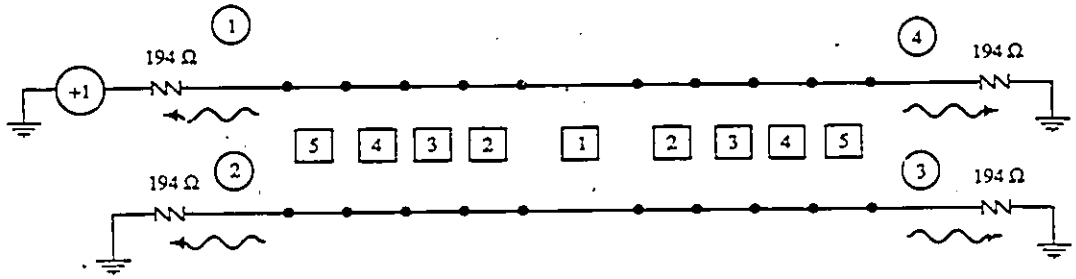

Figure 5.6: Details of the 9 subsection decomposition (one quarter of the structure is shown) and equivalent transmission line model.

section and a 17 section model for circuit GRE063 have been included for comparison. The results are presented next.

GRE049 (Figure 5.7)

The measurements on this circuit reveal a wideband behavior of the transmission coefficients with values around -1.5 dB for s_{31} and -7 dB for s_{41}. This wideband behavior is common to all circuits studied here. The reflection coefficients are also fairly constant between 27 GHz and 34 GHz and dip significantly at the upper end of the band. In addition, s_{41} displays another deep minimum at the lower end of the band. The performances achieved for these two responses (-15 dB) could be improved with a better design. The portion of the band beyond 37 GHz will always be ignored here because of a housing resonance occurring there which disturbed the frequency responses.

This circuit is the only one considered in this work for which the simulation is not in close agreement with the measurements. The calculated s_{41} and the s_{31} responses are respectively higher and lower than the corresponding measured ones with, on the other hand, a similar wideband behavior. Regarding the reflection coefficients however, little correlation is apparent. A 15 subsection model does not improve the agreement.

GRE054 (Figure 5.8)

This circuit has a response that is very similar to the previous one's. The data are only available from 26.5 to 32 GHz in this case. The direct (s_{41}) and coupled (s_{31}) coefficients are around -5 dB and -2 dB respectively over the frequency band considered. The reflection coefficients vary between -15 dB at 28 GHz, and below -25 dB above 31 GHz. It is clear that the simulated responses are in very close agreement with the measurements, with a slight shift towards the higher frequencies.

circuit GRE049

Subsection data

i \ mm	w_i	s_i	b_i	l_i
1	0.229	0.51	3.56	11.1
2	0.254	0.61	4.3	0.754
3	0.333	1.09	5.79	0.754
4	0.467	1.91	7.32	0.754
5	0.533	3.49	9.04	0.99

Experimental (continuous curves) and calculated (discrete points) responses

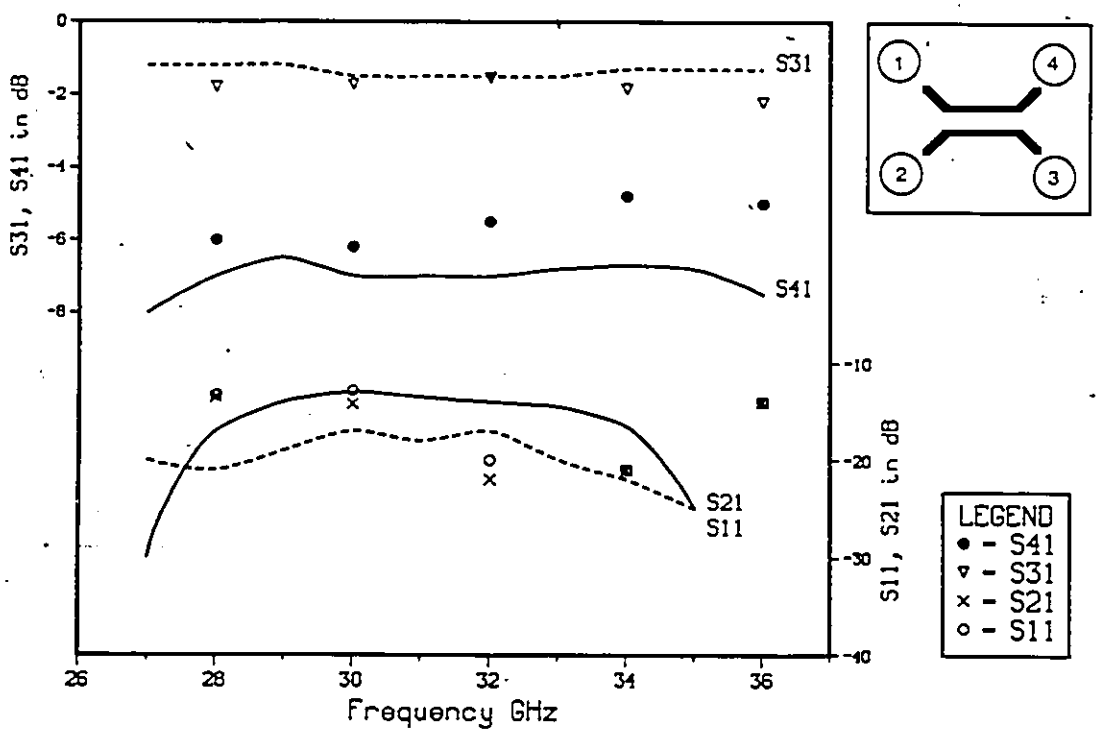

Figure 5.7: Data and experimental and calculated frequency responses for circuit GRE049.

circuit GRE054

Subsection data

i \ mm	w_i	s_i	b_i	l_i
1	0.381	1.40	3.56	11.1
2	0.362	1.52	4.3	0.754
3	0.352	1.81	5.79	0.754
4	0.381	2.25	7.32	0.754
5	0.533	3.49	9.04	0.99

Experimental (continuous curves) and calculated (discrete points) responses

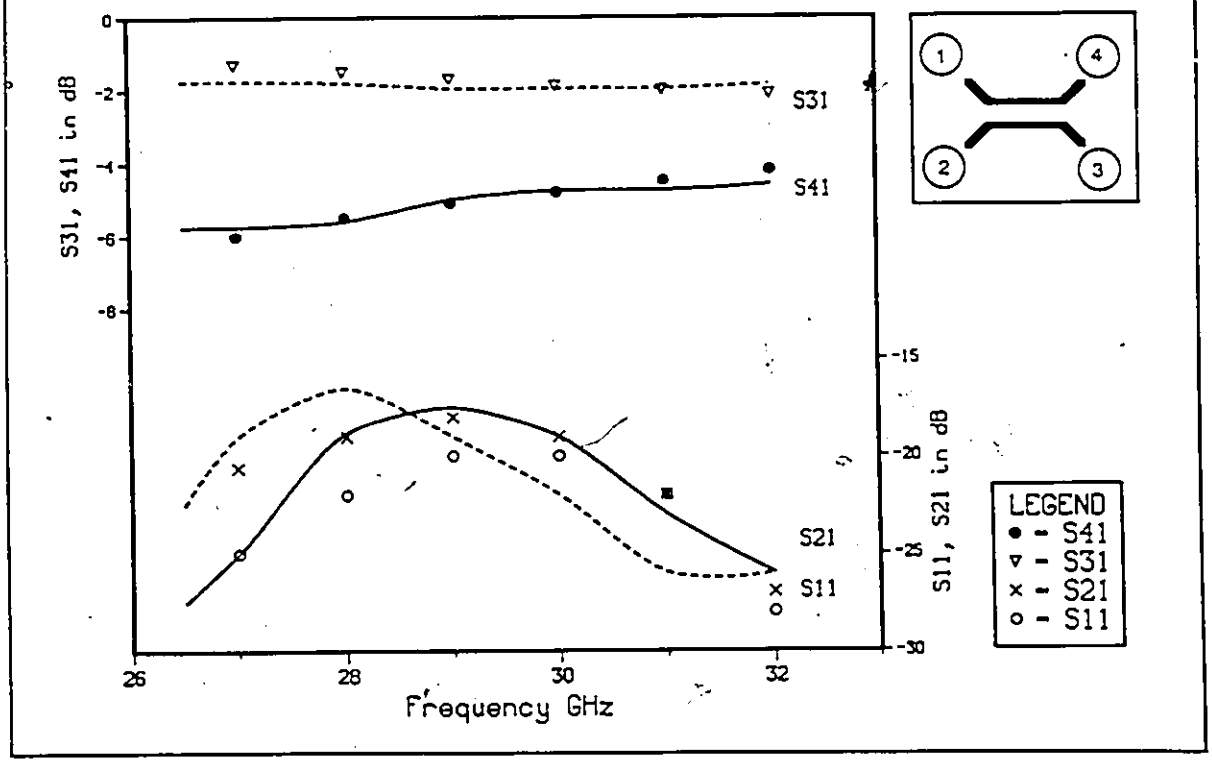

Figure 5.8: Data and experimental and calculated frequency responses for circuit GRE054.

circuit GRE063

Subsection data

i \ mm	w_i	s_i	b_i	l_i
1	0.178	1.40	3.56	11.1
2	0.305	2.083	6.81	3.25

Experimental (continuous curves) and calculated (discrete points) responses

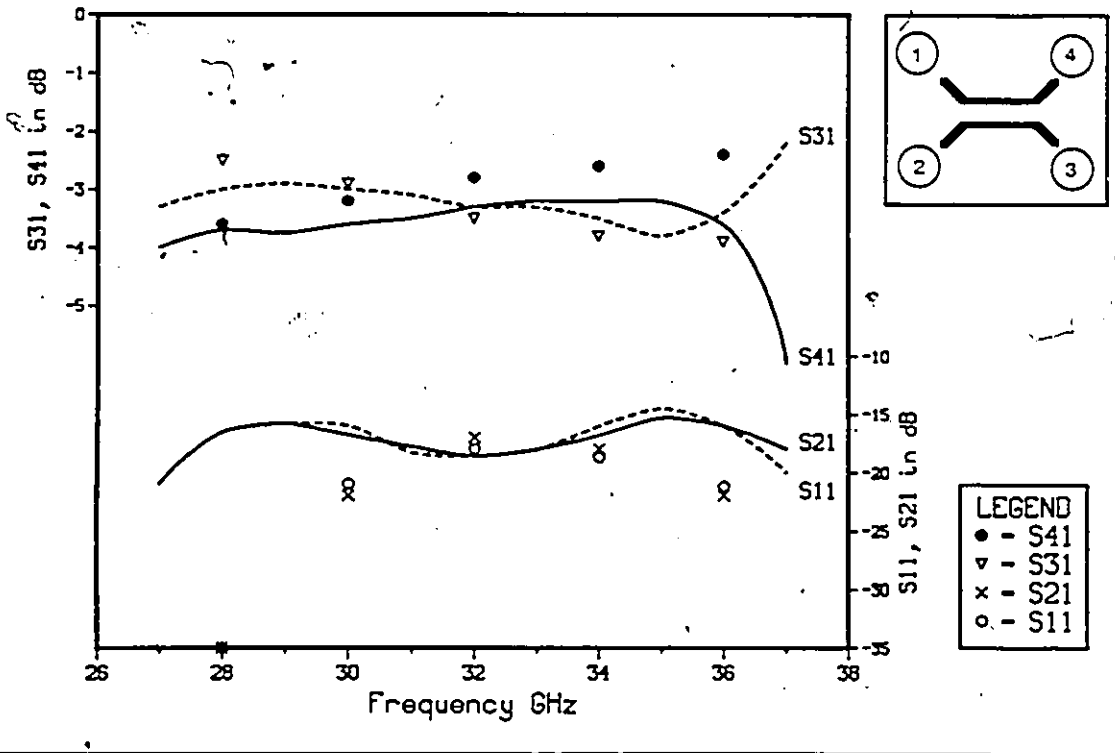

Figure 5.9: Data and experimental and calculated frequency responses for circuit GRE063 (3 subsection model).

circuit GRE063

Subsection data

i \ mm	w_i	s_i	b_i	l_i
1	0.178	1.40	3.56	11.1
2	0.218	1.49	4.3	0.754
3	0.287	1.80	5.79	0.754
4	0.348	2.25	7.32	0.754
5	0.533	3.49	9.04	0.99

Experimental (continuous curves) and calculated (discrete points) responses

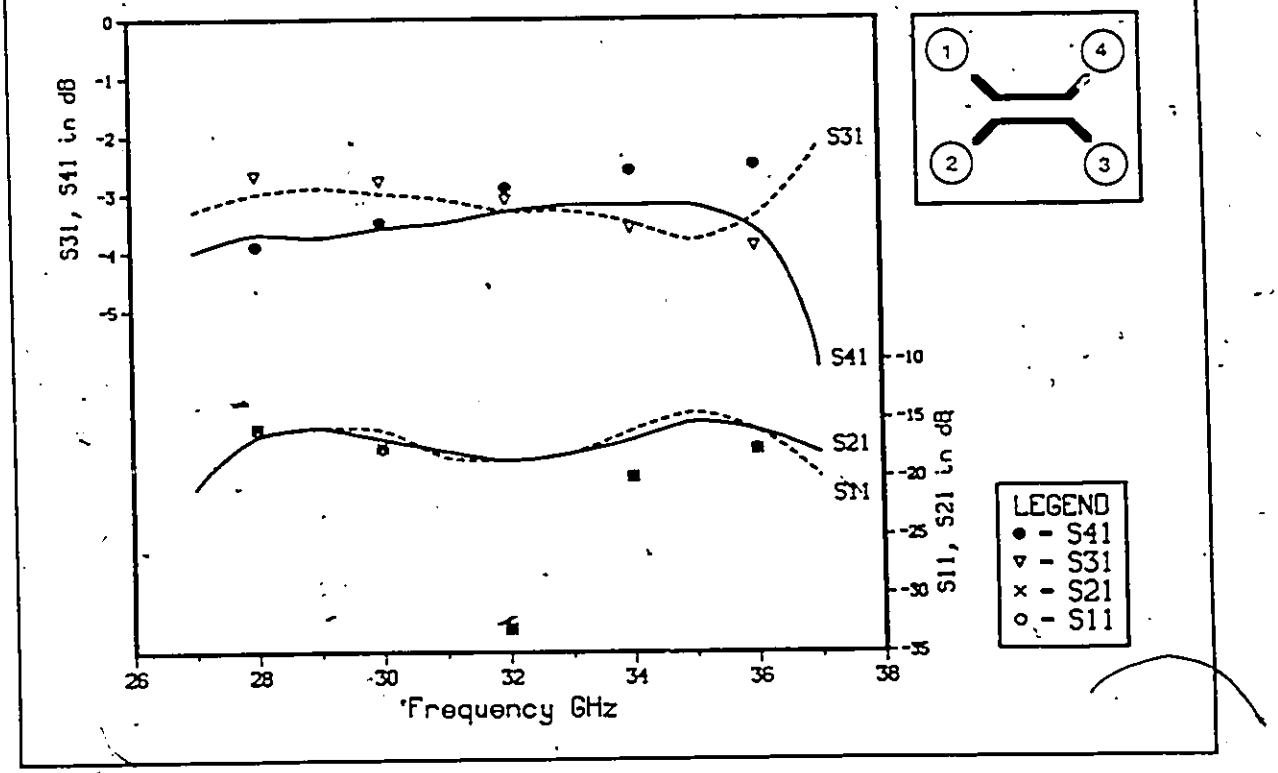

Figure 5.10: Data and experimental and calculated frequency responses for circuit GRE063 (9 subsection model).

circuit GRE063

Subsection data

i \ mm	w_i	s_i	b_i	l_i
1	0.178	1.40	3.56	11.1
2	0.19	1.44	3.92	0.377
3	0.229	1.54	4.69	0.377
4	0.248	1.72	5.45	0.377
5	0.282	1.91	6.21	0.377

i \ mm	w_i	s_i	b_i	l_i
6	0.314	2.11	6.97	0.377
7	0.409	2.36	7.73	0.377
8	0.533	3.01	8.58	0.493
9	0.533	4.0	9.57	0.493

Experimental (continuous curves) and calculated (discrete points) responses

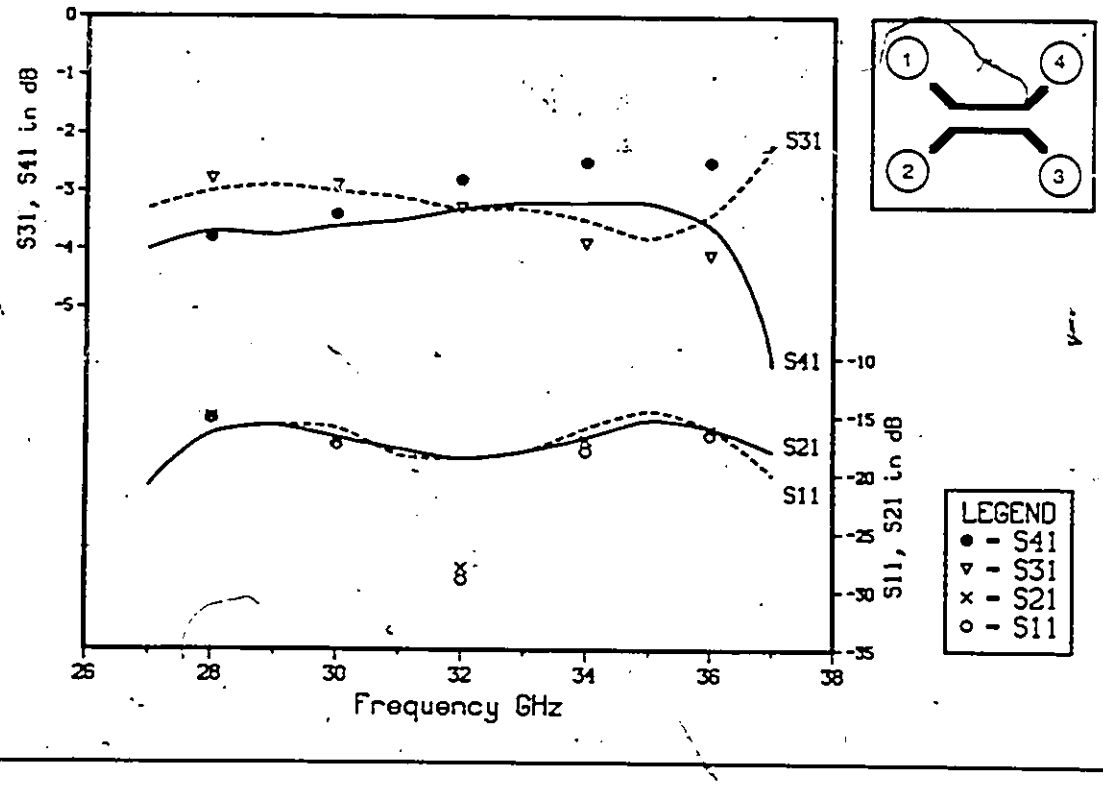

Figure 5.11: Data and experimental and calculated frequency responses for circuit GRE063 (17 subsection model).

circuit GRE064

Subsection data

i \ mm	w_i	s_i	b_i	l_i
1	0.14	1.40	3.56	11.1
2	0.16	1.50	4.3	0.754
3	0.21	1.83	5.79	0.754
4	0.347	2.27	7.32	0.754
5	0.533	3.49	9.04	0.99

Experimental (continuous curves) and calculated (discrete points) responses

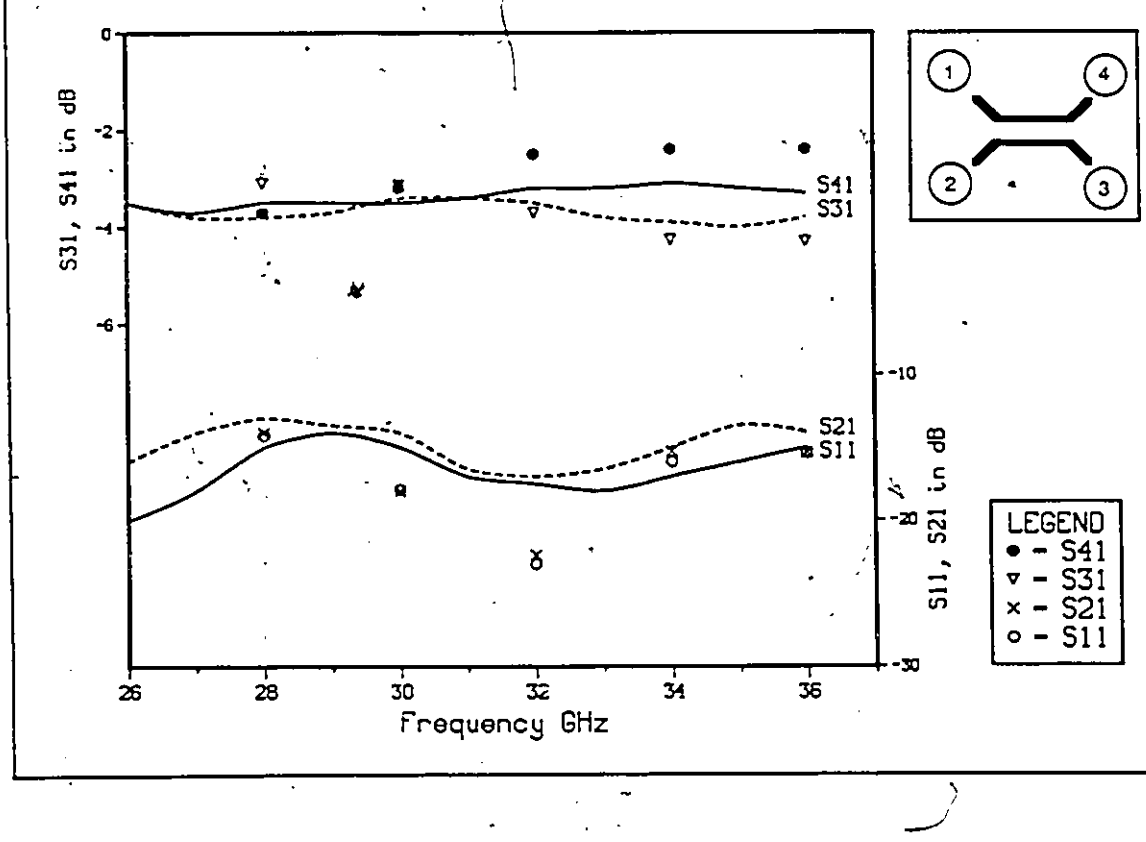

Figure 5.12: Data and experimental and calculated frequency responses for circuit GRE064.

circuit GRE101

Subsection data

i \ mm	w_i	s_i	b_i	l_i
1	0.254	1.90	3.56	11.1
2	0.267	1.94	4.3	0.754
3	0.286	2.91	5.79	0.754
4	0.343	2.36	7.32	0.754
5	0.533	3.49	9.04	0.99

Experimental (continuous curves) and calculated (discrete points) responses

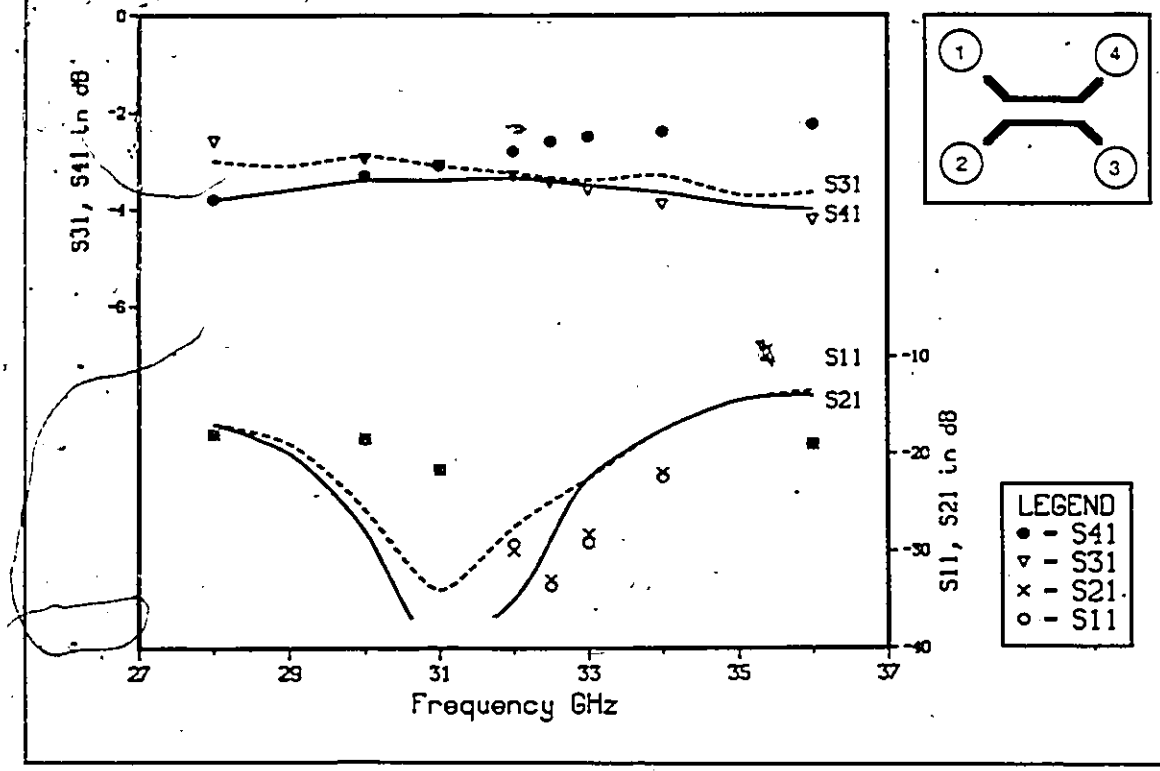

Figure 5.13: Data and experimental and calculated frequency responses for circuit GRE101.

GRE063 (Figures 5.9 to 5.11)

Three models with different discretization steps were used to simulate this coupler. The 3 section model is a rough approximation of the circuit while the 9 and 17 section models are increasingly finer ones. Those simulations were carried out to verify whether or not a finer step size resulted in a better agreement with the experiment. As shown in the frequency responses, it is the case.

GRE063 is a circuit that provides an equal power split between ports 3 and 4 with reflection levels of -15 to -20 dB from 27 to 36 GHz. All three simulations predicted the transmission coefficients with comparable accuracy. As was expected however, there is a net difference in favor of the 17 section model concerning the reflection coefficients. Indeed, with this model, a close agreement is obtained both in the absolute levels and the frequency behaviors of the s_{11} and s_{21} responses. The pronounced dip in the calculated curves at 32 GHz is not as strong in practice but this difference can be attributed to parasitic reflections as, for instance, in the waveguide-to-finline tapers. A very good agreement is obtained with the 17 section and the 9 section models.

GRE064 (Figure 5.12)

The frequency response is similar to that of the previous circuit and, again, a good agreement is achieved with a 9 subsection model. The calculated response appears to be slightly shifted towards the low frequencies.

GRE101 (Figure 5.13)

This 3–dB hybrid has been optimized for good return loss and isolation (s_{11} and s_{21}) between 30 and 32 GHz. Here again the 9-section model gives good agreement with the experiment. The dip in the reflection curves seems shifted in frequency but the model is able to predict the very low levels of these coefficients. For such low reflection

coefficients a better accuracy would be obtained if the waveguide-to-finline tapers (−20 to −25 dB) were included in the simulation.

A point of interest here is that the experimental transmission responses do not seem to cross each other. This is in contradiction with the theory (see Figure 3.11) but is also observable locally on the other circuits' responses. This results in the simulated s_{41} response departing from the real one by almost 2 dB at 36 GHz. This effect is attributed to the housing resonance occurring at the top of the band.

5.3.4 Discussion

For all circuits studied in this section the experimental transmission coefficients were more constant over frequency than predicted by the simulations. The reason for this is not known. The phenomenon can be attributed to the continuously varying nature of the slots' profile. Such constructions are known to improve the bandwidth of directional couplers (see [7]). At the high end of the frequency band, another factor that might influence the responses in that sense is the housing resonance occurring around 38GHz. Nonetheless, the accuracy of the simulations for these coefficients is very good in most cases (the exception is GRE049).

It is worth mentioning here that the discretization of GRE063 in only three subsections resulted in as good a prediction of s_{31} and s_{41} as the 17 subsection model. This somewhat unexpected observation can be explained by the effective coupling length concept introduced in [4]. If the structure of interest is varying very smoothly, its even and odd propagation constants will also vary smoothly. Averaging the value of the electrical length over a longer distance does not, in these cases, significantly change the final result of equation (5.1). This is what happened with GRE063. The way the dimensions of the subsections are determined amounts to averaging the line characteristics over the length of the subsection. In the case of a circuit varying not so slowly, it is likely that more subsections would be necessary to predict the transmission coefficients with

a comparable accuracy.

Regarding the reflection coefficients, however, this simple averaging method is not representative of the reality. In practice it is not true that the impedances are constant and therefore small reflections are produced as the signals travel down the slots. In order to represent these accurately, a larger number of subsections is necessary. This is clearly demonstrated by a comparison of the 3 and 17 section models of GRE063. The former yields reflection responses that bear no resemblance to the experimental results. With the 17 section model on the other hand, a good agreement is achieved. In most cases simulated here, (again GRE049 is the only exception) fairly good predictions of s_{11} and s_{21} were obtained by a decomposition of the circuits into 9 subsections.

Let us remember here that the waveguide-to-finline tapers have been neglected in the analyses. Indeed, their low reflections levels of around -20 to -25 dB would affect significantly only the response of GRE101 because in the other cases, the coupled slots themselves generate larger reflections (-15 to -20 dB). For design purposes, the accuracy of the prediction of the reflections is not as important as that for the transmission responses. In general, one is interested in minimizing them over the entire band considered without paying much attention to their actual level below a certain point. For this reason it makes sense not to include the waveguide-to-finline tapers in the simulations. On the other hand, following an approach similar to the one used in this work, this can be done very easily if deemed necessary.

The calculated and measured frequency curves for circuit GRE049 do not display the close agreement reached in the other cases. This is quite puzzling considering the accuracy achieved with the simulation of GRE054, which has a similar frequency behavior. On the basis of the good results obtained in general, the discrepancy can hardly be attributed to the modelling approach itself. Many factors can be suspected (inaccuracy of the data supplied by [5], fabrication defect) but since the circuit itself

is not available, no conclusion can be drawn on this point. Our opinion is that this result is not significant and accordingly, it will not be considered in our assessment of the validity of the simulation procedure.

In view of the results presented in this section we can conclude that the proposed procedure permits a successful prediction of a non-uniform finline hybrid's performances. The method has the advantage of being conceptually very simple and totally objective in the sense that it does not rely on previous experience. The only necessary information consists of the dimensions of the circuit. The approach also requires a means of accurately calculating the even and odd mode characteristics of coupled finline slots. Here, the spectral domain method has been used for numerical efficiency but other approaches are also possible. Finally, a circuit analysis program such as TOUCHSTONE is necessary to compute the final responses.

The quality of the simulations can always be improved by increasing the number of subsections. It has been observed here that in all cases, reasonably converging results were obtained with 9 subsections. For other geometries, a larger number might be necessary. Of course the amount of computation increases with the number of subsections. The even and odd parameters must be computed for each of them at every frequency point of interest because finlines are dispersive. This is the reason why the numerical efficiency of the spectral domain approach is desirable.

It is believed that the proposed simulation procedure can be very useful in designing finline coupled slot circuits and in particular hybrid couplers. It also opens the door to a deeper investigation of these circuits as, for instance, the evaluation of the advantage of using curved slots or stepped profiles. The exact theoretical analysis of these problems is very difficult, and a trial-and-error approach is simply too costly. The approach could also be advantageously integrated in a CAD package in the form of user-defined models allowing the analysis and, (if enough computing power is available) the optimization of

complete systems.

5.4 Conclusion

This chapter has reported the successful simulation of finline couplers realized with unilateral coupled slots. The characteristics of the structures are calculated by the spectral domain method which combines accuracy and relative numerical efficiency. A circuit analysis program is then used to compute the frequency response. The accuracy of the simulation is achieved by including in the model the non-uniformly coupled slots necessary to connect the main coupling section to the ports of the coupler.

The establishment of a simple and accurate simulation procedure for finline couplers is a significant contribution because, so far, engineers have had to rely on a trial-and-error approach to design these circuits. It is very unlikely that this simulation procedure will allow the total elimination of empirical optimization from the design process. However, it does make the operation a whole lot less dependent upon the designer's previous experience (or inexperience), and opens the door to the investigation of new configurations.

Bibliography

[1] G.B. Gajda and C.J. Verver, "Millimeter-Wave QPSK Modulator in Fin Line," in *1986 IEEE MTT-S Int. Microwave Symp. Digest*, pp. 233-236.

[2] A. Beyer, D. Kóther, I. Wolff, "Development of a Coupler in Finline Technique," in *1985 IEEE MTT-S Int. Microwave Symp. Digest*, pp. 139-142.

[3] H. Callsen, L.P. Schmidt, K. Solbach, "Broadband Finline Directional Couplers," translated from German in Bhartia, Pramanick, "E-Plane Integrated Circuits," Artech House, 1987.

[4] R. Rudokas, T. Itoh, "Passive Millimeter-Wave IC Components Made of Inverted Strip Dielectric Waveguides," *IEEE Trans. Microwave Theory Tech.*, vol. MTT-24, pp. 978-981, Dec. 1976.

[5] G.B. Gajda, Private Communication, Communications Research Center, Government of Canada, Ottawa, Ontario, Canada.

[6] A.M.K. Saad and K. Schünemann, "Design of Fin-Line Tapers, Transitions and Couplers," in *Proc. 11th Eur. Microwave Conf.*, Amsterdam, 1981, pp.305-308.

[7] J.E. Adair, G.I. Haddad, "Coupled Mode Analysis of Non-Uniform Coupled Transmission Lines," *IEEE Trans. Microwave Theory and Tech.*, vol. MTT-17, pp. 746-752, Oct. 1969.

Chapter 6

Conclusion

This thesis has reported a study of finline coupled slots applied to hybrid couplers and the proposition of a simulation procedure for these circuits. A review of E-plane directional couplers was given in the first chapter to identify the advantages of the coupled slot configuration over the other alternatives: ease of fabrication, large bandwidth, high frequency application, forward coupling. It was also pointed out that the design of this type of circuit had been so far mainly an empirical process, due to the inability to analyze non-uniform coupled slots. The theory of coupled lines was then presented, bringing to light the fundamental importance of the normal modes of propagation for the characterization of coupled line circuits. This fact was then applied in conjunction with the spectral domain approach to the analysis of uniform coupled slots in finline. The spectral domain approach is an efficient numerical method that tackles a boundary value problem by first carrying out a Fourier transform of the spatial quantities, to work in the so-called Fourier or spectral domain. This facilitates the field matching process at the interfaces containing field discontinuities.

Finally, by simple consideration of circuit theory, a simulation procedure for non-uniform slots was introduced. They are decomposed in a number of uniform subsections that can be treated independently with the spectral domain analysis discussed above. The procedure has been tested with a number of finline hybrids and the results have been compiled in Chapter 5. The simulation method should prove very useful for the

design of coupled slot circuits and in particular finline hybrids. The implementation of the technique in a CAD package is certainly possible. With enough computation power or using specialized algorithms to determine the parameters of uniform coupled slot sections, it is even conceivable to run computer optimization for complete systems including, among others, coupled slot components.

Appendix A

Computer Program CPLFIN

This appendix constitutes the reference document for the spectral domain program introduced in chapter 4. It contains the complete mathematical expressions for the transverse admittance and those for the calculation of power. Those interested in modifying the program should find this appendix quite useful. The TURBO-PASCAL code itself is also included. Meaningful variable names have been used all along and because the program is fairly straightforward, no separate algorithm is given here. The reader is simply referred to the listings.

As it stands now, the whole program is separated into three disk files: CPLFIN.PAS, CPLFIN.AUX and a data file. CPLFIN.PAS contains the main procedures and is the executable source code. It has an INCLUDE statement that fetches the auxiliary procedures from CPLFIN.AUX (calculation of transverse admittance and power among others). The data are input via a data file whose name must be supplied by the user at execution time. This data file must be written in a specified format, described in the sample file DATA_FIL.PAS. All three files are listed here.

SOME DEFINITIONS

FOURIER SERIES

$$f(x) = \sum_{n=-\infty}^{\infty} c_n e^{-j\alpha_n x}$$

$$c_n = \frac{1}{T}\int_T f(x)\, e^{j\alpha_n x}\, dx \qquad n = 0, \pm 1, \pm 2, \ldots$$

$$\alpha_n = n \cdot \frac{2\pi}{T} \qquad T \text{ is period in } x.$$

if $c_n = -c_{-n}$ then

$$f(x) = \underset{0}{\not{c}_0} + \sum_{n=1}^{\infty} b_n \sin \alpha_n x \qquad b_n = -2j c_n$$

if $c_n = c_{-n}$ then

$$f(x) = c_0 + \sum_{n=1}^{\infty} a_n \cos \alpha_n x \qquad a_n = 2 c_n$$

PARSEVAL'S RELATION

$$\frac{1}{T}\int_T |f(x)|^2\, dx = \sum_{n=-\infty}^{\infty} |c_n|^2$$

VARIOUS CONSTANTS

- $k_0 = 2\pi/\lambda_0 = \omega\sqrt{\mu_0\varepsilon_0}$ = wavenumber in free space.
- $k_i = 2\pi/\lambda_i = \omega\sqrt{\mu_0\varepsilon_0\varepsilon_{ri}}$ = wavenumber in ε_{ri}
- $\beta = 2\pi/\lambda_g = \omega\sqrt{\mu_0\varepsilon_0\varepsilon_{eff}}$ = propagation constant of the structure (unknown)

EXPRESSIONS FOR TRANSVERSE ADMITTANCES

(Procedure get_transv_adm)

Equation (4.11)

CASE #1: $\gamma_1^2 > 0$ and $\gamma_2^2 > 0$ $\left(\gamma_1 = \sqrt{\gamma_1^2}\ ;\ \gamma_2 = \sqrt{\gamma_2^2}\right)$

$$Y^h = j\omega\varepsilon_0\left(\frac{-1}{K_0^2}\right)\left\{\gamma_1 \coth(\gamma_1 h) + \gamma_2\left[\frac{\gamma_1 \coth(\gamma_1 e) + \gamma_2 \tanh(\gamma_2 d)}{\gamma_2 + \gamma_1 \coth(\gamma_1 e)\tanh(\gamma_2 d)}\right]\right\}$$

$$= j\omega\varepsilon_0\left(\frac{-1}{K_0^2}\right)\cdot \bar{h}\ .$$

$$Y^e = j\omega\varepsilon_0\left\{\frac{\varepsilon_{r1}}{\gamma_1}\coth(\gamma_1 h) + \frac{\varepsilon_{r2}}{\gamma_2}\left[\frac{\frac{\varepsilon_{r1}}{\gamma_1}\coth(\gamma_1 e) + \frac{\varepsilon_{r2}}{\gamma_2}\tanh(\gamma_2 d)}{\frac{\varepsilon_{r2}}{\gamma_2} + \frac{\varepsilon_{r1}}{\gamma_1}\coth(\gamma_1 e)\tanh(\gamma_2 d)}\right]\right\}$$

$$= j\omega\varepsilon_0 \cdot \bar{e}\ .$$

CASE #2: $\gamma_1^2 > 0$ and $\gamma_2^2 < 0$ $\left(\gamma_1 = \sqrt{\gamma_1^2}\ ;\ \gamma_2 \leftarrow j\gamma_2'\ ,\ \gamma_2' = \sqrt{-\gamma_2^2}\right)^{\ddagger}$

$$Y^h = j\omega\varepsilon_0\left(\frac{-1}{K_0^2}\right)\left\{\gamma_1 \coth(\gamma_1 h) + \gamma_2'\left[\frac{\gamma_1 \coth(\gamma_1 e) - \gamma_2' \tan(\gamma_2' d)}{\gamma_2' + \gamma_1 \coth(\gamma_1 e)\tan(\gamma_2' d)}\right]\right\}$$

$$= j\omega\varepsilon_0\left(\frac{-1}{K_0^2}\right)\cdot \bar{h}\ .$$

$$Y^e = j\omega\varepsilon_0\left\{\frac{\varepsilon_{r1}}{\gamma_1}\coth(\gamma_1 h) + \frac{\varepsilon_{r2}}{\gamma_2'}\left[\frac{\frac{\varepsilon_{r1}}{\gamma_1}\coth(\gamma_1 e) + \frac{\varepsilon_{r2}}{\gamma_2'}\tan(\gamma_2' d)}{\frac{\varepsilon_{r2}}{\gamma_2'} - \frac{\varepsilon_{r1}}{\gamma_1}\coth(\gamma_1 e)\tan(\gamma_2' d)}\right]\right\}$$

$$= j\omega\varepsilon_0 \cdot \bar{\bar{e}}\ .$$

‡ "←" means "is replaced by".

CASE #3: $\gamma_1^2 < 0$ and $\gamma_2^2 < 0$ $\left(\gamma_1 \leftarrow j\gamma_1',\ \gamma_1' = \sqrt{-\gamma_1^2}\ ;\ \gamma_2 \leftarrow j\gamma_2',\ \gamma_2' = \sqrt{-\gamma_2^2}\right)$

$$Y^h = j\omega\varepsilon_0\left(\frac{-1}{K_0^2}\right)\left\{\gamma_1' \cot(\gamma_1' h) + \gamma_2'\left[\frac{\gamma_1' \cot(\gamma_1' e) - \gamma_2' \tan(\gamma_2' d)}{\gamma_2' + \gamma_1' \cot(\gamma_1' e)\tan(\gamma_2' d)}\right]\right\}$$

$$= j\omega\varepsilon_0\left(\frac{-1}{K_0^2}\right)\cdot \bar{h}\ .$$

$$Y^e = j\omega\varepsilon_0\left\{-\frac{\varepsilon_{r1}}{\gamma_1'}\cot(\gamma_1' h) - \frac{\varepsilon_{r2}}{\gamma_2'}\left[\frac{\frac{\varepsilon_{r1}}{\gamma_1'}\cot(\gamma_1' e) - \frac{\varepsilon_{r2}}{\gamma_2'}\tan(\gamma_2' d)}{\frac{\varepsilon_{r2}}{\gamma_2'} + \frac{\varepsilon_{r1}}{\gamma_1'}\cot(\gamma_1' e)\tan(\gamma_2' d)}\right]\right\}$$

$$= j\omega\varepsilon_0 \cdot \bar{e}\ .$$

Equations (4.16) AND (4.17)

For all cases, with $\bar{h}$ and $\bar{e}$ defined on the previous page.

$$Y_{11} = \frac{j\omega\varepsilon_0}{(\alpha_n^2 + \beta^2)}\left[\alpha_n^2 \cdot \bar{e} - \varepsilon_{eff} \cdot \bar{h}\right].$$

$$Y_{12} = Y_{21} = j\omega\varepsilon_0\ \frac{\alpha_n \beta}{(\alpha_n^2 + \beta^2)}\left[\bar{e} + \frac{1}{K_0^2}\cdot \bar{h}\right].$$

$$Y_{22} = \frac{j\omega\varepsilon_0}{(\alpha_n^2 + \beta^2)}\left[\beta^2 \cdot \bar{e} - \frac{\alpha_n^2}{K_0^2}\cdot \bar{h}\right].$$

EXPRESSIONS FOR POWER CALCULATION

(Procedure **get_total_power** and function **power_term**)

Field expressions using equations (4.44) and (4.46)

MEDIUM 1

$$E_{x1} = \sum_{n=-\infty}^{\infty} j\,\Delta\,\Upsilon_1\,Ch_1(x).$$

$$H_{y1}^{*} = \sum_{n=-\infty}^{\infty} \left[j\,\alpha_n\,\gamma_1^{*}\,\Theta_1^{*} - j\,\frac{K_1^2}{\rho}\,\Upsilon_1^{*} \right] Ch_1^{*}(x).$$

$$E_{y1} = -\sum_{n=-\infty}^{\infty} \left[\rho\,\beta^2\,\Theta_1 - \alpha_n\,\gamma_1\,\Upsilon_1 \right] Sh_1(x).$$

$$H_{x1}^{*} = \sum_{n=-\infty}^{\infty} \Delta\,\Theta_1^{*}\,Sh_1^{*}(x).$$

MEDIUM 2

$$E_{x2} = \sum_{n=-\infty}^{\infty} j\,\Delta\,\Upsilon_1\,\psi_1(x)$$

$$H_{y2}^{*} = \sum_{n=-\infty}^{\infty} j\,\alpha_n\,\gamma_2^{*}\,\Theta_1^{*}\,\psi_2^{*}(x) - j\,\frac{K_2^2}{\rho}\,\Upsilon_1^{*}\,\psi_1^{*}(x).$$

$$E_{y2} = -\sum_{n=-\infty}^{\infty} \rho\,\beta^2\,\Theta_1\,\psi_3(x) - \alpha_n\,\gamma_2\,\Upsilon_1\,\psi_4(x).$$

$$H_{x2}^{*} = \sum_{n=-\infty}^{\infty} \Delta\,\Theta_1^{*}\,\psi_3^{*}(x).$$

MEDIUM 3

$$E_{x3} = \sum_{n=-\infty}^{\infty} j\,\Delta\,\Upsilon_3\,Ch_3(x).$$

$$H_{y3}^{*} = \sum_{n=-\infty}^{\infty} \left[j\,\alpha_n\,\gamma_3^{*}\,\Theta_3^{*} - j\,\frac{K_3^2}{\rho}\,\Upsilon_3^{*} \right] Ch_3^{*}(x).$$

$$E_{y3} = -\sum_{n=-\infty}^{\infty} \left[\rho\,\beta^2\,\Theta_3 - \alpha_n\,\gamma_3\,\Upsilon_3 \right] Sh_3(x).$$

$$H_{x3}^{*} = \sum_{n=-\infty}^{\infty} \Delta\,\Theta_3^{*}\,Sh_3^{*}(x).$$

Auxiliary quantities see equations (4.48)

$$\psi_1(x) = \varepsilon_{12}\, Ch_{1d}\, Ch_2(x) + \gamma_{12}\, Sh_{1d}\, Sh_2(x).$$

$$\psi_2(x) = Sh_{1d}\, Sh_2(x) + \gamma_{12}\, Ch_{1d}\, Ch_2(x).$$

$$\psi_3(x) = Sh_{1d}\, Ch_2(x) + \gamma_{12}\, Ch_{1d}\, Sh_2(x).$$

$$\psi_4(x) = \varepsilon_{12}\, Ch_{1d}\, Sh_2(x) + \gamma_{12}\, Sh_{1d}\, Ch_2(x).$$

Expressions for Poynting vectors equations (4.51) and (4.52)

MEDIUM 1 :

$$E_{x1}\, H_{y1}^* \Rightarrow \sum_{n=-\infty}^{\infty} \Delta \left|Ch_1(x)\right|^2 \left(-\alpha_n \gamma_1^*\, T_1\, \Theta_1^* + \frac{K_1^2}{\rho} \left|T_1\right|^2\right).$$

$$E_{y1}\, H_{x1}^* \Rightarrow -\sum_{n=-\infty}^{\infty} \Delta \left|Sh_1(x)\right|^2 \left(\rho\, \beta^2 \left|\Theta_1\right|^2 - \alpha_n\, \gamma_1\, T_1\, \Theta_1^*\right).$$

MEDIUM 2:

$$E_{x2}\, H_{y2}^* \Rightarrow \sum_{n=-\infty}^{\infty} \Delta \left(-\alpha_n \gamma_2^*\, \Theta_1^*\, T_1\, \psi_1(x)\, \psi_2^*(x) + \frac{K_2^2}{\rho} \left|T_1\right|^2 \left|\psi_1(x)\right|^2\right).$$

$$E_{y2}\, H_{x2}^* \Rightarrow -\sum_{n=-\infty}^{\infty} \Delta \left(\rho\, \beta^2 \left|\Theta_1\right|^2 \left|\psi_2(x)\right|^2 - \alpha_n\, \gamma_2\, T_1\, \Theta_1^*\, \psi_3^*(x)\, \psi_4(x)\right).$$

MEDIUM 3:

$$E_{x3}\, H_{y3}^* \Rightarrow \sum_{n=-\infty}^{\infty} \Delta \left|Ch_3(x)\right|^2 \left(-\alpha_n\, \gamma_3^*\, T_3\, \Theta_3^* + \frac{K_3^2}{\rho} \left|T_3\right|^2\right).$$

$$E_{y3} H_{x3}^{*} \Rightarrow -\sum_{n=-\infty}^{\infty} \Delta \left|Sh_3(x)\right|^2 \left(\rho \beta^2 \left|\Theta_3\right|^2 - \alpha_n \gamma_3 \Upsilon_3 \Theta_3^{*}\right).$$

Because when $\tilde{\xi}_{(n)}$ is real, $\tilde{\zeta}_{(n)}$ is imaginary and vice-versa we obtain:

$$\left|\Upsilon_1\right|^2 = \frac{1}{\left|\gamma_2 G_2 \Delta\right|^2}\left(\alpha_n^2 r^2 \left|\tilde{\xi}_{(n)}\right|^2 + \beta^2 \left|\tilde{\zeta}_{(n)}\right|^2\right) = \frac{1}{\left|\gamma_2 G_2 \Delta\right|^2} \times E_1 .$$

$$\left|\Upsilon_3\right|^2 = \frac{1}{\left|\gamma_3 Sh_{30} \Delta\right|^2}\left(\alpha_n^2 r^2 \left|\tilde{\xi}_{(n)}\right|^2 + \beta^2 \left|\tilde{\zeta}_{(n)}\right|^2\right) = \frac{1}{\left|\gamma_3 Sh_{30} \Delta\right|^2} E_1 .$$

$$\left|\Theta_1\right|^2 = \frac{1}{\left|\rho \Delta G_1 \beta\right|^2}\left(\alpha_n^2 \left|\tilde{\zeta}_{(n)}\right|^2 + \beta^2 r^2 \left|\tilde{\xi}_{(n)}\right|^2\right) = \frac{1}{\left|\rho \Delta G_1 \beta\right|^2} E_3 .$$

$$\left|\Theta_3\right|^2 = \frac{1}{\left|\rho \Delta Sh_{30} \beta\right|^2} E_3 .$$

$$\Upsilon_3 \Theta_3^{*} = \frac{\alpha_n}{\gamma_3 \rho \Delta^2 \left|Sh_{30}\right|^2}\left(\left|\tilde{\xi}_{(n)}\right|^2 - r^2 \left|\tilde{\xi}_{(n)}\right|^2\right) = \frac{\alpha_n}{\gamma_3 \rho \Delta^2 \left|Sh_{30}\right|^2} E_2 \ddagger$$

$$\Upsilon_1 \Theta_1^{*} = \frac{\alpha_n}{\gamma_2 \rho \Delta^2 G_1^{*} G_2} E_2 \ddagger .$$

---

‡ Imaginary terms not included.

Expressions for the total power, equation (4.52)

CASE #1: $\gamma_1^2 > 0$; $\gamma_2^2 > 0$. $\gamma_1 = \sqrt{\gamma_1^2}$ and $\gamma_2 = \sqrt{\gamma_2^2}$.
Other variables defined by (4.48).

$$P = \frac{b}{2} \sum_{n=-\infty}^{\infty} \Delta \, \mathrm{Re} \left\{ \frac{1}{\rho \Delta^2} \left(\frac{K_1^2}{|\gamma_2 G_2|^2} \cdot E_1 - \gamma_{12} \frac{\alpha_n^2}{G_1 G_2} E_2 \right) \int_{-p}^{-d} |Ch_1(x)|^2 \, dx \right.$$

$$+ \frac{1}{\rho \Delta^2} \left(\frac{E_3}{G_1^2} - \gamma_{12} \frac{\alpha_n^2}{G_1 G_2} E_2 \right) \int_{-p}^{-d} |Sh_1(x)|^2 \, dx$$

$$+ \frac{1}{\rho \Delta^2} \frac{K_2^2}{|\gamma_2 G_2|^2} E_1 \int_{-d}^{0} \psi_1^2(x) \, dx$$

$$- \frac{1}{\rho \Delta^2} \frac{\alpha_n^2}{G_1 G_2} E_2 \int_{-d}^{0} \psi_1(x) \psi_2(x) \, dx$$

$$+ \frac{1}{\rho \Delta^2} \frac{E_3}{G_1^2} \int_{-d}^{0} \psi_3^2(x) \, dx$$

$$- \frac{1}{\rho \Delta^2} \frac{\alpha_n^2}{G_1 G_2} E_2 \int_{-d}^{0} \psi_3(x) \psi_4(x) \, dx$$

$$+ \frac{1}{\rho \Delta^2} \left(\frac{K_3^2}{|\gamma_1 Sh_{30}|^2} E_1 - \frac{\alpha_n^2}{|Sh_{30}|^2} E_2 \right) \int_{0}^{h} |Ch_3(x)|^2 \, dx$$

$$\left. + \frac{1}{\rho \Delta^2} \left(\frac{E_3}{|Sh_{30}|^2} - \frac{\alpha_n^2}{|Sh_{30}|^2} E_2 \right) \int_{0}^{h} |Sh_3(x)|^2 \, dx \right\}$$

CASE #1 (cont'd)

$$P = \frac{b}{2\rho} \sum_{n=-\infty}^{\infty} \frac{1}{\Delta} \operatorname{Re}\left\{ \left(\frac{K_1^2}{|\gamma_2 G_2|^2} E_1 - \gamma_{12} \frac{\alpha_n^2}{G_1 G_2} E_2 \right) I_1 \right.$$

$$+ \left(\frac{E_3}{G_1^2} - \gamma_{12} \frac{\alpha_n^2}{G_1 G_2} E_2 \right) I_2$$

$$+ \frac{K_2^2}{|\gamma_2 G_2|^2} E_1 I_3$$

$$- \frac{\alpha_n^2}{G_1 G_2} E_2 I_4 + \frac{1}{G_1^2} E_3 I_5 - \frac{\alpha_n^2}{G_1 G_2} E_2 I_6$$

$$+ \left(\frac{K_3^2}{|\gamma_1 Sh_{30}|^2} E_1 - \frac{\alpha_n^2}{|Sh_{30}|^2} \right) I_7$$

$$\left. + \left(\frac{E_3}{|Sh_{30}|^2} - \frac{\alpha_n^2}{|Sh_{30}|^2} E_2 \right) I_8 \right\} .$$

CASE #2: $\gamma_1^2 > 0$ and $\gamma_2^2 < 0$. Variables of equations (4A8) must be redefined. (Assume $\gamma_3 = \gamma_1$).

- $\gamma_1 \leftarrow \sqrt{\gamma_1^2}$
- $\gamma_2 \leftarrow j\,\gamma_2'$; $\gamma_2' \leftarrow \sqrt{-\gamma_2^2}$
- $\gamma_{12} \leftarrow -j\,\gamma_{12}'$; $\gamma_{12}' \leftarrow \gamma_1/\gamma_2'$
- $Ch_3(x) \leftarrow \cosh(\gamma_1(x-h))$
- $Sh_3(x) \leftarrow \sinh(\gamma_1(x-h))$
- $Ch_2(x) \leftarrow C_2(x)$; $C_2(x) = \cos(\gamma_2'(x+d))$
- $Sh_2(x) \leftarrow j\,S_2(x)$; $S_2(x) = \sin(\gamma_2'(x+d))$
- $Ch_1(x) \leftarrow Ch_1(x)$
- $Sh_1(x) \leftarrow Sh_1(x)$
- $G_1 \leftarrow G_1'$; $G_1' = Sh_{1d}\,C_2(0) + \gamma_{12}'\,Ch_{1d}\,S_2(0)$
- $G_2 \leftarrow j\,G_2'$; $G_2' = \varepsilon_{12}\,Ch_{1d}\,S_2(0) - \gamma_{12}'\,Sh_{1d}\,C_2(0)$
- $G_{12} \leftarrow -j\,G_{12}'$; $G_{12}' \leftarrow G_1'/G_2'$
- $\psi_1(x) \leftarrow \psi_1'(x)$; $\psi_1'(x) = \varepsilon_{12}\,Ch_{1d}\,C_2(x) + \gamma_{12}'\,Sh_{1d}\,S_2(x)$
- $\psi_2(x) \leftarrow j\,\psi_2'(x)$; $\psi_2'(x) = Sh_{1d}\,S_2(x) - \gamma_{12}'\,Ch_{1d}\,C_2(x)$
- $\psi_3(x) \leftarrow \psi_3'(x)$; $\psi_3'(x) = Sh_{1d}\,C_2(x) + \gamma_{12}'\,Ch_{1d}\,S_2(x)$
- $\psi_4(x) \leftarrow j\,\psi_4'(x)$; $\psi_4'(x) = \varepsilon_{12}\,Ch_{1d}\,S_2(x) - \gamma_{12}'\,Sh_{1d}\,C_2(x)$

CASE #2 (cont'd)

$$P = \frac{b}{2\rho} \sum_{n=-\infty}^{\infty} \frac{1}{\Delta} \mathrm{Re}\left\{ \left(\frac{K_1^2}{|\gamma_2' G_2'|^2} E_1 + \gamma_{12}' \frac{\alpha_n^2}{G_1' G_2'} E_2 \right) I_1 \right.$$

$$+ \left(\frac{E_3}{G_1'^2} + \gamma_{12}' \frac{\alpha_n^2}{G_1' G_2'} E_2 \right) I_2$$

$$+ \frac{K_2^2}{|\gamma_2' G_2'|^2} E_1 I_3' - \frac{\alpha_n^2}{G_1' G_2'} E_2 I_4'$$

$$+ \frac{E_3}{G_1'^2} I_5' - \frac{\alpha_n^2}{G_1' G_2'} E_2 I_6'$$

$$+ \left(\frac{K_3^2}{|\gamma_1 Sh_{30}|^2} E_1 - \frac{\alpha_n^2}{|Sh_{30}|^2} E_2 \right) I_7$$

$$\left. + \left(\frac{E_3}{|Sh_{30}|^2} - \frac{\alpha_n^2}{|Sh_{30}|^2} E_2 \right) I_8 \right\} .$$

$I_1, \ldots, I_8$ are defined in a manner similar to CASE #1.

CASE #3: $\gamma_1^2 < 0$ and $\gamma_2^2 < 0$. Variables of equations (4.48) must be redefined (assume $\gamma_3 = \gamma_1$).

- $\gamma_1 \leftarrow j\gamma_1'$; $\gamma_1' = \sqrt{-\gamma_1^2}$
- $\gamma_2 \leftarrow j\gamma_2'$; $\gamma_2' = \sqrt{-\gamma_2^2}$
- $\gamma_{12} \leftarrow \gamma_{12}'$; $\gamma_{12}' = \gamma_1'/\gamma_2'$
- $Ch_3(x) \leftarrow C_3(x)$; $C_3(x) = \cos(\gamma_1'(x-h))$
- $Sh_3(x) \leftarrow jS_3(x)$; $S_3(x) = \sin(\gamma_1'(x-h))$
- $Ch_2(x) \leftarrow C_2(x)$; $C_2(x) = \cos(\gamma_2'(x+d))$
- $Sh_2(x) \leftarrow jS_2(x)$; $S_2(x) = \sin(\gamma_2'(x+d))$
- $Ch_1(x) \leftarrow C_1(x)$; $C_1(x) = \cos(\gamma_1'(x+p))$
- $Sh_1(x) \leftarrow jS_1(x)$; $S_1(x) = \sin(\gamma_1'(x+p))$
- $Sh_{1d} \leftarrow jS_{1d}$; $S_{1d} = S_1(-d)$
- $Ch_{1d} \leftarrow C_{1d}$; $C_{1d} = C_1(-d)$
- $Sh_{30} \leftarrow jS_{30}$; $S_{30} = S_3(0)$
- $G_1 \leftarrow jG_1'$; $G_1' = S_{1d}C_2(0) + \gamma_{12}' C_{1d} S_2(0)$
- $G_2 \leftarrow jG_2'$; $G_2' = \varepsilon_{12} C_{1d} S_2(0) + \gamma_{12}' S_{1d} C_2(0)$
- $G_{12} \leftarrow G_{12}'$; $G_{12}' = G_1'/G_2'$
- $\psi_1(x) \leftarrow \psi_1'(x)$; $\psi_1'(x) = \varepsilon_{12} C_{1d} C_2(x) - \gamma_{12}' S_{1d} S_2(x)$
- $\psi_2(x) \leftarrow \psi_2'(x)$; $\psi_2'(x) = -S_{1d} S_2(x) + \gamma_{12}' C_{1d} C_2(x)$
- $\psi_3(x) \leftarrow j\psi_3'(x)$; $\psi_3'(x) = S_{1d} C_2(x) + \gamma_{12}' C_{1d} S_2(x)$
- $\psi_4(x) \leftarrow j\psi_4'(x)$; $\psi_4'(x) = \varepsilon_{12} C_{1d} S_2(x) + \gamma_{12}' S_{1d} C_2(x)$.

CASE #3 (cont'd)

$$P = \frac{b}{2\rho} \sum_{n=-\infty}^{\infty} \frac{1}{\Delta} \mathrm{Re}\left\{ \left(\frac{K_1^2}{|\gamma_2' G_2'|^2} E_1 + \gamma_{12}' \frac{\alpha_n^2}{G_1' G_2'} E_2 \right) I_1' \right.$$

$$+ \left(\frac{E_3}{|G_1'|^2} - \gamma_{12}' \frac{\alpha_n^2}{G_1' G_2'} E_2 \right) I_2'$$

$$+ \frac{K_2^2}{|\gamma_2' G_2'|^2} E_1 I_3' + \frac{\alpha_n^2}{G_1' G_2'} E_2 I_4'$$

$$+ \frac{E_3}{|G_1'|^2} I_5' - \frac{\alpha_n^2}{G_1' G_2'} E_2 I_6'$$

$$+ \left(\frac{K_3^2}{|\gamma_1' S_{30}|^2} E_1 + \frac{\alpha_n^2}{|S_{30}|^2} E_2 \right) I_7'$$

$$\left. + \left(\frac{E_3}{|S_{30}|^2} - \frac{\alpha_n^2}{|S_{30}|^2} E_2 \right) I_8' \right\}.$$

$I_1', \ldots, I_8'$ defined in a manner similar to case #1.

For cases # 1,2,3 we have

$$\text{total power} = P = \frac{b}{2\rho} \sum_{n=-\infty}^{\infty} \text{power term}(n) \; .$$

Since in all cases power term(n) = power term(-n) we obtain:

$$\text{total power} = \frac{b}{2\rho} \left[\text{power term}(0) + 2 \sum_{n=1}^{\infty} \text{power term}(n) \right]$$

$$= \frac{b}{\rho} \cdot \left[\frac{\text{power term}(0)}{2} + \sum_{n=1}^{\infty} \text{power term}(n) \right] .$$

CPLFIN.PAS

```
{ Program cplfin.pas. Version 3. october, 1987.

  This version uses an input file instead of interactive input.
  A number of executions with different data can be specified
  in this data file.  See DATA_FIL.PAS.

  Calculation of epsilon effective and impedance
  of coupled slots in unilateral finlines for both the even and
  odd modes of excitation.  Two basis-functions are used.
  See thesis by Sylvain Labonte, chapter 4 and appendix A.}

const
   c                    =2.9979e11;    {millimeters/second}
   eta0                 =377;          {ohms}
type
   array2x2             =array[1..2,1..2] of real;
   screenline           =string[80];
   string8              =string[8];
   string3              =string[3];
var
   eps_eff              :real;     {epsilon effective of coupled slots}
   eps_even_guess,
   eps_odd_guess        :real;     {initial guesses}
   z                    :real;     {characteristic impedance of each slot in the presence of the other}

   a,b,w,s,d,e,h,u,v,p,q,r  :real;     {physical dimensions}
   freq,k0,k1,k2,k3         :real;     {signal's characteristics and wave numbers}
   epsr1,epsr2              :real;     {properties of substrate and}
   epsr12,epsr12_2          :real;     {derived quantities}

   total_power,voltage      :real;     {for characteristic impedance calculation}
   basis_func_ratio         :real;     {the relative amplitudes of basis functions}
   nterms_eps               :integer;  {number of spectral terms for eps. eff}
   nterms_z                 :integer;  {number of spec terms for impedance}
   nterms_ratio             :integer;  {number of spec terms for basis_func_ratio}
   nruns,index              :integer;     {total number of executions and}
                                          {index of data_vector to modify at each execution}
   basis_func: array[0..2000] of array2x2;  {fourier series coef.of basis_func}
   transv_adm               :array2x2;     {admittance matrix for each spectral term}
   eigen_matrix             :array2X2;     {the matrix to solve for basis_func_ratio}
   data_vector              :array[1..30] of real;

   mode                     :string[4];
   output_file              :text;
   output_line              :integer;
   outfilename              :string[15];
   counter,i                :integer;
   date,time                :string8;
   day                      :string3;
{_____________________________________________________________________}

{Include math package for hyperbolic and bessel functions and the
routines to get the date and time}

{$I MATH_PAK.LIB}
{$I CALENDAR.LIB}
```

```
{Include the routines transv_ada and power_term plus misc. routines}

{$I CPLFIN.AUX}
{_____________________________________________________________________}

function conv_criterion(x_low,x_high,y_low,y_high: real):real;
{
   the convergence criterion used in root finding algorithm for eps_eff.
   The root is known to be between x_low and x_high
}
begin
   conv_criterion:=abs(0.001*(y_high-y_low)/(x_high-x_low));
{    conv_criterion:=1.e-10}
end;
{_____________________________________________________________________}

procedure get_voltage;
{equals the integral of Ey field across one slot}
{see p.54 and foll.}

begin
   voltage:=b*basis_func_ratio;
{  voltage:=w;}
end;
{_____________________________________________________________________}

procedure get_basis_func(n: integer);

  {calculates a 2x2 matrix whose elements are fyfy, fyfz, fzfy, fzfz,
   the basis functions (transforms) of the Efields in y and z for the nth
   spectral term. See page 54 and foll.}

var
   alphan:              real;
   fy,fz:               real;
   temp:                real;
begin
   alphan:=pi*n/b;

   if mode='EVEN' then          {even mode excitation}
   begin

      if n=0 then fy:=0
      else fy:=(sin(alphan*q)+sin(alphan*r))*bessj0(alphan*w/2); {cosine with edge term}
{      else fy:=(cos(alphan*(b-v))-cos(alphan*(b-u))+cos(alphan*u)-
             cos(alphan*v))/alphan/b;}      {constant}

      if n=0 then fz:=0
      else fz:=(sin(alphan*q)+sin(alphan*r))*bessjn(2,alphan*w/2)/alphan; {cosine}

   end
   else begin                   {odd mode excitation}

      if n=0 then fy:=2.   {cosine with edge term}
{      if n=0 then fy:=2*w/b}    {constant}
      else fy:=(cos(alphan*q)+cos(alphan*r))*bessj0(alphan*w/2);  {cosine with edge term}
{      else fy:=(sin(alphan*(b-u))-sin(alphan*(b-v))+sin(alphan*v)-
             sin(alphan*u))/alphan/b;}   {constant}
```

```
      if n=0 then fz:=0
      else fz:=(cos(alphan*r)+cos(alphan*q))*bessjn(2,alphan*w/2)/alphan;

   end;

   basis_func[n][1,1]:=fy*fy;
   basis_func[n][1,2]:=fy*fz;
   basis_func[n][2,1]:=basis_func[n][1,2];
   basis_func[n][2,2]:=fz*fz;

end;
{_____________________________________________________________________}

function char_eq(eeff: real;first_time: boolean): real;    {eeff is local}

   {computes the char. eq.(det. of the eigen_matrix) for a given eeff.
    Each term of the 2x2 eigen_matrix is a "semi-infinite" summation (trun-
    cated after nterms_eps) of the products of a basis_func(n) and a
    transv_adm(n,eeff) see equation (4.38) p.57.
    Basis_func(n) is computed only once and stored in the array
    basis_func[n].  }

var
   n,i,j,line         :integer;
   resultmat          :array2x2;

begin

   for i:=1 to 2                    {clear  eigen_matrix}
   do begin
      for j:=1 to 2  do
      eigen_matrix[i,j]:=0.;
   end;

   if mode='ODD ' then      {there is an n=0 term for the odd mode only}
   begin
      get_transv_adm(0,eeff);
      get_basis_func(0);
      eigen_matrix[1,1]:=transv_adm[1,1]*basis_func[0][1,1]/2;
   end;

   if first_time then
   begin
      for n:=1 to nterms_eps do       {compute basis_func[n] for all n up to}
      begin                           {nterms_eps}
(*         gotoxy(53,12);write(n:4);*)
         get_basis_func(n);           {basis_func[n] is a 2d matrix}
         get_transv_adm(n,eeff);
         mtimes(basis_func[n],transv_adm,resultmat);    {matrix "scalar" prod}
         mplus(resultmat,eigen_matrix,eigen_matrix);    {matrix add.}
      end
   end
   else
   begin
      for n:=1 to nterms_eps do      {basis_func[n] has been calculated earlier}
      begin
(*         gotoxy(53,12);write(n:4);   *)
```

```
        get_transv_ada(n,eeff);
        mtimes(basis_func[n],transv_ada,resultmat);    {matrix "scalar" prod}
        mplus(resultmat,eigen_matrix,eigen_matrix);    {matrix add.}
      end
    end;

    char_eq:=determinant_of(eigen_matrix);

(*  if mode='ODD ' then line:=21;          {print intermediate results}
    if mode='EVEN' then line:=19;
    gotoxy(1,line); clreol;
    write(eigen_matrix[1,1]:3,' ',eigen_matrix[1,2]:3,' ',
          eigen_matrix[2,1]:3,' ',eigen_matrix[2,2]:3);*)
end;
{_____________________________________________________________}

procedure get_eps_eff;          {eps_eff is global}

    {Finds a root for the characteristic equation (see pages 49 and 58) }

var
    eeff_low,eeff_high,eeff_mid:        real;
    F_low,F_high,F_mid:                 real;
    conv:                               real;
    it:                                 integer;
    flag:                               boolean;
    str1,str2,str3:                     screenline;

begin
    gotoxy(1,24); clreol;
    write_bv('Solving for epsilon effective... ');

    if mode = 'EVEN' then eeff_low:=eps_even_guess    {initial guesses}
    else eeff_low:=eps_odd_guess;

    eeff_high:=eeff_low;
    flag:=true;

    repeat                              {vary low and high in a systematic way}
      eeff_low:= eeff_low*0.9;          {so that the interval contains a root}
      eeff_high:=eeff_high*1.1;

      str(eeff_low:6:3,str1); str(eeff_high:6:3,str2);
      gotoxy(35,24); write('['+str1+','+str2+' ]   ');

      F_low:=char_eq(eeff_low,flag);  {the flag only indicates whether char_eq}
      flag:=false;                    {is executed for the first time or not}
      F_high:=char_eq(eeff_high,flag);

    until ((F_low*F_high) <= 0) or (eeff_high > epsr2);

{problem here because eeff_high can be higher than epsr2 with the root
 lower than epsr2.  This test must be improved.}

    if eeff_high > epsr2 then   {set parameters so that the remaining of this}
    begin                       {routine is skipped}
      it:=10;
      F_mid:=1;
```

This algorithm must be improved so as to make sure that the value found for epsilon effective (root of char_eq), is indeed the highest one smaller than epsilon relative (for the dominant mode).

See pages 49 and 58 of thesis.

```
   end
   else                        {find the root between low and high}
   begin
      eeff_mid:=eeff_low;
      F_mid:=F_low;
      it:=0;
   end;

   conv:=conv_criterion(eeff_low,eeff_high,F_low,F_high);
(*   str(conv:3,str3); gotoxy(35,24); clreol; write_bw(str3);*)

   while (abs(F_mid) > conv) and (it < 10)
   do begin

      if (F_mid*F_low) >= 0          {eeff_mid and eeff_low on same side}
      then begin
         eeff_low:=eeff_mid;
         F_low:=F_mid;
      end
      else begin                     {eeff_mid and eeff_low not on same side}
         eeff_high:=eeff_mid;
         F_high:=F_mid;
      end;

      eeff_mid:=regulafalsi(eeff_low,eeff_high,F_low,F_high);
      F_mid:=char_eq(eeff_mid,flag);

      it:=it+1;

      gotoxy(56,24); write(it,'  ',F_mid:3);

   end;

   if (abs(F_mid) <= conv)        {the root is found}
   then eps_eff:=eeff_mid
   else  eps_eff:= -1;            {no root found}

end;
{_____________________________________________________________________}

procedure get_basis_func_ratio;

 {This procedure solves the system [eigen_matrix][a,b]=0 for a/b, the
 relative amplitude of Efield y over z (here called the basis_func_ratio
 and in the thesis called r, see page 58).
 At this point the determinant of eigen_matrix has been used to compute
 eps_eff.  However even though the determinant converged to a constant value
 with nterms_eps spectral terms, each entry of eigen_matrix generally needs
 more. Therefore more spectral terms are included in eigen_matrix prior to
 the solution of the system.}

var
   n                    :integer;
   resultmat            :array2x2;
begin

   for n:=nterms_eps to nterms_ratio do     {computation of eigen_matrix }
   begin                                    {for larger spectral terms}
```

```
(*      gotoxy(53,14);write(n:4);*)
      get_basis_func(n);          {basis_func[n] is a 2d matrix}
      get_transv_ada(n,eps_eff);
      mtimes(basis_func[n],transv_ada,resultmat);    {matrix "scalar" prod}
      mplus(resultmat,eigen_matrix,eigen_matrix);    {matrix add.}
   end;

   basis_func_ratio:=-eigen_matrix[2,2]/eigen_matrix[2,1];
end;
{_____________________________________________________________________}

procedure weigh_basis_functions;

 { This procedure multiplies basis_func[n][1,1] by sqr(basis_func_ratio)
 to account for the relative amplitudes of the y and z Efields in computation
 of power. (see Expressions for Poynting vectors, appendix a)

var
   n                    :integer;
begin
   for n:=0 to nterms_z do
   begin
      basis_func[n][1,1]:=sqr(basis_func_ratio)*basis_func[n][1,1];
   end
end;
{_____________________________________________________________________}

procedure get_total_power;

(see appendix a)

var
   n:                   integer;
   temp:                real;

begin

   if mode='ODD ' then         {only ODD mode has a n=0 term}
      temp:=power_term(0)/2
   else temp:= 0.0;

   for n:=1 to nterms_z do     {calculate the total power in the cross-section}
   begin
(*      gotoxy(53,13);write(n:4);*)
      temp:=temp+power_term(n);
   end;

   total_power:=temp*b/eta0*sqrt(eps_eff);
end;
{_____________________________________________________________________}

procedure get_z;
var
   str1,str2               :screenline;
begin
   gotoxy(1,24); clreol; write_bw('Solving for impedance...  ');

   get_basis_func_ratio;  (get the relative amplitudes of Ey and Ez)
```

```
  weigh_basis_functions; {multiply the basis_functions by basis_func_ratio}
  get_voltage;           {voltage also depends on basis_func_ratio}
  get_total_power;

{*  str(voltage:4,str1); str(total_power:4,str2);
  gotoxy(35,19); clreol; write_bw('  '+str1+'  '+str2);*}

  z:=sqr(voltage)/2/(total_power/2);
  gotoxy(1,24); clreol;
end;
{_____________________________________________________________}

procedure compute_and_print_results;
var
  n                    :integer;
  alphan               :real;
begin
  gotoxy(1,output_line);write(mode,' MODE  ');

  get_eps_eff;

  gotoxy(12,output_line);
  case trunc(eps_eff) of
      -1: begin
          writeln('  Eeff is:  No convergence');
          z:=0;              {bypass the calculation of z}
          end;
     else begin
          write('  Eeff is:  ',eps_eff:7:3);
          get_z;
          end;
  end;
  gotoxy(35,output_line);
  write('  V**2/2P impedance is:   ',z:7:0,'   ohms');
end;
{_____________________________________________________________}

procedure output_onto_file;
begin
  if mode='EVEN' then
  begin
  writeln(output_file,'=============================================================='+day+' '+date+' '+time);
  writeln(output_file,'   a   ','   h   ','   b   ','   w   ','   s   ','   d   ',
         'epsr2 ','  freq','   n_eps','  n_z','   n_rat');
  writeln(output_file,a:6:3,' ',h:6:3,' ',b:6:3,' ',w:6:3,' ',s:6:3,' ',d:6:3,
         ' ',epsr2:4:1,'  ',freq:3,' ', nterms_eps:4,'  ',nterms_z:4,' ',nterms_ratio:5);
  writeln(output_file,'_____________________________________________________________________________');
  end;

  writeln(output_file,mode,' MODE','   eps= ',eps_eff:6:3,'  z= ',z:4:0);
  writeln(output_file,'Ratio= ',basis_func_ratio:5:1);
  writeln(output_file);
end;
{_____________________________________________________________}

procedure echo_data;
begin
  clrscr;
```

```
   writeln('        Spectral Domain Analysis of Coupled Unilateral Finlines');
   writeln('    This program calculates epsilon effective and impedance using the');
   writeln('SDA-method. Two basis functions are used for the slot''s Ey and Ez fields');
   writeln('Waveguide width  (a) in mm        > ',a:6:3);
   writeln('Distance from wall to metal (h) mm > ',h:6:3);
   writeln('Waveguide height (b) in mm        > ',b:6:3);
   writeln('Slot width (w) in mm              > ',w:6:3);
   writeln('Slot Spacing (s) in mm            > ',s:6:3);
   writeln('Substrate thickness (d) in mm     > ',d:6:3);
   writeln('Relative dielectric constant      > ',epsr2:5:1);
   writeln('Operating frequency in Hz         > ',freq:3);
   writeln('Nterms spectral terms for epsilon > ',nterms_eps:4);
   writeln('Ntermsz spec terms for z          > ',nterms_z:4);
   writeln('Nterms_ratio                      > ',nterms_ratio:5);
   writeln('_____________________________________________________________________');

end;
{_____________________________________________________________}

procedure update_data_vector;
begin
    data_vector[index]:=data_vector[15+counter];
end;
{_____________________________________________________________}

procedure get_data_from_vector;
begin
   a:=data_vector[1];
   h:=data_vector[2];
   b:=data_vector[3];
   w:=data_vector[4];
   s:=data_vector[5];
   d:=data_vector[6];
   epsr2:=data_vector[7];
   eps_even_guess:=data_vector[8];
   eps_odd_guess:=data_vector[9];
   freq:=data_vector[10];
   nterms_eps:=trunc(data_vector[11]);
   nterms_z:=trunc(data_vector[12]);
   nterms_ratio:=trunc(data_vector[13]);
   nruns:=trunc(data_vector[14]);
   index:=trunc(data_vector[15]);

   freq:=freq*1e9;              {freq in hertz}
   u:=s/2;                      {derived physical dimensions}
   v:=s/2+w;
   p:=a-h;
   e:=a-d-h;
   q:=s/2+w/2;
   r:=b-q;
   epsr1:=1;
   k0:=2*pi*freq/c;             {wave numbers}
   k1:=sqrt(epsr1)*k0;
   k2:=sqrt(epsr2)*k0;
   k3:=k1;
   epsr12:=epsr1/epsr2;         {derived quantities}
   epsr12_2:=sqr(epsr12);
   Date_Time_Week(date, time, day);
```

```
end;
{_____________________________________________________________________}

procedure input_data_vector;
{
 The outputs are: outfilename, data_vector}

var
   inputfile              :text;
   string15               :string[15];
   endfile,dataread       :boolean;
   IOres,i                :integer;
            {_____________________________________________}

            procedure seek_delimiter(var endfile:boolean);   {local procedure}
            begin
               repeat
                  readln(inputfile,string15);
                  endfile:=eof(inputfile);
               until (string15='---------------') or endfile;
            end;
            {_____________________________________________}

begin
   repeat
      write('Enter input file name:   ');readln(string15);
      {$I-}
      assign(inputfile,string15);
      reset(inputfile);
      {$I+}
      IOres:=IOresult;
      if IOres <> 0 then
         writeln('Unable to open file:  ',string15)
      else begin
         seek_delimiter(endfile);
         if endfile then
         begin
            writeln('Unable to find data in this file');
            dataread:=false;
         end
         else begin
            readln(inputfile,outfilename);

            for i:=1 to 14 do
               readln(inputfile,data_vector[i]);
            if data_vector[14]>1 then
            begin
               seek_delimiter(endfile);
               if endfile then
               begin
                  write'n('Unable to find data in this file');
                  dataread:=false;
               end
               else begin
                  i:=15;
                  repeat
                     readln(inputfile,data_vector[i]);
                     i:=i+1;
```

```
            until eof(inputfile);
            dataread:=true;
          end;
        end
        else dataread:=true;
      end;
    end;
    close(inputfile);
  until (IOres = 0) and dataread;
end;
{_____________________________________________________________}

(************************* MAIN BLOCK BEGINS ********************************)

begin

  for i:=1 to 30 do        {clear data_vector}
    data_vector[i]:=0;

  input_data_vector;       {read from disk: outfilename and data_vector}
  get_data_from_vector;    {assign values to a,h,b,w,s,d,epsr2,
                            eps_even_guess,eps_odd_guess,
                            freq,nterms_eps,nterms_z,
                            nterms_ratio,nruns,index+derived quantities,
                            as obtained from data_vector}

  assign(output_file,outfilename);
  rewrite(output_file);

  for counter:=1 to nruns
  do begin
    echo_data;

    mode:='EVEN';
    output_line:=18;
    compute_and_print_results;   {print on screen}
    output_onto_file;

    mode:='ODD.';
    output_line:=20;
    compute_and_print_results;
    output_onto_file;

    update_data_vector;          {execution with different data}
    get_data_from_vector;
  end;
  close(output_file);
  ring_bell;
end.
```

CPLFIN.AUX

```
{
    This file is to be included in CPLFIN.PAS for calculation of
    coupled finline characteristics.
{
{_____}

procedure ring_bell;
begin
   write(^g);
end;
{_____}

procedure write_bw(message:screenline);

   {Writes the message black on white.  Message must be a CHARACTER string.}

begin
   textbackground(white+blink); textcolor(black+blink);
   write(message);
   textbackground(black); textcolor(white);
end;
{_____}

procedure mplus(mat1,mat2:array2x2; var result: array2x2);
{2x2 matrix addition}

var
   i,j:                integer;
begin
   for i:=1 to 2
   do begin
      for j:=1 to 2 do
      result[i,j]:=mat1[i,j]+mat2[i,j];
   end;
end;
{_____}

procedure mtimes(mat1,mat2:array2x2; var result: array2x2);
{2x2 matrix term by term multiplication}

var
   i,j:                integer;
begin
   for i:=1 to 2
   do begin
      for j:=1 to 2 do
      result[i,j]:=mat1[i,j]*mat2[i,j];
   end;
end;
{_____}

function determinant_of (mat: array2x2):real;
begin
   determinant_of:=mat[1,1]*mat[2,2]-mat[1,2]*mat[2,1];
end;
{_____}

function regulafalsi(x_low,x_high,y_low,y_high:real): real;
```

```
{algorithm for root search.  The root is between x_low and x_high}

begin
   regulafalsi:=x_low-y_low*(x_high-x_low)/(y_high-y_low);
end;
{_____________________________________________________________________}

function gam_square(alphan,eeff,epsr: real): real;
{see thesis p.47 equation 4.14}

begin
   gam_square:=sqr(alphan)+(eeff-epsr)*sqr(k0);
end;
{_____________________________________________________________________}

procedure get_transv_adm(n: integer; eeff:real);        {eeff is local}

   {computes the transv. admittance for a spect. term n, and for one epsilon
   effective, eeff. transv_adm is a 2x2 matrix.  See appendix A for the
   expressions of admittance.}

var
   gamma2_square,gamma1_square:   real;
   gamma2,gamma1:                 real;
   alphan:                        real;
   beta_2,delta,beta:             real;
   g1_h,g1_e,g2_d:                real;
   er1_g1,er2_g2:                 real;
   Ye,Yh:                    real;

begin
   alphan:=pi*n/b;
   beta_2:=eeff*sqr(k0);
   beta:=sqrt(beta_2);
   delta:=sqr(alphan)+beta_2;

   gamma1_square:=gam_square(alphan,eeff,epsr1);
   gamma2_square:=gam_square(alphan,eeff,epsr2);

   if gamma1_square < 0            {both gamma's are imaginary}
   then begin

      gamma1:=sqrt(-gamma1_square);
      gamma2:=sqrt(-gamma2_square);
      g1_h:=gamma1*h;
      g1_e:=gamma1*e;
      g2_d:=gamma2*d;
      er1_g1:=epsr1/gamma1;
      er2_g2:=epsr2/gamma2;
      Ye:=er1_g1*cot(g1_e)-er2_g2*tan(g2_d);
      Ye:=Ye/(er2_g2+er1_g1*cot(g1_e)*tan(g2_d));
      Ye:=-er1_g1*cot(g1_h)-er2_g2*Ye;
      Yh:=gamma1*cot(g1_e)-gamma2*tan(g2_d);
      Yh:=Yh/(gamma2+gamma1*cot(g1_e)*tan(g2_d));
      Yh:=gamma1*cot(g1_h)+gamma2*Yh;
   end
   else begin                      {gamma1 real, gamma2 imaginary}
      if gamma2_square < 0
```

```
    then begin
       gamma1:=sqrt(gamma1_square);
       gamma2:=sqrt(-gamma2_square);
       g1_h:=gamma1*h;
       g1_e:=gamma1*e;
       g2_d:=gamma2*d;
       er1_g1:=epsr1/gamma1;
       er2_g2:=epsr2/gamma2;
       Ye:=er1_g1*coth(g1_e)+er2_g2*tan(g2_d);
       Ye:=Ye/(er2_g2-er1_g1*coth(g1_e)*tan(g2_d));
       Ye:=er1_g1*coth(g1_h)+er2_g2*Ye;
       Yh:=gamma1*coth(g1_e)-gamma2*tan(g2_d);
       Yh:=Yh/(gamma2+gamma1*coth(g1_e)*tan(g2_d));
       Yh:=gamma1*coth(g1_h)+gamma2*Yh;
    end
    else begin                          (both gamma's real)
       gamma1:=sqrt(gamma1_square);
       gamma2:=sqrt(gamma2_square);
       g1_h:=gamma1*h;
       g1_e:=gamma1*e;
       g2_d:=gamma2*d;
       er1_g1:=epsr1/gamma1;
       er2_g2:=epsr2/gamma2;
       Ye:=er1_g1*coth(g1_e)+er2_g2*tanh(g2_d);
       Ye:=Ye/(er2_g2+er1_g1*coth(g1_e)*tanh(g2_d));
       Ye:=er1_g1*coth(g1_h)+er2_g2*Ye;
       Yh:=gamma1*coth(g1_e)+gamma2*tanh(g2_d);
       Yh:=Yh/(gamma2+gamma1*coth(g1_e)*tanh(g2_d));
       Yh:=gamma1*coth(g1_h)+gamma2*Yh;
    end;
  end;

  transv_adm[1,1]:=(sqr(alphan)*Ye-eeff*Yh)/delta;
  transv_adm[1,2]:=alphan*beta*(Ye+Yh/sqr(k0))/delta;
  transv_adm[2,1]:=transv_adm[1,2];
  transv_adm[2,2]:=(beta_2*Ye-sqr(alphan/k0)*Yh)/delta;

end;
{_____________________________________________________________________}

function power_term(n: integer):real;

   {These are the big formulae for the expression of power for each spectral
   term in the cross-section for the three conditions on gamma1 and gamma2.
   See appendix A}

var
  alphan,alphan_2,beta_2,delta,
  gam1,gam2,gam1_2,gam2_2,gam12,gam12_2,
  fy_2,fz_2,e1,e2,e3,
  s1d,s1d_2,c1d,c1d_2,c20,s20,s30,
  sh1d,sh1d_2,ch1d,ch1d_2,ch20,sh20,sh30,
  g1,g2,g12,
  p1,s1,p2,s2,p3,s3,cc2,ss2,sc2,
  i1,i2,i3,i4,i5,i6,i7,i8,
  temp,I1,f2                          :real;

begin
```

```
alphan:=pi*n/b; alphan_2:=sqr(alphan);
beta_2:=eps_eff*sqr(k0);
delta:=alphan_2+beta_2;

gam1_2:=gam_square(alphan,eps_eff,epsr1);
gam2_2:=gam_square(alphan,eps_eff,epsr2);

fy_2:=basis_func[n][1,1]; fz_2:=basis_func[n][2,2];
e1:=alphan_2*fy_2+beta_2*fz_2; e2:=fz_2-fy_2; e3:=alphan_2*fz_2+beta_2*fy_2;


if gam1_2 < 0          {both gamma's are imaginary}
then begin
   gam1:=sqrt(-gam1_2); gam2:=sqrt(-gam2_2);
   gam12:=gam1/gam2; gam12_2:=sqr(gam12);

   s1d:=sin(gam1*(p-d)); s1d_2:=sqr(s1d); c1d:=cos(gam1*(p-d)); c1d_2:=sqr(c1d);
   c20:=cos(gam2*(d)); s20:=sin(gam2*(d)); s30:=sin(gam1*h);
   g1:=s1d*c20+gam12*c1d*s20; g2:=epsr12*c1d*s20+gam12*s1d*c20; g12:=g1/g2;

   f2:=alphan_2*e2/g1/g2;

   s1:=sin(2*gam1*(p-d))/4/gam1; p1:=(p-d)/2;
   s2:=sin(2*gam2*d)/4/gam2; p2:=d/2;
   s3:=sin(2*gam1*h)/4/gam1; p3:=h/2;
   cc2:=s2+p2; ss2:=p2-s2; sc2:=sqr(sin(gam2*d))/2/gam2;

   i1:=c1d*s1d*sc2;

   i1:=p1+s1; i2:=p1-s1;
   i3:=epsr12_2*c1d_2*cc2+gam12_2*s1d_2*ss2-2*epsr12*gam12*i1;
   i4:=epsr12*gam12*c1d_2*cc2+gam12*s1d_2*ss2-(epsr12+gam12_2)*i1;
   i5:=s1d_2*cc2+gam12_2*c1d_2*ss2+2*gam12*i1;
   i6:=gam12*s1d_2*cc2+epsr12*gam12*c1d_2*ss2+(epsr12+gam12_2)*i1;
   i7:=p3+s3; i8:=p3-s3;

   temp:=e1/sqr(gam2*g2)*(sqr(k1)*i1+sqr(k2)*i3)+
         f2*(gam12*(i1-i2)+i4-i6)+
         e3/sqr(g1)*(i2+i5)+
         ((sqr(k3/gam1)*e1+alphan_2*e2)*i7+delta*fy_2*i8)/sqr(s30);
end
else begin
   if gam2_2 < 0      {gamma1=real, gamma2 imaginary}
   then begin

   gam1:=sqrt(gam1_2); gam2:=sqrt(-gam2_2);
   gam12:=gam1/gam2; gam12_2:=sqr(gam12);

   sh1d:=sinh(gam1*(p-d)); sh1d_2:=sqr(sh1d); ch1d:=cosh(gam1*(p-d)); ch1d_2:=sqr(ch1d);
   c20:=cos(gam2*(d)); s20:=sin(gam2*(d)); sh30:=sinh(gam1*h);
   g1:=sh1d*c20+gam12*ch1d*s20; g2:=epsr12*ch1d*s20-gam12*sh1d*c20; g12:=g1/g2;

   f2:=alphan_2*e2/g1/g2;

   s1:=sinh(2*gam1*(p-d))/4/gam1; p1:=(p-d)/2;
   s2:=sin(2*gam2*d)/4/gam2; p2:=d/2;
   s3:=sinh(2*gam1*h)/4/gam1; p3:=h/2;
   cc2:=s2+p2; ss2:=p2-s2; sc2:=sqr(sin(gam2*d))/2/gam2;
```

```
    i1:=chld*shld*sc2;

    i1:=p1+s1; i2:=s1-p1;
    i3:=epsr12_2*chld_2*cc2+gam12_2*shld_2*ss2+2*epsr12*gam12*i1;
    i4:=-epsr12*gam12*chld_2*cc2+gam12*shld_2*ss2+(epsr12-gam12_2)*i1;
    i5:=shld_2*cc2+gam12_2*chld_2*ss2+2*gam12*i1;
    i6:=-gam12*shld_2*cc2+epsr12*gam12*chld_2*ss2+(epsr12-gam12_2)*i1;
    i7:=p3+s3; i8:=s3-p3;

    temp:=e1/sqr(gam2*g2)*(sqr(k1)*i1+sqr(k2)*i3)+
          f2*(gam12*(i1+i2)-i4-i6)+
          e3/sqr(g1)*(i2+i5)+
          ((sqr(k3/gam1)*e1-alphan_2*e2)*i7+delta*fy_2*i8)/sqr(sh30);

    end
    else begin                  {both gamma's real}

    gam1:=sqrt(gam1_2); gam2:=sqrt(gam2_2);
    gam12:=gam1/gam2; gam12_2:=sqr(gam12);

    shld:=sinh(gam1*(p-d)); shld_2:=sqr(shld); chld:=cosh(gam1*(p-d)); chld_2:=sqr(chld);
    ch20:=cosh(gam2*(d)); sh20:=sinh(gam2*(d)); sh30:=sinh(gam1*-h);
    g1:=shld*ch20+gam12*chld*sh20; g2:=epsr12*chld*sh20+gam12*shld*ch20; g12:=g1/g2;

    f2:=alphan_2*e2/g1/g2;

    s1:=sinh(2*gam1*(p-d))/4/gam1; p1:=(p-d)/2;
    s2:=sinh(2*gam2*d)/4/gam2; p2:=d/2;
    s3:=sinh(2*gam1*h)/4/gam1; p3:=h/2;
    cc2:=s2+p2; ss2:=s2-p2; sc2:=sqr(sinh(gam2*d))/2/gam2;

    i1:=chld*shld*sc2;

    i1:=p1+s1; i2:=s1-p1;
    i3:=epsr12_2*chld_2*cc2+gam12_2*shld_2*ss2+2*epsr12*gam12*i1;
    i4:=epsr12*gam12*chld_2*cc2+gam12*shld_2*ss2+(epsr12+gam12_2)*i1;
    i5:=shld_2*cc2+gam12_2*chld_2*ss2+2*gam12*i1;
    i6:=gam12*shld_2*cc2+epsr12*gam12*chld_2*ss2+(epsr12+gam12_2)*i1;
    i7:=p3+s3; i8:=s3-p3;

    temp:=e1/sqr(gam2*g2)*(sqr(k1)*i1+sqr(k2)*i3)-
          f2*(gam12*(i1+i2)+i4+i6)+
          e3/sqr(g1)*(i2+i5)+
          ((sqr(k3/gam1)*e1-alphan_2*e2)*i7+delta*fy_2*i8)/sqr(sh30);
    end;
  end;

  power_term:=temp/delta;
end;
{_____________________________________________________________}
```

DATA_FIL.PAS

```
this is the data file for the program CPLFIN.
Enter the correct data in column 1 of each line.
The order in which the entries appear must be kept.
------------------------------------------------------------------------------
gre049.dat          :output filename.
7.112               :(1) waveguide width (a) in mm.
3.556               :(2) Distance from wall to metal (h) mm.
3.556               :(3) Waveguide height (b) in mm.
0.229               :(4) Slot width (w) in mm.
0.508               :(5) Slot Spacing (s) in mm.
0.254               :(6) Substrate thickness (d) in mm.
10.2                :(7) Relative dielectric constant.
1.5                 :(8) Initial guess for eps_even.
1.5                 :(9) Initial guess for eps_odd.
28                  :(10) Operating frequency in GHz.
200                 :(11) Nterms spectral terms for epsilon.
50                  :(12) Ntermsz spec terms for z.
200                 :(13) nterms_ratio.
1                   :(14) Total number of executions (nruns (15).
******************************************************************************
after the next row of -- enter on different rows first the index of the
parameter to vary at each execution (1 to 13) and next, the different values
taken by this parameter. maximum 15 executions.
------------------------------------------------------------------------------
12                  :index (1 to 13)
200
250
300
400
```